Master's thesis

2019

Katalin Sandor Johansen

NTNU
Norwegian University of
Science and Technology
Faculty of Engineering
and Environmental Engineering
Department of Civil

Katalin Sandor Johansen

Internal Rain Gutter for BIPV Roof

Dimensioning the Internal Rain Gutter for ZEB Laboratory's BIPV Roof

July 2019

NTNU
Norwegian University of
Science and Technology

NTNU
Norwegian University of
Science and Technology

NTNU
Norwegian University of
Science and Technology

Internal Rain Gutter for BIPV Roof

Dimensioning the Internal Rain Gutter for ZEB Laboratory's BIPV Roof

Katalin Sandor Johansen

Civil and Environmental Engineering
Submission date: July 2019
Supervisor: Tore Kvande
Co-supervisor: Anna Eknes Stagrum

Norwegian University of Science and Technology
Department of Civil and Environmental Engineering

Preface

This master thesis was written at the Institute for Civil and Environmental Engineering at Norwegian University of Science and Technology (NTNU) in the spring of 2019 for the 2-year MSc Program. The thesis constitutes the work related to the course TBA4905 Building and Material Engineering within the specialization building and material engineering and constitutes 30 course credits. This thesis is an investigation for the new ZEB Laboratory through Klima 2050, a research center for risk reduction through climate adaptation of buildings and infrastructure.

The objective of this thesis to dimension the interior rain gutters for the ZEB Laboratory's BIPV roof with respect to expected future climate and optimization the roof area for renewable energy production. Veidekke, the ZEB Laboratory contractors, will consider the final recommendations of this thesis in the design and construction of the roof and roof drainage system. A presentation of the thesis with a limited summary of results was presented in an article for Byggindustrien nr.10-2019 and is included in the appendix.

I would like to extend a big thank you to my supervisors, Tore Kvande and Anna Eknes Stagrum, for allowing me the opportunity to investigate such an interesting topic and for providing excellent guidance, help, and feedback throughout the entire process. Additionally, I would like to thank Jan Ove Busklein, Øystein Holmberget, and Ole Aunrønningen for crucial help and guidance in the laboratory. Without their assistance, none of the results in this thesis would have been possible. Thanks to Einar Bergheim for allowing us to use the SINTEF laboratory for this experiment. Finally, a thank you to Charlott Sandor Johansen and Tom Johansen for excellent editing and Erlend Andenæs for general writing advice.

Abstract

The ZEB Laboratory is designed to be an office and educational building, while also providing an arena for testing Zero Emission Building (ZEB) solutions. The building aims to reduce material use and generate renewable energy through a large 30-degree, mono-pitched, south-facing roof composed of $525m^2$ of fully-integrated continuous building-integrated photovoltaics (BIPVs). This produces a relatively large, slick, steep, and impervious surface, which, during downpours, can cause large amounts of rainwater to stream down the roof with high velocity. The purpose of this thesis is to dimension the internal roof gutter for the ZEB Laboratory to ensure runoff capture during high-intensity rainfall events, while also ensuring optimal use of the south-facing area for energy production. As the building is expected to maintain a lifetime of 60 years, the design needs to be adapted to future high-intensity rain loads as a result of climate change.

The experiment tested a large-scale sample roof in a Rain and Wind Box (RAWI-box) at 30 degrees with different dimensions of gutter opening; 120mm, 240mm, and 480mm. Water volumes representing rain loads pertaining to ZEB's location in Trondheim were modified to reflect expected future design loads and then tested on the sample roof. Grating covers were also tested in each case to see if the covers had an effect on gutter interception capabilities. As these water quantities and its application exceeded the capabilities of the RAWI-box, a special set-up was constructed which ultimately caused failures in the apparatus. A qualitative evaluation of the video results evaluated the performance of the various gutter sizes.

The results indicate that smaller gutter openings increase the chance of roof runoff projection overshooting the gutter and increases the intensity of frequency of back-splash (water splashing up and over the edge of the gutter). Grating covers reduce the probability of these phenomena for all gutter opening sizes. Based on experimental observation, the recommended gutter size opening for ZEB Laboratory is 240 mm. With a modified gutter design and with the use of grating covers, the opening size can be set to a range of 200-300 mm, depending on the level of risk building owners are willing to accept. Observations from this experiment can be useful in future gutter design for buildings with large mono-pitched BIPV roofs.

Sammendrag

ZEB Laboratoriet skal bli et kontor og utdanningsbygg, samtidig som det vil benyttes til forskning og utvikling av løsninger for nullutslipps bygninger. Bygningen planlagt og vil bli bygget med fokus på redusert materialbruk, samt å generere fornybar energi gjennom et stort sørvendt 30-graders skråtak bestående av 525 m^2 med fullstendig integrerte solceller (BIPV). En slik konstruksjon vil gi et relativt stor, glatt, bratt og ugjennomtrengelig takflate. Under kraftige regnskyll vil et tak med en slik utførelse medføre at store mengder regnvann vil strømmer nedover taket med stor hastighet. Formålet med denne oppgaven er å dimensjonere en innvendig takrennen til ZEB-laboratoriet for å kunne sikre kontrollert avrenning ved ekstreme regnskyll, samtidig som det skal sikres optimal bruk av sørvendt område for energiproduksjon. Da bygningen forventes å ha en levetid på 60 år, må designet være spesielt tilpasset fremtidig høy intensitet av nedbør i form av regn på grunn av antatte klimaendringer.

Forsøket besto av et fysisk eksperiment som testet et stort tak i et regn- og vindkammer (RAWI-boks) ved 30 grader med forskjellige dimensjoner av takrenneåpninger; 120mm, 240mm og 480mm. Vannmengdene som representerer regnbelastninger knyttet til ZEBs lokasjon, Trondheim, ble modifisert for å gjenskape forventede fremtidige dimensjonerende belastninger og deretter påført test-taket. Gitterdeksler ble også testet i hvert enkelt tilfelle for å se om dekslene hadde en effekt på kapasiteten på avløpet. Da testingen av slike vannmengdene med et slikt oppsett var langt utover RAWI-boksens kapasitet, ble kapasiteten justert med spesialtilpassninger, noe som til slutt førte til feil i testapparatet. Kvalitativ evaluering av videoresultatene ble brukt til å identifisere ytelsen til rennestørrelsene.

Resultatene indikerte at mindre renneåpninger vil gi større sannsynlighet for at avrenningen ifra taket ikke blir fanget av rennen og i hyppigere og kraftigere spruting fra strålen av som treffer kanten på innsiden takrennen. Ved å benytte en rist over takrennen vil man kunne redusere sannsynligheten for at dette oppstår for alle åpningsstørrelser. Basert på observasjonene fra forsøket, er den anbefalte takrenneåpningen 240 mm. Med et modifisert takrennedesign og bruk av rist, kan åpningsstørrelsen settes til en rekkevidde på 200-300 mm, alt avhengig av hvilken risiko byggherre er villige til å akseptere. Generelle observasjoner fra dette eksperimentet kan være nyttige i fremtidig konstruksjon av takrenner for bygninger med store integrerte BIPV tak.

Contents

List of Figures

List of Tables

Definitions

Back-splash Describes when water splashes over the edge of the gutter in a reflected angle approximately perpendicular to the runoff projection's trajectory.

Building Integrated Photovoltaics (BIPV) Multifunctional photovoltaic materials that replace conventional building materials, usually in the building envelope, and perform the replaced material's functionality to a comparable degree [1].

Catchment Area The catchment area is the roof area that collects and channels rainwater.

Climate Adaptation "The process of adjustment to actual or expected climate and its effects, in order to moderate harm or exploit beneficial opportunities" [2].

Climate Factor Factors that represent the expected relative change of predicted rain intensity from current values due to climate change [3] .

Embodied Emissions The energy that is necessary for the production of materials multiplies by a CO_2 factor. Gives indication of the emissions associated with production of material [4].

Flow Water moving with a velocity in a stream or a sheet downhill.

Grating cover A metal mesh-like structure that is placed on top of gutters to prevent debris from entering and clogging gutters.

Green House Gases (GHG) "Greenhouse gases are those gaseous constituents of the atmosphere, both natural and anthropogenic, that absorb and emit radiation at specific wavelengths within the spectrum of terrestrial radiation emitted by the Earth's surface, the atmosphere itself and by clouds.Water vapour (H2O), carbon dioxide (CO_2), nitrous oxide (N_2O), methane (CH_4) and ozone (O_3) are the primary GHGs"[2].

Intensity Duration Frequency (IDF) "Curve showing the probability that various short-period rainfall rates for various durations of precipitation at a given location will be exceeded" [5].

Intercept In this thesis, to intercept or interception of water, is runoff water that is caught be the gutter.

Internal Gutter Gutter set within the perimeter of the roof to intercept and convey rainwater to drainage outlets. Otherwise known as "box gutter", as it describes the gutter being "boxed" in from all sides.

Laminar "Flow associated with low velocities, characterized by a smooth appearance" [6].

Mitigation "A human intervention to reduce emissions or enhance the sinks of greenhouse gases" [2].

Overshoot Runoff from roof that passes over the gutter and is not caught and drained.

Overtopping/overflow Water flows over the brim of the gutter, in this thesis refers to gutter having insufficient hydraulic capacity.

Qualitative Results that cannot be related to quantity, descriptive information that cannot be measured.

Quantitative Results that are measureable by quantity or amount.

RAWI BOX Apparatus used to simulate driving-rain conditions on building components mounted in a frame by pulsating air pressures and water spray by moving nozzles.

Reliability The consistency of results.

Representative Concentration Pathways (RCP) "Scenarios that include time series of emissions and concentrations of the full suite of greenhouse gases (GHGs) and aerosols and chemically active gases, as well as land use/land cover (Moss et al., 2008). The word representative signifies that each RCP provides only one of many possible scenarios that would lead to the specific radiative forcing characteristics based biophysical, techno-economic, and/or socio-behavioural trajectories and involve various dynamics, goals and actors across different scales" [2].

Return Period The return period of rain intensity is the "average time interval in years between the occurrence of rainfall of a given intensity and that of an equal or greater intensity"[5].

Runoff That part of the precipitation which is not infiltrated or stored on surface but flows over the surface [5, 7].

Runoff Projection In this thesis, refers the "jet" or "waterfall" that occurs when runoff from the roof enters free fall into gutter.

Short-term extreme rain events Heavy rainfall events, usually with a duration of 1-60 minutes, that could case problems for drainage systems. In this thesis, the short-term extreme rainfall events act as design values for roof drainage systems .

Turbulent "Flow associated with intense mixing and unsteady flow" [6].

Uncertainty "A state of incomplete knowledge that can result from a lack of information or from disagreement about what is known or even knowable" [2].

Validity If experimental result or procedure represents the actual process or phenomenon to a sufficient degree.

ZEB: Zero Emission Building A building that generates enough renewable energy to compensate for all CO2- equivalent GHG emissions throughout the building's lifetime [4, 8, 9].

Chapter 1

Introduction

1.1 Background

Due to the release of vast amounts of anthropogenic greenhouse gases since the Industrial Revolution, humans have indisputably affected the global environment and climate. Globally, climate trends indicate an overall warming of the atmosphere and resultant changes in weather systems globally with regional variations [10]. These trends are already being observed and prediction scenarios indicate that they will continue to prevail and intensify in the future. Effects include increases in frequency and intensity of extreme weather events such as; heavy precipitation, storm cycles, droughts, and extreme temperatures. These climate changes will enhance the vulnerability of the built environment to damages caused by amplified environmental strains. In order to preserve and prolong their intended lifetimes, buildings need to be designed for future climate. In short, buildings need to be resilient and adapted to future climate changes.

The global community sees the importance and urgency of addressing the global challenges involving climate change, primarily the need to curb emissions of greenhouse gases. In order to limit current atmospheric warming to 1.5- 2°C, as suggested by the UN to abate climate-related consequences, deep global reductions of anthropogenic greenhouse gas (GHG) emissions of approximately 40-25 % respectively by 2030 are necessary [10]. The building and construction industry is currently responsible for 39% [11] of energy related CO_2 emissions globally and approximately one-third of global final energy use. There is an urgent need to focus on reforming this sector to mitigate GHG emissions as well as adapting to any future climate changes. To reach current emissions ambitions, a reduction of energy intensity pr square meter of approximately 30% is needed by 2030. To facilitate these reductions, there is an increasing focus on transitioning the global building stock into high-performance low-emission and low-energy, sustainable, and resilient buildings[11].

In order to achieve the necessary reductions in GHG emissions, countries are establishing passive, zero emission, and zero energy buildings standards and adopting stricter mandatory building codes for energy use in buildings. For example, the EU Energy Performance of Buildings Directive requires all new buildings and all new public buildings to be nearly zero-energy by the end of 2020 and 2018, respectively [12]. A zero emission buildings (ZEBs) aims to lower the GHG of buildings by reducing energy demand through energy efficient measures and offsetting its entire lifecycle carbon footprint by producing renewable energy on- or near site [9]. Though a greater number of these projects and buildings are being developed, market penetration is slow and there is a need to demonstrate the

capability of developing ZEB buildings with readily available technology and design solutions.

1.2 ZEB Laboratory- Mitigation and Adaptation

ZEB Laboratory, a collaboration project between NTNU and SINTEF at the Gløshaugen campus in Trondheim, aims to enhance knowledge related to zero emission buildings. ZEB Laboratory is designed to be a fully functioning building for office and educational use. It will simultaneously act as a living lab to test and develop new and sustainable technologies, techniques, and solutions related to zero emission buildings. The intention is for ZEB Laboratory to have the ability to remove, replace and change elements in the building facade and systems. This will enable research on various technologies and solutions when exposed to real environmental conditions and interactions with actual users. Figure 1.1 is the proposed building design.

Figure 1.1: Proposed ZEB Laboratory [13]

ZEB Laboratory aims to reach ZEB COM status. This implies that the building generates enough onsite renewable energy throughout its 60-year lifetime to compensate for the emissions related to material use, construction, and operation of the building [14]. In order to achieve this, energy efficiency measures and measures to reduce material use and the embodied energy of construction materials are paramount. Despite the attempt to minimize the embodied energy, the building must have substantial energy production from both thermal and electrical sources. Photovoltaic solar power is the main renewable energy production method for this project as it is abundantly available and produces virtually no emissions during operation. In order to reduce material use and maximize energy production while maintaining a holistic architectural image, building integrated photovoltaics (BIPV) will be utilized in the east-, west-, and south-facing facade and roof [14].This reemphasizes the architects visual expression for the building, which is a polished silicon crystal, the semiconducting material most commonly used in photovoltaic cells. The seamless and continuous panels will give the building a black metallic luster to further enhance the semblance invoked by the buildings' polygonal shape [14].

BIPVs are photovoltaics, which are integrated into the building envelope and replace conventional construction materials while generating renewable electricity from solar power. BIPVs can be integrated into the building envelope by replacing building components materials in the facade, the roof or other building aspects such as shading systems [1]. BIPVs must meet standards regarding the functionality of the conventional building envelope component that the BIPVs replace. In the ZEB Laboratory, the BIPVs will replace traditional cladding and roofing materials. The functionality of these materials include privacy screening, thermal insulation, acoustic protection, and structural support. However, one of the most important functionalities that the BIPV must replace is protection against the elements.

The climate in Trondheim, where ZEB laboratory will be built, is expected to become increasingly warmer and wetter. Climate changes in Trondheim is particularly associated with increased frequency and intensity of short-duration heavy rainfall events, storm water floods, increased risk of landslides and avalanches, and increases in storm surges[15]. ZEB Laboratory therefore needs to incorporate adaptation to these climatic changes in the building design. Due to the building's location, the most important adaptions to the design are associated with increased rainfall and storm-water runoff from heavy precipitation events to prevent moisture-related damage.

ZEB Laboratory's profile and orientation is optimized in order to ensure maximum possible solar radiation in its allotted location. The building is oriented directly southward with a mono-pitched roof with a slope of 30 degrees that faces directly south. This makes the roof and south-facing facade valuable area for solar energy production. The 550 m^2 roof is roughly 20 meters long with a height difference of height of almost 11 meters, four stories to the north and three stories towards the south [16]. Approximately 525 m^2 of high efficiency BIPVs in a fully integrated continuous solution is planned. The underlying roof design is a compact roof with a drainage and ventilation gap between BIPV roofing elements and the underlying structure [16]. The BIPV roofing system must be as impervious as possible to prevent wind and rain penetration onto the underlying roofing system. This implies joints have to be sealed and a minimum of extruding parts, which additionally gives the roof a smooth and homogeneous appearance.

1.3 Challenges of rain gutter design for BIPV roof

The BIPV panels have a low coefficient of friction, making the entire roof a relatively large, slick, and impervious surface. As short-duration heavy rain events are expected to increase in frequency and intensity, the roof in particular needs to be adapted to handle these climate changes. During heavy downpours, large amounts of rainwater runoff will stream down along the roof towards the outer edge and towards the south facade. Directing this runoff water down the facade of the building is deemed unacceptable [16]. The BIPVs planned for the south facade are expected to have larger openings or gaps between the panels, making the facade more susceptible to water and moisture related damages. Overshoot and uncollected storm-water runoff will also contribute to increased risk of urban flooding, which should be avoided. Additionally an entrance and a pergola, seen in Figure 1.2, are located on the south side of the building, make this a vulnerable area due to increased public traffic.

The most covetable solution is a type of catchment and drainage system implemented at the outer edge that can handle extreme rainfall events. However, a rain gutter and drainage system along

Figure 1.2: South facade and roof of ZEB Laboratory [17]

the outside perimeter (eave gutter) sufficiently sized to intercept the runoff without unacceptable overshoot or overflow, would shade the topmost section of BIPVs on the south facade. This would reduce energy production and should therefore be avoided [16]. A rain gutter of this size, likely 400mm in diameter, would also decrease the building's intended visual expression aesthetic. This is certainly an issue not only for the ZEB Laboratory, but also for similar BIPV projects in urban areas where a large south facing mono-pitched BIPV roof will account for large portions of the building's renewable energy production.

Therefore, the architect's proposed solution to ensure proper handling of the rainwater runoff from the ZEB Laboratory roof, is an internal gutter integrated into the roof surface close to the bottom edge of the roof as seen in Figure 1.3.

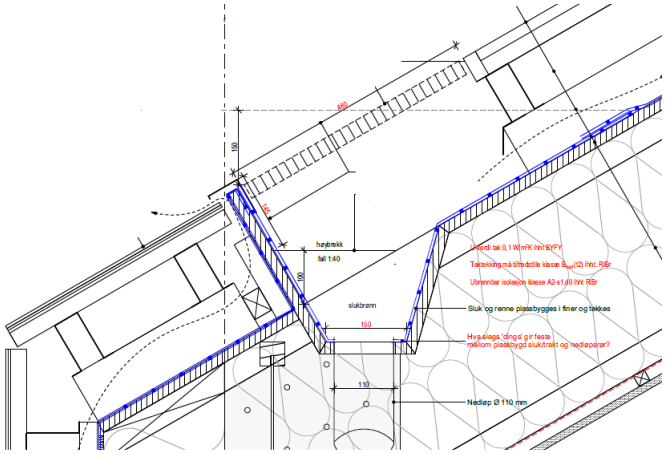

Figure 1.3: Architect's proposed solution of an internal gutter integrated into the roof's surface [18]

1.4 Objective and Scope

The purpose of this thesis is to optimize the dimensions of this gutter design to maximize the amount of BIPV modules placed on the roof to, in turn, maximize energy production, all while adequately collecting and draining the runoff rainwater from the roof. This also implies that certain architectural restrictions placed on the design are not violated, so that the intended visual expression is not compromised. The primary architectural restrictions are no parapet and no external roof gutter. The focus of the thesis is to determine the width of the opening in the surface of the roof to sufficiently intercept rainwater runoff from the roof above without an unacceptable overshoot. As rainwater-roof interactions are quite hard to fully understand and predict, a simplified experiment was performed with a sample roof to visually observe and the performance of the rain gutter.

In order to adequately address this issue, a series of research questions was used to direct the investigation:

In order to adequately address this problem, a series of research questions have been used to direct the investigation:

1. What are the current and future dimensioning rain loads for ZEB Laboratory in Trondheim?
2. How well does the architect's suggested design, with respect gutter opening, perform with regards to overshoot?
3. What rain gutter design will meet functional requirements while also maximizing solar energy potential?

1.5 Limitations

The scope of this thesis is limited to the design of the ZEB Laboratory and the design of its roof gutter due to short-term high intensity rain events. Even though other precipitation impacts may be relevant, this thesis is limited to effects of rainwater runoff for short-duration high intensity design rainfall. The dimensioning is based on the possibility of runoff overshoot and the design of the roof drainage system as a whole will thus not be investigated. Therefore only preliminary calculations of the hydraulic capacity of the gutter will be mentioned in some parts of this report. Sufficient drainage of the roof gutter will depend on the number of outlets and downspouts placed along the length of the roof, and in this case, gutter overflow is not considered in the dimensioning of the system. The gutter design will be limited to the dimension design. Other relevant aspects of gutter design, such as material selection, are not inspected in this thesis.

This investigation is building specific to ZEB Laboratory and more particularly, to the location where it will be built, as mostly climatic factors govern the dimensioning of this roof gutter. Rain intensity and angle of the roof are both factors inherently linked to location. The latitude and optimal solar energy potential govern the roof angle, while weather and rain are linked to a myriad of factors such as local topography, geography, and temperature. Despite the research case being quite location specific for this investigation, there are generalizations and lessons learned that are applicable to other projects and locations. This investigation is also based on the assumption of a full-roof building integrated photovoltaic system with a minimum of extruding parts and crevices

that will inhibit the flow of water. In reality, there will be some extruding parts and openings depending on the specific product and installation systems used.

1.6 Layout

The main layout of this thesis is summarized below:

Introduction Motivation and background for this thesis.

Theoretical Framework The theoretical framework gives the context for the development of the experimental method and for the discussion and interpretation of results. The results of the literature search are presented in this section, as it forms the basis for the experimental method.

Method A description of the literature search and the qualitative experimental methodologies used in this thesis.

Results An unbiased presentation of the results from the experiment. The qualitative results are primarily based on stills from video footage of the experiment. These videos are available on "https://www.youtube.com/channel/UC0u565OUCAWqgAoxXOfKsIg".

Discussion A discussion and interpretation of the relevant results, in an attempt to adequately answer the research questions.

Conclusion Findings of this thesis summarized in a purposed solution for the roof gutter design for ZEB Laboratory.

Further Works Discussion of relevant findings for further investigation and research.

Chapter 2

Theoretical Framework

2.1 Zero Emission Buildings

Although there is no universally accepted definition or standard for zero emission buildings (ZEB), ZEB can be described as a building that generates enough renewable energy to compensate for all CO_2- equivalent GHG emissions the building emits throughout its lifetime [4, 8, 9]. The GHG emissions from buildings are generally determined through a life cycle assessment (LCA), where emissions from the different lifecycle phases (production, construction, operational and end of life) are determined. The number of phases, and their respective emissions, included in LCA depends on the building's ZEB ambition level [8]. The different ZEB ambition levels and the included lifecycle phases are listed below in ascending order and are illustrated in figure 2.1 [9].

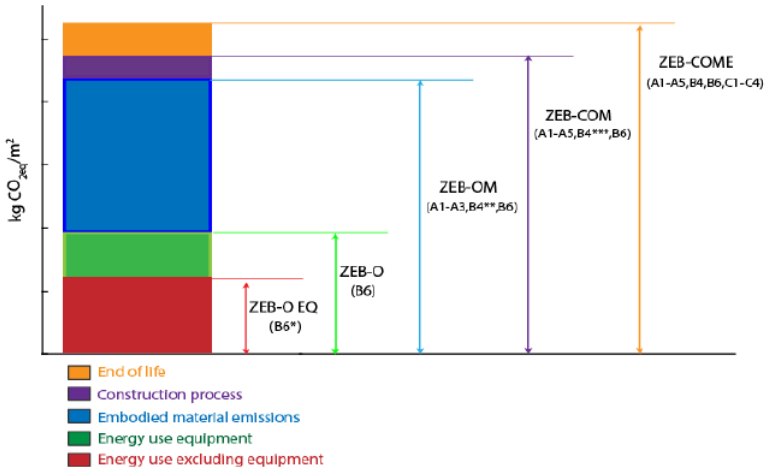

Figure 2.1: Emissions included in ZEB Ambition Levels [9]

- **ZEB-O-EQ** The building's renewable energy production compensates for GHG emissions related to the energy demand during the operational phase except for the electrical equipment plugged into electrical outlets.
- **ZEB-O** The building's renewable energy production compensates for emissions related to the energy demand during the operational phase.
- **ZEB-OM** The building's renewable energy production compensates for GHG emissions re-

lated to energy demand during the operational phase and the production of building materials used throughout the building's entire lifetime.

- **ZEB-COM** The building's renewable energy production compensates for GHG emissions related to energy demand during the operational phase, the production of building materials used throughout the building's entire lifetime, and the construction phase (including transport and installation).

- **ZEB-COME** The building's renewable energy production compensates for GHG emissions related to energy demand during the operational phase, the production of building materials used throughout the building's entire lifetime, the construction phase, and the end of life phase. The end of life includes demolition, transport, waste processing, and disposal. The end of life could reduce emissions due to recycling of building materials.

- **ZEB-COMPLETE** The building's renewable energy production compensates for GHG emissions related to energy demand during all phases of life previously mentioned,in addition to maintenance, repair, and renovation.

The total emission balance of a building can be expressed in the following equation, were energy demand is electric [8, 9]:

$$\Delta E = EE_c + EE_m + EE_{plet} + EE_e + \sum_{n}^{n=0} \Delta E_{O,N} \tag{2.1}$$

Where the variables are:

- ΔE Total emission balance $\left[kgCO_2eq/m^2\right]$

- EE_c Embodied emissions from construction

- EE_m Embodied Emissions from material production

- EE_plet Embodied Emissions from maintenance, repairs, renovation

- EE_e Embodied Emissions from end of life

- $\sum_{n}^{n=0} \Delta E_{O,N}$ The sum of the emission balance of energy demand during the operational phase during the entire lifetime, n. $\Delta E_O, N$ is basically the difference in the buildings total energy demand and the total renewable energy produced (i.e. by photovoltaics).

The emissions included in the equation will depend on the ambitions of the ZEB. This equation can be illustrated in a graph that visually depicts the emissions being "paid back" from the renewable energy produced exported from the building. Figure 2.2 depicts an example of a building's energy balance. Equation 2.1 and Figure 2.2, illustrate that a high annual production of renewable energy can result in a net zero emissions balance within a buildings lifetime.

ZEB could also refer to Zero Energy Building, which generally refers to a building that generates a sufficient amount of renewable energy equivalent to or exceeding the buildings annual net energy demand [4]. For the purpose of this thesis, ZEB refers to Zero Emission Buildings.

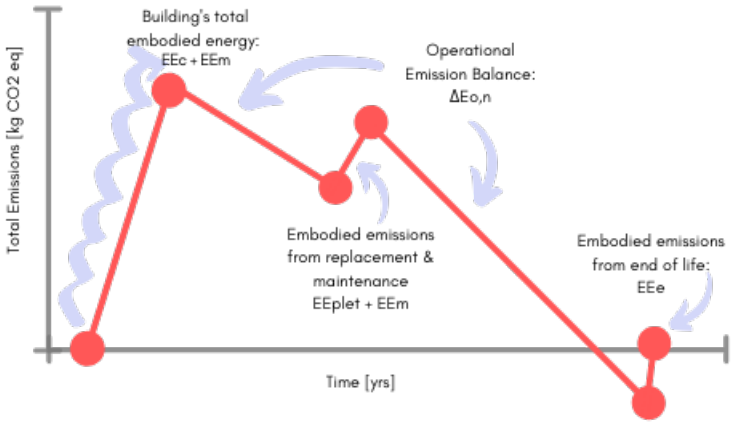

Figure 2.2: Depiction of a ZEB building's emission balance

2.2 Building Integrated Photovoltaics

As solar energy is inexhaustible and have no direct emissions during energy production, photovoltaic cells energy are currently one of the most promising methods of renewable energy production [19]. Thus utilizing photovoltaics as a main renewable energy source in ZEBs is a viable and favorable solution. Building integrated photovoltaics (BIPVs) are multifunctional photovoltaic materials that replace conventional building materials, usually in the building envelope, and perform the replaced material's functionality to a comparable degree [1]. BIPVs therefore provide a cost-effective way of enhancing sustainability in buildings by reducing material consumption and labor while providing a low-emission energy source [20].

The solar irradiance is abundant even in Norway, which receives 700-1000 kWh/m^2 annually [20]. The optimal angle for annual solar production in Norway is 30-45°, and are generally placed on roofs [20]. But due to the low angle of incidence in high latitudes for long periods of the year, photovoltaics mounted on facades also have the potential to harvest a decent amount of solar energy [21]. High latitudes have lower temperatures, which ensure that the modules maintain expected efficiencies since PV cells are more efficient when cold [22].

Photovoltaic cells (PV) are semiconductor devices that convert sunlight directly into electricity through the photovoltaic effect. The photovoltaic cell is based on two layers of semiconducting material manipulated to hold different charges, which when exposed to photons give rise to an electric current between them [23]. Different cell technologies exists with varying ranges of efficiency of converting solar power into electrical energy; crystalline silicon wafer technology (12-20%), thin-film technology (5-13%) , and organic or inorganic nano-cell technology [24].

The cells are interconnected to form modules in order to generate enough voltage and power output. Photovoltaic cells are connected together and encapsulated between a stable transparent front material and a backing material offering protection against mechanical damage, weather, and moisture [23]. Clear toughened glass with high transmittance is usually used. Thin-film modules can be formed into a single substrate with a flexible or fixed transparent front material, generally plastic

or glass [19]. A multitude of mounting structures and frames for mounting modules have been developed especially for BIPV to allow for integration into architectural design.

Partial Mounting systems : used for installing conventional standardized PV modules into sections of roofs, as modules are not customized to roof dimensions [25].

Full roof solution : roof was conceived architecturally as a solar collecting surface. BIPVs characterizes the whole roof system with special frames, roof-components, boards, joints, etc. to ensure functionalities are met while maintaining the distinct aesthetic of a full-roof system [25].

Prefab : "fastening system and other functionalities are already integrated into PV module" [25].

Solar tiles : PVs are integrated into roof as tiles and are meant to resemble conventional roof tiles [25].

Solar glazing : Laminates used for roofs made of glass or other transparent materials [25].

Curtain wall : PVs that replace transparent walls or glass walls [25].

Rain screen façade : Replace traditional cladding materials and usually consists of sub-frame structure, air gap, and cladding panel [25].

BIPVs that replace traditional roofing materials have to fulfill the functionalities that these traditional materials usually provide. The fulfillment of rain tightness and climate screen aspects are imperative to avoid avoiding moisture-related damages. Joints and screws interacting throughout the system have to be water tight and penetrations in the construction have to be adapted to materials to ensure air and water tightness [26].

Even though PVs do not emit GHGs during operation, the production of the cells and associated components do have substantial emissions. Therefore the resultant embodied energy of a BIPV system generally represents a large fraction of the building's total emissions [27]. However, with advancements in technology and more efficient production methods, the embodied energy of PVs are expected to significantly reduce in the future [8].

2.3 Rain

Estimating the expected precipitation load for a building's lifetime is one of the most crucial aspects in designing and sizing a successfully performing roof drainage system. Rainfall is generally the type of precipitation that is critical when designing roof drainage systems, with exceptions for some regions and roofing materials, such as glass, were snow is dimensioning [28]. In Trondheim, were ZEB is located, rainfall will be the dimensioning factor, and therefore this thesis will focus on rain and downpours.

Precipitation is "liquid or solid products of condensation or sublimation of water vapor falling from clouds or deposited from air on to ground."[5] Occurs when water vapor condenses on small nuclei in an air mass that has reached saturation point for water vapor, usually through cooling. The type of precipitation expelled depends on temperature and atmospheric conditions; types include drizzle, rain, snow, sleet, hail, or any combination of these [7]. Rain is liquid precipitation with drop size larger than 0.5mm with terminal velocities greater than 3 m/s [28]. Terminal velocity of

raindrops increases with drop size. Maximum terminal velocity is usually around 8-9 m/s when the drop has a diameter of around 5mm. Drops larger than this size will be torn apart by air resistance into smaller drops [28]. Generally, greater rainfall intensities correspond to a larger median drop size. Drops of the largest diameters ($\leq$5mm) are usually only present in high intensity rainfall events. Rainfall intensity is the amount of rainfall or depth of rainfall at a particular point during a set time interval, commonly denoted in mm/s or mm/hr. Rainfall intensities can vary from light to heavy, and typically classified as [7]:

- **Light rain** rain intensity less than 2.5 mm/h [7]
- **Moderate rain** rain intensity between 2.5 mm/h and 7.5 mm/h [7]
- **Heavy rain** rain intensity greater than 7.5 mm/h [7]

2.3.1 Rainfall Intensity

Rainfall intensity varies temporally and spatially, and storm events can therefore have an "average" rainfall intensity lesser than the peak rainfall intensity experienced throughout the event. Higher intensity rainfall events therefore tend to correspond to shorter time durations. In Norway, high intensity rainfall events are usually caused by either large frontal systems that last little more than a day or by convective showers and cloudbursts, generally in the summer, that last for minutes to hours [28, 29]. These high intensity showers are usually used in dimensioning infrastructure, as they represent the largest strains on the infrastructure systems and have the largest damage potential. In these cases, drainage infrastructure need to handle very large volumes of water with high velocities in a short time-period, which can lead to a variety of challenges related to flooding. High intensity rainfall that falls in the span of minutes to a few hours are therefore crucial in designing storm water handling and drainage systems in urban areas.

2.3.2 Rainfall Measurement

Rainfall is measured by rain gauges, which are types of horizontal funnels that lead rain to a storage area and the depth, or volume over unit area, is measured over a period of usually 24 hours [30]. To accurately measure rainfall intensity for short durations, periods of minutes and hours, the Norwegian Meteorological Institute (MET) [29] uses tipping or weight pluviometers. For tipping pluviometers, the rain enters a funnel drips into a scale that balanced on an edge held in place by a magnet until it reaches a calibrated amount (0.1- 0.2 mm water). The magnet releases to empty the scale and a second scale moves into position. The release of the magnet is time-registered and data is transferred in real-time. The real-time data enables calculation of the rain intensity for a specific time interval [29]. Weight pluviometers are based on the continuous weighing of accumulated water in a bucket, which is related to time data. There are some small variations in the results depending on the type of pluviometer but this is accounted for in calibrations. Uncertainties in actual catch rate for pluviometers due to wind effects and height placement are minimal when it comes to high intensity rainfall.

2.3.3 IDF Curves

Estimation of dimension of extreme values is based on extrapolation of available data from the pluviometers to give values with certain return periods. The return period of rain intensity is the "average time interval in years between the occurrence of rainfall of a given intensity and that of an equal or greater intensity."[5] The return period will give an indication of the probability of exceeding a given rainfall intensity. To illustrate this, Intensity-Duration-Frequency (IDF) curves show "the probability that various short period rainfall rates for various durations (1 minute to 24 hours) of precipitation at a given location will be exceeded" [5] under different return periods (2-200 years). IDF data for Norway is available through the Norwegian Centre for Climate Services (NCCS), which is a collaboration between the Norwegian Meteorological Institute, The Norwegian Water Resources and Energy Directorate (NVE), NORCE and the Bjerknes Centre for Climate Research. NCCS aims to provide climate information to promote and facilitate research on climate adaptation and climate change [31].

For ZEB Laboratory, four weather stations in the Trondheim vicinity provide relevant data: Blakli, Voll, Tyholt, and Risvollan. Figure 2.3 shows the location of these stations in comparison to ZEB Laboratory and their relevant IDF curves are presented in Aection A in the Appendix. The most relevant station for meteorological data in Trondheim is considered to be Voll-Tyholt[32]. The meteorological stations at Tyholt and Voll are effectively the same station that was moved from Tyholt to Voll. The different data series reflect the station location during different time periods. For the purpose of this thesis the Voll meterological station will be used, which has been in operation since 2002 [31]

Figure 2.3: Meteorological stations in Trondheim compared to ZEB Laboratory

The data the NCCS uses in their IDF curves are filtered to ensure that estimates are not based on outlier values or insufficient data sets. Recommended data sets require measurements from at least 10 seasons that meet the defined criteria for data set reliability.

Figure 2.4 illustrates IDF for Trondhiem (Voll). The experimental calculations were based on these numbers.

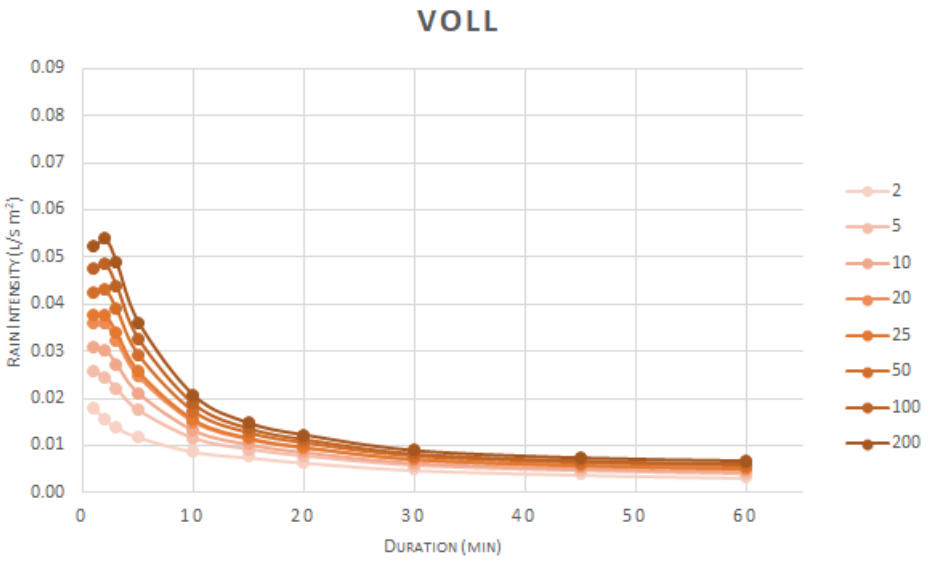

Figure 2.4: IDF for Voll- Current values

2.4 Expected Climate Change

As buildings are expected to have a specified lifetime, usually 60 years, it is necessary predict the future climate in order to have an idea of the environmental stresses that the building may experience. Without any noticeable reductions in current greenhouse gas emissions, the Norwegian government's climate predictions towards the end of the century are based on median to high emission scenario. Annual temperatures are expected to increase by 4.5 °C [33] with a range from (3.3 °C to 6.4 °C) with regional variation. As warmer air can hold more moisture than cold air, the annual precipitation is expected to increase by approximately 18%.

The Climate in Norway 2100,[33], mentions that rainfall intensity data already indicates a trend in increasing intensity in heavy rainfall events in Norway. Since 1900, there has been approximately a 20% increase in intensity of high intensity rainfall events.[29]. Extreme precipitation events are expected to increase in both intensity and frequency by the end of the century [15, 29, 33].

2.4.1 Climate Models

Global climate models were used in determining these future climate predictions. Global climate models involve physical and mathematical representations of the physical processes and interactions (forcings and feedbacks) seen in climate systems and used to quantify climate change under various emissions scenarios. Global models are based on a grid size of 100x100 km, which is too coarse for quantifying future climate in specific regions in Norway [33]. In order to get detailed climate predictions for regional use, the global models are empiric-statistically or dynamically down-scaled [29]. Empirical/Statistical observations and create statistical links from global to regional scale while dynamical down-scaling creates regional climate models (RCM) [2].

These are used in conjunction with scenarios representing the possibilities for future development of anthropogenic GHG emissions, or the so-called Representative Concentration Pathways (RCP) [33]. These RCPs show future projection of GHG emissions dependent on a variety of factors

such as population growth, technological development, socio-economic circumstances, and climate policies. The scenarios used in the context of this thesis are RCP4.5 and RCP8.5, as results are readily available for comparison and these scenarios are deemed more realistic to base design on considering the current rate of emissions [33]. This emissions pathways are characterized as:

- **RCP 4.5** Intermediate emissions: consisting of stable/ slight increases emissions until 2040 and then significant reduction of emissions. This scenario requires stringent climate policies that require a 40% reduction of GHG emissions of 2012-level emissions by 2080. This scenario predicts a global temperature rise of 2°C by 2100 compared to pre-industrial levels. [10, 33]

- **RCP 8.5** High Emissions: continuous emissions with a "business as usual" development. This scenario assumes a three-fold increase in GHG emissions with rapid increase in methane emissions and a human population increase to 12 billion by 2100. This scenario predicts a global temperature rise of more than 4°C by 2100 compared to pre-industrial levels. [10, 33]

2.4.2 Climate Factors

To dimension future buildings and infrastructure for future climate strains, in this case rainfall intensity, climate factors (K_f) have been developed based on the predictions made by the regional climate models. Climate factors can be defined as the expected relative change of predicted rain intensity from current values due to climate change [3]. Climate factors are multiplied with current design rainfall intensity to get target future design values. Climate factors are dependent on RCP and RCM but also on the return period, duration of rainfall, location, and reference period for predictions [29].

Table 2.1: Recommended climate factors[%] for change in design short-duration rainfall until 2071-2100, M5= 5 yr return period, M50= 50 yr return period [34]

	<M50		**≥ M50**	
Duration	**Low M5**	**High M5**	**Low M5**	**High M5**
≤ 1hr	40	40	50	50
2-3 hr	40	30	40	30
4-6 hr	30	30	40	30
7-24 hr	30	20	30	30

Table [34] indicates that the climate factor will increase with increasing return period and for shorter duration events [34]. The geographical representations in Figure 2.5 shows the median climate factors for Norway for a return period of 5 years for a 1-hour duration. Table **??** shows Norwegian Meteorological Institute's recommendation for climate factors for design values of high intensity short-duration rainfall. For the purpose of this thesis, only the values associated with a duration of less than 1 hour are significant. Based on the information presented so far, the chosen values of 1.4 and 1.5 are dimensioning climate factors for high intensity short-term rainfall events in Trondheim with return periods less than 50 years and greater or equal to 50 years respectively. This will give an acceptable error of margin, as there are a multitude of assumptions and uncertainties involved with future climate predictions.

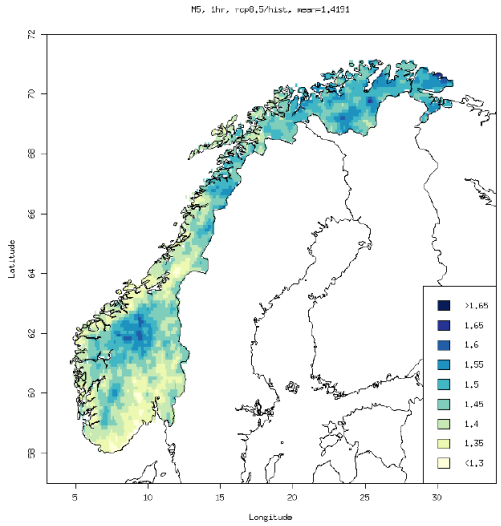

Figure 2.5: Mean value for climate factors for M5 and 1 hr [34]

2.5 Precipitation and Buildings

Precipitation is one of the most critical environmental strains that buildings experience. In Norway, approximately three-quarters of all building-related damages are accredited to water and moisture, and roughly one-fourth of these damages are attributed to precipitation alone [35]. With increasing intensity and frequency of short-duration heavy rainfall, there is an increased risk of moisture-related damages in buildings. As two-thirds of damages related to the building envelope and 22% [35] of damages are solely related to roofs, appropriately designed roof drainage systems may be crucial in handling the increased runoff from the expected in increase rain load.

To ensure that buildings are adapted and resilient towards increased rain load in the future, appropriately sized roof drainage systems are important to handle the increased rainwater runoff loads.

2.5.1 Roof Drainage

The main purpose of rain gutters is to collect and convey rainwater water away from the roof to protect the interior, facade, and foundation from rainwater infiltration. As mentioned previously in chapter 1, it is not possible to position gutters on the outside of ZEB Laboratory's perimeter. This makes internal gutters a viable solution. Internal or Box gutters are commonly used in large commercial buildings, while eave gutters are more commonly associated with residential buildings [36]. Internal gutters are "graded channel, generally of rectangular shape, for conveyance of rainwater located within the roof of a building" [37]. Different types of box or internal gutters include valley gutters, parapet gutters and boundary wall gutters [38].

Gutter components Figure 2.6 depicts the general components associated with a general internal or box gutter in a roof.

Catchment Area The catchment area is the roof area that collects and channels rainwater. The surface characteristics and geometry, will determine how the runoff flows on the roof. The slope,

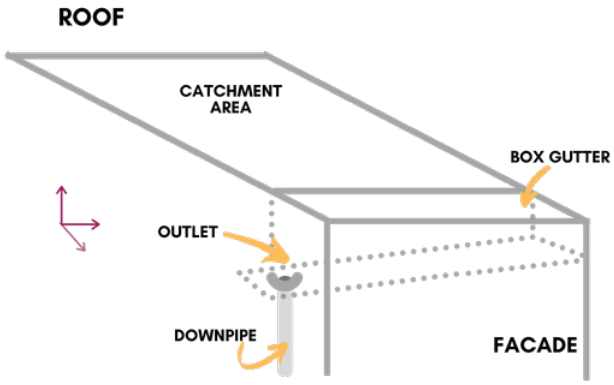

Figure 2.6: General components of an internal roof gutter system

length, roughness and infiltration properties of roofing material, and the corrugation of roofing affects the trajectory and quantity of rainwater runoff flow.

Internal Gutter The box or internal gutter intercepts runoff flow along the length from the catchment area and conveys it to a drainage outlet. The shape of gutters may be semi-circular, of similar rounded shape, or of a rectangular or trapezoidal shape. The shape and dimensions of the gutter will determine the hydraulic capacity of the gutter. To convey water efficiently to the discharge outlet and avoid ponding, some slope in the gutter may be necessary. The fall of the slope is recommended to be less than 1/100, and a slope less than 3mm pr m are considered to be nominally level for design purposes [38, 39]. The hydraulic capacity of a gutter is usually determined with nominal fall as it will give a conservative estimate of the hydraulic capacity of the gutter in question.

Discharge Outlet The discharge outlet is "an opening in the sole of the gutter which discharges water directly into the head of the rainwater pipe" [38]. The size and shape of opening will determine the draining capacity of the roof gutter.

Downpipes Downpipes lead the rainwater vertically down from roof elevation to ground level to storage tanks for greywater systems, expulsion to terrain, or sewage systems. Though the piping system usually runs at atmospheric pressure, outlets and piping systems could be designed to function siphonically [38].

2.5.2 Grating covers

Gutter grating are coverings with openings, usually mesh-like, that are installed on top of the gutters. Grate coverings thus allow rainwater to drain through but block larger pieces of debris from entering the gutter. This prevents debris build-up and clogging, especially in and around the drainage outlet. Though the primary purpose is to prevent debris from entering the roof gutter, they may also have a decelerating effect on the velocity of runoff flow. This is suggested by investigations into the effects of grate covers on street drainage systems[40].

2.6 Hydraulic dimensioning

Correct dimensioning of the hydraulic capacity of the system to prevent exceedance of the system is essential, but so is maintaining a balance to avoid costly over-design [41]. The risk level of the drainage system is determined by the potential consequences of failure in the system. The risk categories for roof drainage are classified 1-4, with category 4 representing the greatest consequence potential [38, 42]. Though it is acceptable for the roof drainage system to be exceeded occasionally, the failure or overflow of internal gutters is inherently associated with higher risk of significant damage to the building itself and its contents. Box or internal gutters tend to be in risk category 2 or 3, thus the EU standard suggests a return period of $1.5L_y$, where L_y is the lifetime of the building, [38] and a 2-minute duration.

2.6.1 Standard for Roof drainage: NS 12056-3

The Norwegian standard for Gravity drainage systems inside buildings- Roof drainage is based on the European standard of the same name. This standard describes methods for the layout and dimensioning of all parts of the of roof drainage system for different types and shapes of gutter systems. Though the standard does give insight into a lot of design aspects related to dimensioning of the roof gutter system, it does not take into account design issues associated with specific types of roofs. For example, overshoot for BIPV or corrugated roofs.

The rational method is used to estimate the peak rate of flow from the catchment in all roof cases. The calculation of hydraulic design capacity of the internal gutter system is done according to the method outlined in the standards. The steps below can summarize design of internal “box” rain gutters: hydraulic capacity according to standard 12056-3 [39].

1. Calculate design flow load Q expected from rainfall, generally from the rational method as described in section 2.6.2
2. Size/ shape of gutter design
3. Determine maximum allowable depth for safe operation without overflow
4. Calculate hydraulic design flow capacity Q_L
5. Ensure Q_L is greater than Q, if not:
    - Add more outlets to reduce drainage length, or
    - Use gutter with larger cross-sectional area

2.6.2 Rational Method

The Rational Method was first introduced by Mulvaney in 1851 and adopted by Kuichling in 1889 [41] and is still used as a method for determining the peak rate of flow resulting runoff from a catchment (hydrology introduction). The premise of this method is that the peak runoff flow is achieved when the entire catchment area contributes. The rational method can be expressed through the equation:

$$Q_p = C \cdot i \cdot A \tag{2.2}$$

where:

- **Qp** is peak flow rate (l/s)
- **i** rainfall intensity (l/s pr m2)
- **A** surface area of catchment (m2)
- **C** is the dimensionless runoff coefficient. The runoff coefficient is the proportion of rainfall input that contributes to peak runoff rate [41] between 0 and unity. It accounts for a multitude of catchment surface characteristics that determine initial losses to depression storage and infiltration of runoff [41]. The European standard [39, 42] recommends a value of 1 for traditional roofing for design purposes.

Assumptions for the Rational Method are [43]:

- "Runoff coefficient constant throughout the design storm" [41]
- Catchment area is constant during design storm
- Rainfall intensity is time-space constant for at least equal to the time of concentration
- The peak runoff rate is maximum when duration is equal to or larger than time of concentration
  - the time of concentration is "excess rainfall to travel from the hydraulically most distant point in drainage area to the design point" [43].
  - Several equations try to describe the time of concentration, some of the suggested equations are:

    Kirpich 1940

$$[7]t_c = 223.2 \left(\frac{L}{S_a^{1/2}} \right)^{0.80} \tag{2.3}$$

    (where L length [km] and Sa is slope)

    Gauckler-Manning [7]

$$: t_c = (n^{0.60} P^{-0.4}) \left(\frac{L}{S_0^{1/2}} \right)^{0.60} \tag{2.4}$$

These assumptions would be unrealistic in some cases and therefore the rational method is generally only applicable for small catchments in urban areas, generally roofs. The rational method is usually accepted in terms of quantifying peak design load for roof gutters, as roofs generally have short concentration times, uniform and constant surface characteristics, and specified and uniform topography [36].

The Rational equation does not specifically account for the slope, surface roughness or permeability that one expects to be defining characteristics of ZEB Laboratory and BIPV roofs. Even though slope, surface friction, and permeability are theoretically incorporated in the runoff coefficient, the coarseness of the assumption of one value to fit all roofs seems like an oversimplification. Coupled with the inaccurate assumption of uniform flow and depth in the catchment area and not including time variation in flow rate, it may be necessary to compare the rational method to other methods that incorporate this into runoff rate estimation.

In reality, the depth of flow generally increases further downstream in a catchment, making the flow actually unsteady and non-uniform. A kinematic approach tries to account for these as well as incorporate catchment slope, roughness and infiltration [41]. With the use of the shallow water equations, one can attempt to estimate the depth and velocity at the downstream end (edge of the roof before gutter) as the increased depth will give a higher discharge rate into the gutter than what is assumed in the rational method.

2.6.3 Shallow water equations

Runoff flow is considered to be free surface flow, or flow that occurs at the fluid interface of liquid and gas. Sheet flow or otherwise known as overland flow, can be used to describe the flow regime during heavy rainfall conditions and initial stages of surface runoff [7]. In design situations the objective is usually to identify flow " at the downstream end of a sloping plane for a known lateral inflow"[7], in this case the lateral inflow is rainfall. The shallow water equations, otherwise known as the Saint Venants equations, can be used in simplifying the problem. Though the shallow water may not be entirely applicable in this case of ZEB Laboratory, mainly due to the steepness of the roof, the method is used to see if they provide a better estimate of the flow than the rational method.

Figure 2.7 depicts the situation.

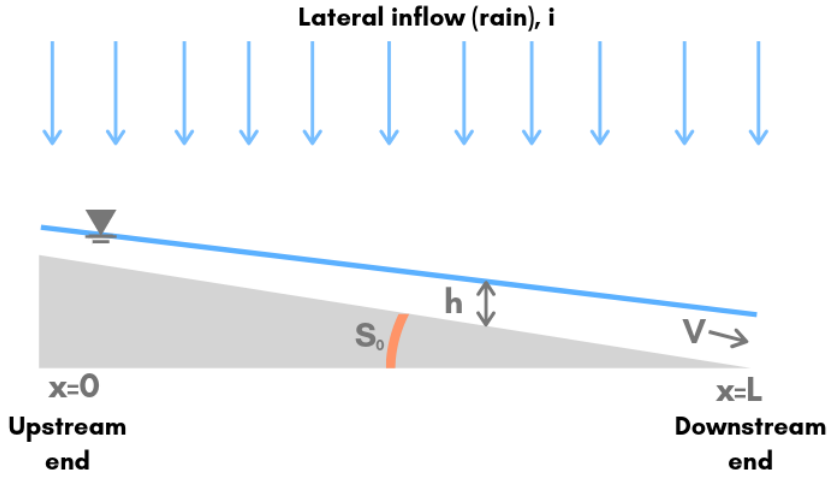

Figure 2.7: Illustration of shallow water flow, inspired by [7]

Fluid flow on a solid surface is governed by the continuity equation for mass and the Navier-Stokes equation for momentum. The shallow water equations are simplifications of these equations: [7] Equation of continuity becomes:

$$\frac{\partial h}{\partial t} + \frac{\partial}{\partial x}(Vh) - i = 0 \tag{2.5}$$

Momentum equation of hydraulic theory of free flow becomes:

$$\frac{\partial V}{\partial t} + V\frac{\partial V}{\partial x} + g(\frac{\partial h}{\partial x} + S_f - S_0) + \frac{iV}{h} = 0 \tag{2.6}$$

Assumptions for the shallow water equations are [7, 41]:

- Pressure at any depth is hydrostatic

- Bed slope is constant and small; $sin\theta = tan\theta = -S_0$
- Depth across section (lengthwise) is constant
- Momentum transferred to flow from lateral inflow is negligible
- Viscous and turbulent stresses are parameterized and combined into a friction slope S_f
- Uniform flow friction equations applies to non-uniform and gradually varied flow
- Velocity is constant; velocity not very dependent on water depth

Kinematic Wave Assumption To further simplify the problem, one utilizes the kinematic wave assumption. This assumption neglects the momentum change and the acceleration terms and assumes that the frictional slope is identical to the bed slope [41]. It implies that water flows downhill are prevented from accelerating or decelerating very much because of frictional resistance of bed is overwhelming all other factors S_f=S_0 (resistance to flow acts the same way in unsteady and steady flow) [7]. The kinematic wave assumption thus describes small perturbations as waves, as water depth varies if the flow is a small departure from an initially uniform state[7]. The waves described, are long and flat with respect to distance but change in velocity with respect to time is negligible and they only propagate downstream. Thus the relevant equations 2.5 and 2.6 are used to create a simplified equation for normal velocity in laminar flow over a smooth slope with rainfall (hydrology, Brutsaert 1972):

$$V = \frac{gS_f h^2}{\nu(3 + cS_f^d P^e)} \tag{2.7}$$

For Re<800 and So $\leq$ 0.03

where:

- **V** Velocity of flow []
- **P** Rainfall intensity [cm/hr] as in this case there is no infiltration so lateral inflow i=P
- **Constants c=2.32, d=0, e=0.4** as proposed by Shen and Li (1973) from experimental data
- $\mathbf{S_f = S_0}$ Bed Slope
- **g** gravity
- ν kinematic viscosity taken at 10°C for these purposes
- **h** depth of flow

$$Re = \frac{VL}{\nu} \tag{2.8}$$

Flow velocity can be estimated to be maximum at downstream end $VL = PL$ [7]. Under steady state conditions or equilibrium conditions, when flow rate at any point, x ,along the catchment equals the total lateral inflow upstream from that point. Time to equilibrium in laminar conditions can be expressed as:

$$t_s = \frac{L}{(K_r i^2)^{1/3}} \tag{2.9}$$

where,

$$K_r = \frac{gS_0}{\nu(3 + cS_f^d P^e)} \tag{2.10}$$

2.6.4 Manning Equation

The flow on the roof can also be described as an open channel flow where the channel is wide and the flow is uniform and two-dimensional. The discharge from the channel can thus be described through the Manning equation [6]:

$$\frac{Q}{A} = V = \frac{1}{n} S_f R_h^{2/3} \tag{2.11}$$

where

- **n**: Manning's coefficient, a resistance coefficient that describes the boundary roughness of the channel based on the material it is made of [6].
- $\mathbf{R}_h$: Hydraulic radius, "wetted perimeter of the channel that is in contact with the flowing liquid" [6]. For wide, shallow channels or two-dimensional flows, the depth of flow (h) can set to be the hydraulic radius [7].
- **Q**: Volumetric flow
- $\mathbf{S}_o$: Slope of channel [dimensionless]
- **V**: Velocity of flow
- **A**: Cross-sectional area of flow

2.6.5 Hydraulic Design Capacity of Gutter

To ensure that the gutters can handle the inflow of rainwater from the roof without overtopping, it is necessary to determine the hydraulic capacity of the gutters. The theoretically-predicted capacity of the gutter predicted by the cross-sectional area neglects flow effects. The theoretical capacity thus is reduced by factors to give an appropriate safety margin [38].

The nominal capacity (Q_n) is the capacity expected under ideal flow conditions after real-flow effects taken into account [39] in [l/s]. The nominal capacity for an internal gutter of rectangular or similar shape (triangular shape included) with a nominal slope is given by:

$$Q_N = 3.89 \times 10^{-5} \cdot {A_W}^{1.25} \cdot F_d \cdot F_s \tag{2.12}$$

where:

- **Aw** cross-sectional area of flow in gutter under freeboard in mm^2 and can be calculated with the dimensions shown in figure5.11. Freeboard allows for fluctuations in water level due to wind. Freeboard is considered to the depth from the top of the gutter where overtopping would occur to the design depth and can be calculated according to table 2.2 [39].

- $\mathbf{F}_d$ depth factor allows for effect of relative depth. Determined by the ratio of W/T, where $W = Z - Y$ and T is the width of flow.
- $\mathbf{F}_s$ is the shape factor, which depends on the ratio S/T. where S is the width of the sole of the gutter in mm. The shape factor for a rectangle would be 1, while a triangular gutter (where $S/T = 0$) F_s= 0.893. [38]

Table 2.2: Minimum freeboard for internal gutters [39]

Gutter depth including freeboard, Z [mm]	Minimum Freeboard, Y [mm]
less than 85	25
85 to 250	0.3Z
greater than 250	75

Design capacity Q_L is the nominal capacity with an additional margin of safety factor (0.9) to account for effects such increased roughness and turbulence due to debris etc [39, 42]. The design capacity for a hydraulically short gutter, a gutter where the length of each gutter section is less than 50x the design depth (W), is given by:

$$Q_L = 0.9 \cdot Q_N \tag{2.13}$$

2.7 Previous Experiments

During this investigation, little to no literature was uncovered that had specifically to due with investigations into roof drainage systems on BIPV roofs. Through the literature search process defined in 3.1, experiments or simulations relating to runoff on green roofs, roof catchment systems, and water quality of roof runoff was most prevalent.

Some literature was found experiments investigating performances of roof gutter systems, but usually focused on the capabilities of the gutter channels themselves. [37, 44]. The literature found that was probably most relevant to this thesis was[45], which used a small-scale evaluation of gutter efficiency based on the different types interception in a gutter scenario. Simulations and investigations into channel flow in roof gutter also were identified in this section, though the numerical modeling was usually based on flow in the roof gutter [46]

Very little literature regarding runoff and BIPVs except for water quality of runoff and rain-tightness of BIPVs [47–49]).

Rain and Wind Box

The large-scale testing apparatus used for the experiment is an apparatus for rain and wind testing, aptly named the RAWI-box, seen in Figure 2.8. Though the main functionality of RAWI-box is for water-tightness against driving rain, its functionality will be modified to suit the goal of this thesis. In order to understand the modifications to the set-up and procedure of the RAWI-box, the original capabilities and uses are mentioned in this section.

Figure 2.8: Rain and Wind (RAWI) Box at SINTEF Laboratory

The RAWI-box is located at the Building and Infrastructure laboratory for SINTEF and NTNU. It is used to simulate driving-rain conditions on building components by pulsating air pressures and water spray by moving nozzles. This tests the water tightness and water leakage of building elements used in facades and roofs[50]. The tilting function of the box enables testing on slopes between 0 and 90 degrees to the horizontal. Usually water-tightness towards driven rain is tested according to Nordtest Method NT Build 421 where the test specimen is subjected to run-off water and driving rain simultaneously. Run-off water is supplied evenly from a row of spray nozzles mounted above the specimen. Approximately 1.7± 0.3 $l/mmin$ of water can be supplied via the run-off water component. The driving rain is applied by movable air and drop nozzles attached to a movable beam that moves vertically along the surface of the specimen. The air supplied from high pressure fans can reach speeds from 0-42 m/s. Approximately 0.3 ± 0.05 $l/m^2 \cdot min$ of water can be supplied via the driving-rain component of the RAWI-box [50]. The RAWI-box is intended to supply approximately 2 $l/m^2 \cdot min$.

The tiltable box consists of a large chamber with a viewing window which houses the machinery associated with supplying water and pulsating air pressure. This chamber also houses a drainage system, which does not interfere with the test sample. The RAWI-box is used for projects internally by SINTEF and NTNU or projects commissioned by external parties. The apparatus has also been used for student projects (i.e. Master and PhD students). Some tests done with roof integrated BIPVs. Although these investigations are mainly focused on the effects of wind-driven rain, some aspects can be applied to this investigation. Relevant past experiments were completed in [47] and [48]. These investigations focused on wind-driven rain exposure on BIPV panels, but the set-up was similar and gives an indication of the intended capabilities and use of the RAWI-box.

Chapter 3

Method

3.1 Literature Search

The purpose of the literature review is to get an overview of relevant literature and experiments addressing concepts related to rainwater runoff and rain gutters on BIPV roofs. The information gleaned from the search was vital in understanding and creating the theoretical framework necessary to develop an experimental method, and for the discussion and interpretation of the results.

3.1.1 Procedure

The methodology of the literature search in this thesis was based on the search strategy in [51] for writing systematic literature review and the exploration phase of the seven step model of comprehensive literature review as described by [52]. Figure 3.1 shows the overall process for the literature review search. Figure 3.1 shows the overall process for the literature search. The method is based on identifying relevant keywords, which are then combined into a logical search string. The search string is developed based on synonyms and truncation of relevant key words that have syntax customized to the chosen databases. Firstly, professors in the field of hydrology and hydrodynamics at NTNU were contacted and presented with the thesis scope and problem statement. They provided insight into concepts and ideas worth investigating and general feedback on the problem statement.

3.1.2 Search Criteria

Keywords are central in the systematic search relating to rainwater runoff and rain gutters on BIPV roofs. Figure 3.2 shows the keywords used in this systematic search, where each section represents synonyms or related words. Searches were made using the keywords composed into phrases with Boolean operators , and with keywords and operators added in consecutive searches to focus the search. This iterative process avoided the screening of large volumes of literature for relevance. When the searches provided a manageable amount of results, usually less than 100, the results were screened for relevance.

The electronic databases that were used included: Scopus, ScienceDirect, Oria, and Google Scholar. The use of several databases were used to avoid bias in a particular database based on the databases'

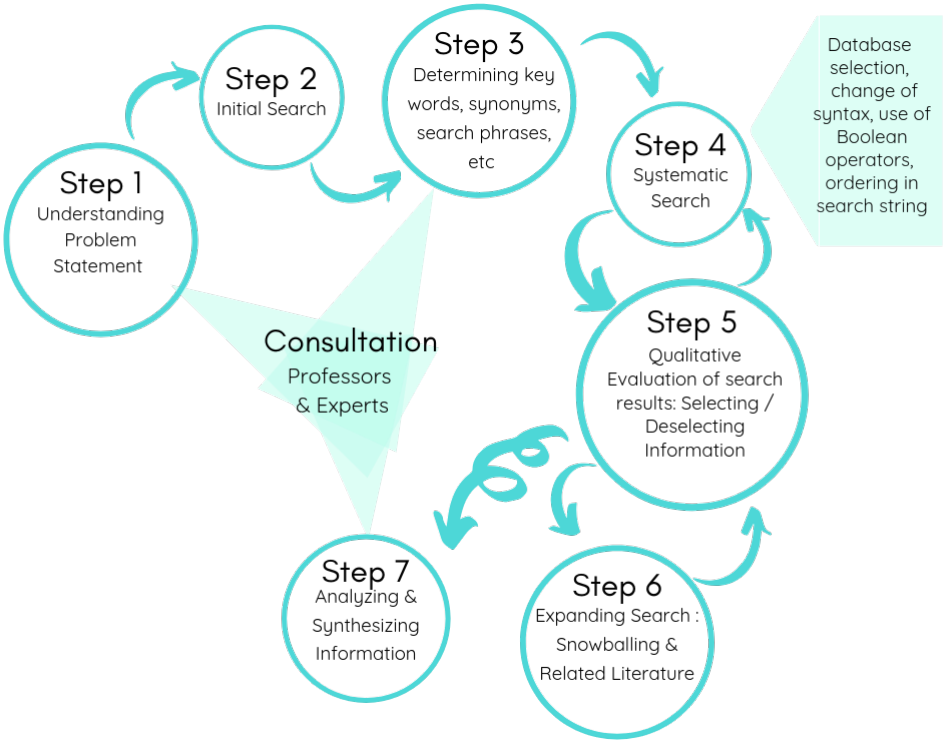

Figure 3.1: Modified Literature Search Process based on [51, 52]

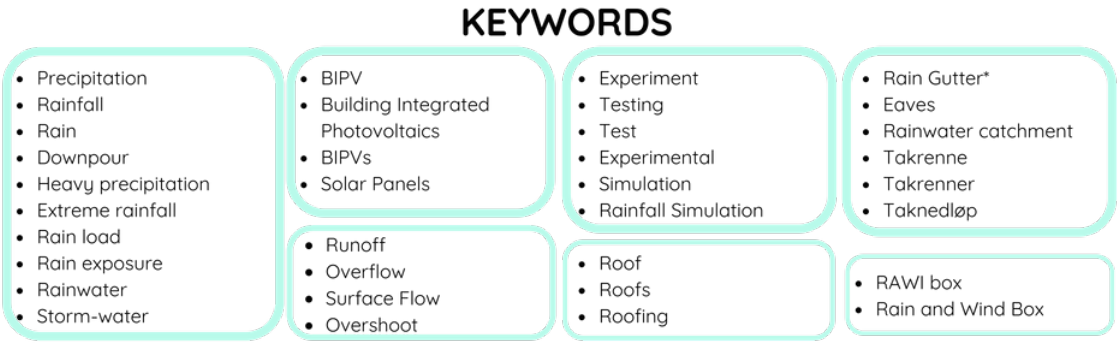

Figure 3.2: Keywords for systematic search

use of search algorithms or available literature.Most of the databases have search options with a search string for all fields. Searches done in Scopus are based on title, abstract, and keywords. Except for a language filter (Norwegian and English), no further limitations or restrictions were placed on the searches.

3.1.3 Selection processes

The screening of relevant literature were based on manual qualitative evaluations done in four steps.

1. Assessment of title, if relevant:
2. Assessment of keywords, if relevant:
3. Assessment of abstract, if relevant:

4. Literature was obtained and viewed. The literature was skimmed for relevance and reliability

The above steps of succession were followed only if the literature met the conditions of the preceding steps.

It was difficult to formulate an adequate search string, meaning a string broad enough to include relevant papers without a large number of irrelevant papers. Snowballing was therefore also used to identify literature that could have been missed due to specific terminology. Snowballing means using the reference list of relevant literature to identify additional papers or literature of interest for further study [53]. Relevant papers found through the four-step systematic search process mentioned above were used as the starting point. Mendeley, the reference handling program, was used, and suggestions based on the complied literature library were further reviewed and evaluated.

Though this method was used to obtain relevant literature for this thesis, the systematic documentation of searches was limited to experiments or concepts directly related to rainwater runoff and rain gutters on BIPV roofs. Relevant standards, SINTEFs building design, and relevant climate data were found through direct searches within these institutions.

3.2 Experimental Design Calculation

The basis of this experiment is to discover how the roof drainage/ rain gutter intercepts rainwater runoff from the roof. Therefore, it is important to identify the quantity of runoff which the drainage system needs to manage and how the runoff behaves when streaming down the roof. Since a full-scale experiment was not possible due to sizing, a challenge lay in recreating the same runoff flow that the real roof would experience.

A scaled model was considered, though ultimately abandoned as the flow would be quite unpredictable and difficult to control, as well as provide an element of uncertainty in whether the unknown roof-runoff and water interactions could be scaled appropriately or cause too much disturbance. This meant that the total amount of runoff from the entire roof catchment had to be determined so that the flow could be applied on the sample roof under test conditions. As the sample roof length is less than 15% of the original roof, the effect of water flowing the “extra 2.67m” of the sample roof is expected to be minimal. Calculations are therefore made with the entire length of the roof to calculate expected flow.

The ZEB Laboratory roof is a polygonal as depicted by Figure 3.3, however the extra section highlighted in red in Figure 3.3 is ignored for the purposes of this investigation. This can be justified by the plans for a gutter that goes along parallel to the edge of this section which will drain runoff from this part of the roof individually. The assumption is that this runoff will gain less speed than the rest of the roof as the drainage length from the roof ridge to the gutter are less than the full length of the rest of the roof. The model was constrained to the size of the testing apparatus, the RAWI-box. As the original roof is polygonal and the model was constrained in the shape of a square, the far left section of the roof, which is angled, was not incorporated in the runoff calculations and the model experiment.

As the roof gutter should be sized and designed based on the maximum runoff flow, finding peak flow was necessary. Two methods were used for comparison to quantify peak runoff flow; the

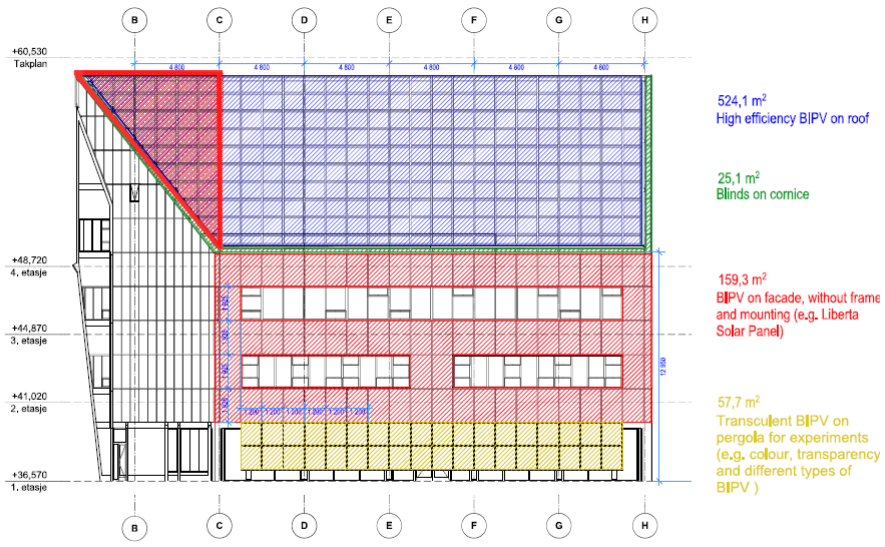

Figure 3.3: ZEB Laboratory Roof, shaded section not included in calculations [17]

rational method and a modified method that utilized both the shallow water equations and the Manning equation.

The IDF data used for these calculations will be the curve presented in 2.3.3 Figure 2.4. The IDF data used for future rain load, is presented in Figure B.2, Figure 2.4 which is multiplied by climate factors 1.4 and 1.5 as described in Section 2.4.2. This give the IDF Curve in Figure 3.4.

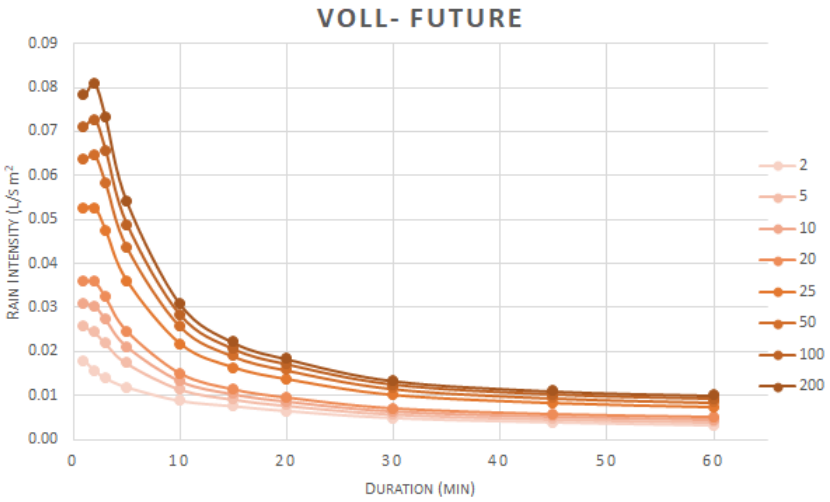

Figure 3.4: Future IDF Curve for Voll, used in calculations in 3.2.1

3.2.1 Rational Method

The Rational method is based on the rational equation 2.2 presented in section 2.6. For this experiment, the values of the variables are:

- C: taken as 1. This is an impermeable roof surface [38, 39, 42]. Even though values for runoff

coefficient for traditional roofs typically vary between 0.75-0.95 [7], design values have to be conservative in the cases where infiltration and storage is minimal and have negligible effect on flow.

- i: will be the rainfall intensity of short-duration (1-60 minutes) rainfall measured at the weather station at Voll in Trondheim, Norway. In order to compare flow rates for different durations and return periods, values from the entire IDF curve will be used for all calculations. Figure A.5 in the appendix B.1 is used. For future rain intensities, the climate factors of 1.4 for return periods of less than 50 years and 1.5 for return periods equal to and greater than 50 years are applied as indicated in section 2.4.2. The resulting IDF values are presented in Figure A.6 in appendix B.1.
- A: effective catchment area of the roof will be 462.3 m2, as it is assumed that wind effects are neglected. As mentioned before, this number ignores the extra "triangular section" of the roof. The length of the roof (L), from ridge to edge, is 19.22m and the width of the roof that will be drained is 24.05m. For clarification, the length of the roof is perpendicular to the gutter and the drainage length parallel to the gutter. The relevant dimensions of the sample roof are 2.67 m by 2.67m but will be discussed further in Section 3.3.1.

In order to find the total flow needed on the sample roof to simulate peak flow, the peak flow on the real roof had to be calculated. The flow per meter width (or drainage length) on the roof: $q = L \cdot C \cdot i$. q is the volumetric flow per meter drainage length. This was multiplied by the sample roof width 2.67m to obtain the total flow necessary for the entire sample per minute. The calculation was repeated for the IDF values for future rain intensity at Voll as well.

The calculations for flow rate based on future rain intensity are presented in table 3.1 and calculations on the flow rate based on present rain intensity are presented in the appendices.

Table 3.1: Total future runoff flow quantities from sample roof [l/min] for specified durations and return periods

Return Period (yr)	1 min	2 min	3 min	5 min	10 min	15 min	20 min	30 min	45 min	60 min
2	76.61	66.83	59.50	50.57	37.34	32.16	27.46	20.61	16.30	13.37
5	110.63	104.85	94.07	74.59	49.02	39.32	33.20	24.62	19.75	16.86
10	133.13	130.03	116.97	90.45	56.74	44.06	36.99	27.29	22.03	19.19
20	154.78	154.17	138.91	105.71	64.20	48.59	40.61	29.88	24.23	21.38
25	161.63	161.85	145.90	110.54	66.52	50.01	41.78	30.70	24.96	22.12
50	195.77	198.68	179.32	134.38	79.08	58.34	48.60	35.57	29.01	26.01
100	218.22	223.76	202.14	150.22	86.80	63.05	52.38	38.20	31.32	28.32
200	240.67	248.80	224.91	166.02	94.47	67.77	56.17	40.88	33.58	30.63

3.2.2 Hybrid Method: Shallow Water equations and Manning equation

As mentioned previously in section 2.6.2, the Rational method does not explicitly account for slope, surface roughness or surface permeability of the roof. The rational method also does not account for non-uniform flow, time variation of flow or water depth build-up at the downstream end of the roof. However, the rational method does provide a good basis for the design of the gutter and the experiment. The calculations based on this hybrid method are done to see if they are comparable to the Rational Method and could be used as an improvement. Further investigation into the velocity

and depth of flow at the edge of the catchment would be interesting, as these could be relevant parameters in understanding water behavior at the transition between roof and gutter.

In the shallow water equations, the Reynold's number for flow is first calculated to check the applicability for laminar flow. The approximation $VL = PL$ is used, where P is the future and present rainfall intensities in the IDF curves used during the rational method and L is the length of the roof. These results can be seen in appendix B.3.

As velocity and water depth at the downstream end of the catchment cannot be found using the rational method, the shallow water approximation for laminar flow over a smooth slope with rainfall 2.7 is rearranged to give the depth of flow at the downstream end of the catchment.

$$h = \left[\frac{\nu(3 + cS_0{}^d P^e)}{gS_0} \cdot PL\right]^{1/3} \tag{3.1}$$

Note! P, rainfall intensity, inside the parenthesis, must be expressed in cm/hr, while the units of the other P is consistent with the other variables. Values of the variables in ZEB Laboratory case are:

- ν : kinematic viscosity of water at 10 ° C is $1.3070x10^{-}6m^2/s$ (introduction)
- Constants: c=2.32, d=0, e=0.4
- S_0= slope of roof 30°is 0.58
- g: is gravity 9.81 m^2/s
- L: roof length 19.22m
- P: will be rainfall intensity of short-duration (1-60 minutes) rainfall measured at the weather station at Voll in Trondheim, Norway. In order to compare flow rates for different durations and return periods, values from the entire IDF curve will be used for all calculations. Figure A.5 in the appendix B.1 is used. For future rain intensities, the climate factors of 1.4 for return periods of less than 50 years and 1.5 for return periods equal to and greater than 50 years are applied as indicated in section 2.4.2. The resulting IDF values are presented in Figure A.6 in appendix B.1.

The results for present and future are shown in figure B.13 and B.14 in appendix B.3. The resultant depth of the flow is then used in the Manning equation for open channel flow to find the velocity of flow at the downstream end of the roof. After substituting in $h = Rh$ as suggested in section 2.6, the Manning equation 2.6.4 becomes:

$$V = \frac{1}{n} S_f h^{2/3} \tag{3.2}$$

where the variables ZEB Laboratory case are:

- $S_f = S_o$ after the kinematic wave assumption. Slope of 30 °is 0.58
- n: manning's coefficient for glass 0.011 [6, 54]

The results are presented in the appendix B.3.

The resultant runoff flow per meter width drainage length is then calculated:

$$q = h \cdot V \tag{3.3}$$

which gives the results for future rain intensity in Table 3.2.

Table 3.2: Total future runoff flow quantities from sample roof [l/min] for specified durations and return periods

Return Period (yr)	1 min	2 min	3 min	5 min	10 min	15 min	20 min	30 min	45 min	60 min
2	84.90	77.24	71.30	63.78	51.87	46.90	42.17	34.81	29.80	26.16
5	109.68	105.64	97.93	83.34	62.43	53.73	47.91	39.19	33.84	30.48
10	124.92	122.86	114.05	95.28	69.01	58.05	51.55	41.99	36.39	33.20
20	138.93	138.54	128.71	106.24	75.13	62.06	54.92	44.63	38.78	35.68
25	143.25	143.39	133.25	109.62	77.00	63.29	55.99	45.45	39.56	36.49
50	156.27	157.92	146.84	119.77	82.74	67.09	59.21	47.91	41.77	38.83
100	168.82	171.86	159.87	129.56	88.25	70.77	62.32	50.28	43.98	41.10
200	181.03	185.38	172.50	139.04	93.60	74.37	65.37	52.64	46.09	43.32

3.3 Experiment

The goal of the test is to apply expected short-term extreme rain events to test the behavior of rainwater run-off on roof comprised of building-integrated photovoltaics. The test also aims to study the catching effect of internal (integrated) roof gutter designs to minimize and prevent overshoot and maximize the amount of runoff caught in an internal roof drainage system. The experiment is based on testing the catchment capabilities of different widths of the internal gutters.

As the original roof covers approximately 550 m^2, a full-scale test would not be feasible. Therefore, a model was used to simulate the phenomena that occurs in the transition zone of the roof and the drainage gutter. The model was constrained to the size of the testing apparatus, the RAWI-box. As the original roof is polygonal and the model was constrained in the shape of a square, the far left section of the roof, which is angled, was not incorporated in the runoff calculations and the model experiment.

Calculations were made to predict the volumetric flow of rainwater runoff that would stream down the 20 meters of original roof under short duration extreme rain events during peak flow. This flow prediction was the basis for simulations and applied to the top of the sample roof to simulate the water flow that would be discharged from the roof above. Materials:

- GoPro 3+ with mount
- Hand-held video camera
- RAWI Box Set-up modified for this experiment
- RAWI Box Set-up modified for this experiment
- Sample roof
- Grate coverings 2x120, 240 mm
- 2x 700 L bins

- Water pump
- Stopwatch

3.3.1 Sample Roof Set-Up

A sample roof area with a 2.75 by 2.75m timber frame and waterproof plywood covering was built for the experiment. The timber frame was built to fit the square template used during testing in the RAWI-box. The frame was clamped down on the sample roof so that the roof dimensions inside the frame were 2.68m by 2.68m. The sample roof was built with (dimension) rafters placed at a standard spacing distance of 60cm and a 2.57m by 0.48m integrated fixed rain gutter. The sample roof set-up with dimensions can be seen in Figure 3.5, 3.6 and 3.7. To standardize the

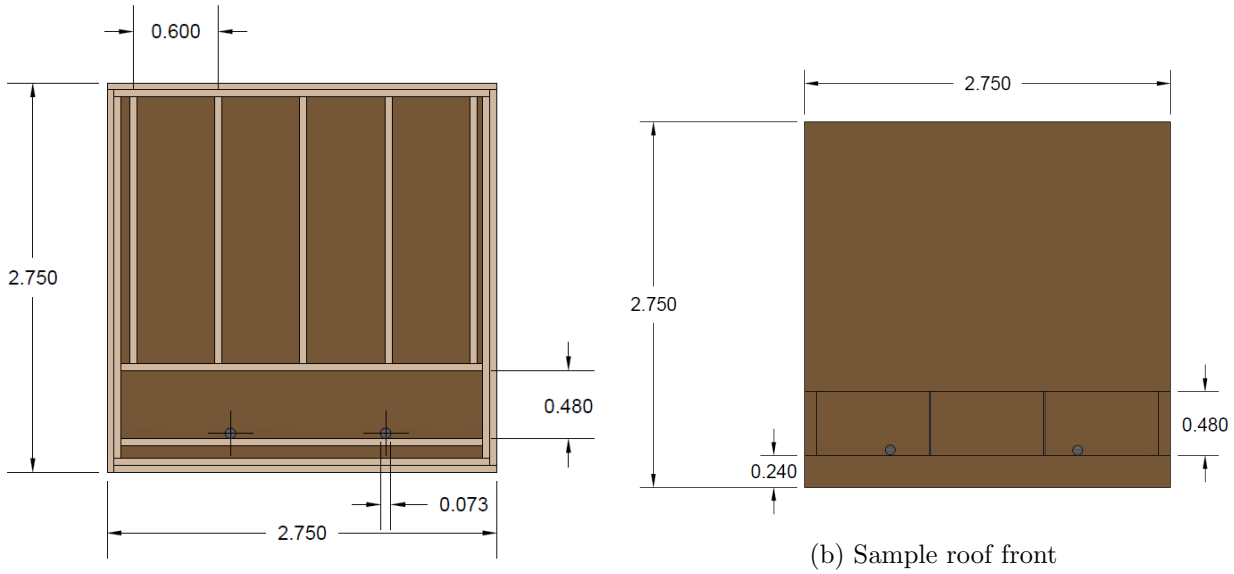

(a) Sample roof back

(b) Sample roof front

Figure 3.5: Sample roof with dimensions

experimental method, the same surface area of roof had to be used as a catchment area for all the different widths of roof gutters. In order to achieve this, the sample roof was built with a rain gutter the size of the largest testing width, 480 mm, and additional sections of plywood were attached to the opening below the gutter to create the smaller gutter widths. Internal gutters dimensions can be seen in Figures 3.5 and 3.6 . To see if there was a "back-splash effect" at the bottom panel of the roof gutter, a 98x48mm stud was mounted flush to the inside of the additional sections of plywood. This simulated the bottom panel for gutters with smaller widths. Grating covers were cut to the same dimensions as the extra sections of the plywood covering, so that they would fit the different dimensions of the rain gutter. Two rods were positioned 84.5mm from each side to prevent the grates from sagging when placed over the gutter opening. Two drainage outlets, both 73mm in diameter, were drilled in the bottom corner of the gutter. Since only the rainwater runoff capabilities of BIPVs were tested, plywood covering was used in place of BIPV panels. Coupled with the fact that the specific BIPVs that will be used for the roof of the ZEB Laboratory are yet to be determined, using actual BIPVs would be too costly. Ideally, glass should have been used to accurately simulate BIPV cells, however, due to difficulties acquiring and correctly mounting glass panes of this size, waterproof film-coated plywood was used instead. This material can be

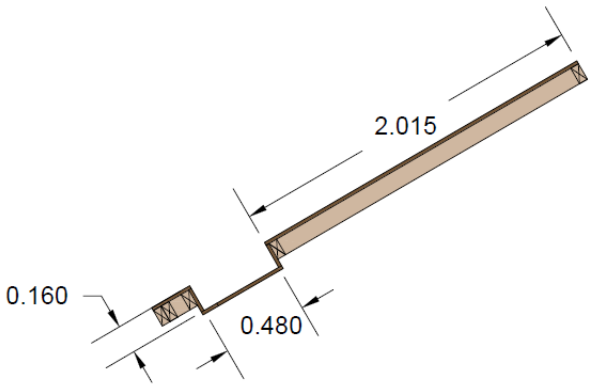

Figure 3.6: Sample roof cross-section

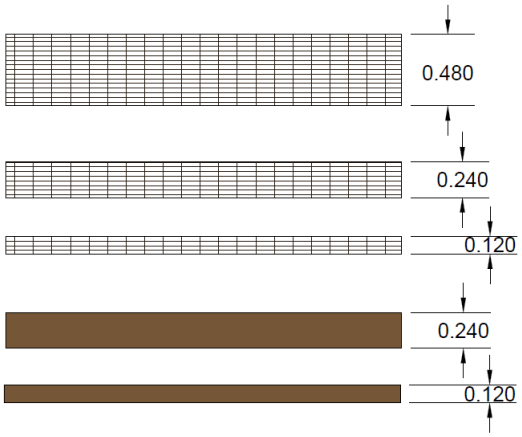

Figure 3.7: Extra sections of material for creating different gutter dimensions

considered to be quite smooth and comparable to glass surfaces. The plywood also allows for easy assembly and mounting of the different configurations/ dimensions of gutters tested. The installation of BIPVs are dependent on the type of BIPV modules and systems used, therefore any protrusions, joints, or openings could affect the runoff geometry of the rainwater. All screw holes, edges, and splices were duct-taped to prevent leakage and ensure an overall smooth surface with no perforations. The plywood surface is devoid of any protrusion, joints, or openings, and therefore acts as a kind of "worst-case" scenario of sheet-flow runoff as there are no obstacles, joints,etc., that slow the flow of runoff.

3.3.2 Modified RAWI Set-up

In order to test the rain gutters for future rainfall intensities, large amounts of water are needed. From section 2.7, it is determined that the RAWI-box's intended procedure can only supply 1.7 l/min x 2.75 m, as driving rain will not be used during this investigation. The RAWI-box's runoff water is supplied from the horizontal row of nozzles located above the sample roof. To increase the total flow rate of water, an additional runoff beam was added at the uppermost location above the sample roof. This increased the total runoff supply to a total of 18l/min for the entire test area. This was still considerably less than what was needed to achieve peak future runoff flow at the steady state, as suggested in Section 2.7.

To achieve water flow quantities more representative of future rainfall intensity, the SINTEF laboratory's fire-hoses were used to attain maximum water flow. A set-up that would give the necessary volumetric water flow rate while simulating rainwater runoff onto the sample roof was identified through trial and error.Two fire-hoses were fed in through a door in the back of the RAWI-box, opposite of the sample roof, and directed towards the top of the test frame via two modified timber boards. The tops of the boards were attached to the nozzle beam at the top of the sample roof with cable ties but were later replaced with polypropylene binder twine due to breakage in the cable ties. This allowed for movement of the beam during tilting of the RAWI-box. The boards were reinforced with furring strips and the hoses were kept in position along the boards with cable ties.

The hose openings were pointed towards the top of the test specimen, but the impact force of the thick water jet created turbulence and radial hydraulic jump in the location where the jet impinges on the surface. This "wake" from the jets created a separation of the runoff water into streams, creating "empty" sections on the roof with no sheet runoff. The break-up of the jet was essential to get a somewhat realistic representation of runoff on the roof surface. In order to break up the jets into "spray", boards angled at 45 ° were attached horizontally between the ends of the two boards supporting the fire hoses. When the water jet hit these boards, the jet was broken into a spray stream that more or less was distributed across the top of the sample roof. Though not an ideal simulation, it was considered better than the original case of continuous solid jets impinging the surface with high impact jets. The set-up is illustrated in figure 3.8.

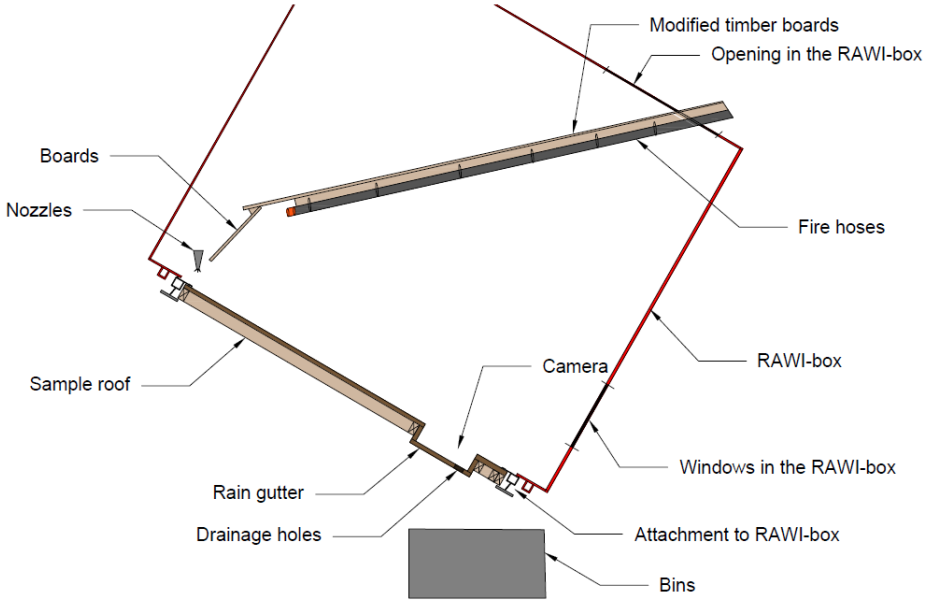

Figure 3.8: Modified RAWI-Box set-up, the box is rotated to 30 °

The set-up enabled testing of extreme water quantities well beyond the capabilities of the RAWI-box and pushed the mechanics of intended use to its limits. Though the experiment was originally intended to have trials with current rain levels and with different types of drainage grates, this modified set-up caused overload of the mechanics of the RAWI-box and the number of trials had to be limited. This will be further described in section 3.3.5.

3.3.3 Experimental Procedure

Initially, the idea was that rainfall runoff quantities calculated in section 3.2 should be used as the actual runoff flow for the experimental portion. However, obtaining quantities that were approximately adequate for testing future rainfall proved difficult. Therefore, the exact rainfall quantities calculated in section 3.2 were abandoned and a range of values that were physically available with the RAWI-box were opted for instead. There was also no automated method of precisely measuring inflow from the modified set-up.

The water flow provided by the runoff nozzle beams, a small portion of the total water flow, was the only directly measurable quantity by instruments already present in the RAWI- box. As there were no instruments available to measure the total influx of water from the fire-hoses, the combined water inflow from the runoff nozzles and the fire-hoses was determined with the method described below.. The method was used for all trials to determine consistency in water flow during peak flow.

Measurement of actual volumetric flow rate:

1. Tilting the box 30 ° on the horizontal axis.
2. Activation of runoff nozzles, providing 18 l/min on the entirety of the sample roof.
3. Simultaneous activation of the two fire-hoses.
4. After the increase of flow through the drainage holes became consistent (after approximately 5-10 seconds), two large 500L basins were placed on pallet jacks and rolled in place directly underneath the drainage holes to collect water.
5. As the bins were rolled underneath the drainage holes, a timer was started.
6. The runoff water was allowed to drain for exactly one minute before the bins were pulled away from the drainage holes.
7. The water was then pumped out into 10L buckets to determine the volume of water in each of the large 500L basins.

The approach was not very precise, but the water amount could be determined to the nearest liter. This measurement approach determines the amount of water that drains into the rain gutter, which means that overshoot, back-splash and water flowing outside of the sample roof would not be included in the measurement (time of concentration was not considered and water build up neglected). The maximum volumetric flow rate achieved was approximately around 200-180 L/min when the fire-hose openings were set to maximum. To achieve less water pressure for the present precipitation levels, the fire-hose head would have to be tightened to partially close the opening. Furthermore, the volumetric flow rate from the fire-hoses depended on the water usage in the rest of the building. This was hard to control and made water pressure inconsistent, which also made it difficult to compare results from the water flow measurements

3.3.4 Recordings of Results

As there was no accurate way of measuring the total inflow and outflow, the amount of overflow could not be precisely determined. Therefore, there was no quantitative way of determining or comparing the efficiency of each dimension of the rain gutters or the effect of a grate. In order to

determine the results and evaluate the efficiency and performance of the different configurations, a GoPro Hero 3+ was used to record video footage of the runoff occurring within the RAWI-box during the experimental runs. The GoPro was positioned next to the rain gutter on the inside wall of the RAWI-box on the left side of the sample roof. The left side of the box was the only side that was lighted, thus giving a clearer image while recording. The GoPro was angled specifically to give optimal view of the gutter and the roof, without being in the direct flow of the runoff. As noted previously, the GoPro gives a hemispherical visual distortion effect on its images. Multiple cameras would have been optimal in order to provide multiple views and angles without being subject to disturbances that might give false observations.

The GoPro was remotely activated via the GoPro app from an IPhone, which also allowed for simultaneous viewing during the experiment. An observer with a handheld video camera was standing by the viewing windows on the backside of the RAWI-box to film from another angle. The video quality and image proved to be quite poor, and was not included in the result section of this report.

3.3.5 Experimental Trials

Table 3.3 lists the different set-ups of variables tested during this investigation. As running the experiment was quite expensive, the number of trials had to be limited.

Table 3.3: Different variables tested in individual trials in experiment

Width of gap [mm]	Grate/ Grill Cover	Rain Intensity for entirety of sample roof [l/min]	Runtime [min]
480	NO		1.0
480	YES		1.0
240	NO	Future Rain Intensity	1.0
240	YES	MAX water flow (ca.200-180 l/min)	1.0
120	NO		1.0
120	YES		1.0
480	NO		1.0
480	YES		1.0
240	NO	Present-day Rain Intensity	1.0
240	YES	Decreased Flow (ca 100 l/min)	1.0
120	NO		1.0
120	YES		1.0

The first set of experiments focused on the expected future rain intensity, so the fire-hose outlet was set to maximum opening. The next set of planned experiments were set with present-day intensity, so the fire-hose openings were to be reduced.

In addition to these experiments, one set-up was chosen and run multiple times in succession. This was done to determine the replicability of the flow rate and the results. Though multiple runs for every set-up would have been optimal, time and cost constraints limited this to one set-up. To further strengthen the robustness and consistency of the results, an extended run time of 2

minutes was suggested to see whether there was any change in runoff behavior at the "transition zone", where the roof and gutter met. This was done to strengthen the argument that despite the limited run-time of 1 minute, the same behavior and results were seen regardless of the length of the experiment.

Another planned experiment consisted of testing a grate which had openings perpendicular to the openings of the original grates. Though these experiments were not performed due to the overexertion of the machine, the intention was to see if the different orientation of openings had different effects on the speed of the runoff flow.

As mentioned previously, the modified set-up of the RAWI-box required to create the desirable test conditions were well beyond the limits of this apparatus. There was a lot of movement and adjustment required for each variation in the set-up, which resulted in quite a few issues in the set-up that continually had to be fixed. This resulted in downtime and delays which further constrained the number of configurations tested. After testing the configuration of 120mm opening for future precipitation levels, the RAWI-box experienced an error message that allowed no further testing. Upon inspection from a technician, the set-up had caused a misalignment within the mechanics of the RAWI-box due to the increased load on the movable nozzle bar inside the RAWI-box. This misalignment was cause a fail-safe error that prevented further use of the RAWI-box, and further experiments were not completed., a. Therefore, the second set of experiments that were planned with the present-day rain intensity of approximately 100 l/min were not performed. The extended run-time experiment was also not performed.

Chapter 4

Results

4.1 Results from measurement of flow

The measurement of the amount of runoff tested in each of the experimental trials is presented in Table 4.1. The water pressure of the hoses were dependent on the total water pressure in the SINTEF building, and not just the laboratories. This means that the water pressure could vary instantaneously, it is assumed that the water pressure for each of the test days were somewhat similar. This is reflected in the results in Table 4.1.

Table 4.1: Measurement of total runoff from sample roof during experiment

#	Set-Up			Rain Intensity [l/min]			Run time [min]
	Date	Size of opening [mm]	Grating	Left	Right	Total	
1	6/5/2019	480	NO	68.0	60.0	128.0	1.0
2	6/5/2019	480	NO	75.0	56.0	131.0	1.0
3	6/5/2019	480	YES	97.0	106.5	203.5	1.0
4	7/5/2019	240	YES	85.0	99.0	184.0	1.0
5	7/5/2019	240	YES	81.7	100.5	182.2	1.0
6	7/5/2019	240	YES	80.0	105.0	185.0	1.0
7	7/5/2019	240	NO	76.0	103.5	179.5	1.0
8	7/5/2019	240	NO	76.0	103.0	179.0	1.0
9	27/5/2019	120	NO	90.0	91.0	181.0	1.0
10	27/5/2019	120	YES	90.5	100.0	190.5	1.0

4.2 Video and Photo Results

Since accurate quantitative data for comparing the efficiency and performance of each gutter opening size was not measurable as described in Section 3.3, qualitative assessment of video footage was used to determine results. Video footage was recorded with the highest quality achievable on

the GoPro Hero 3+ at 30 frames/ second. Photos of individual frames from these video clips are presented throughout this chapter to explain the phenomena that occurred during the experimental trials. Though the pictures are explained in this chapter, a more holistic impression of the trials may be attained through viewing the trial videos. The videos can be viewed on the YouTube channel "https://www.youtube.com/channel/UC0u565OUCAWqgAoxXOfKsIg". The videos are named using the size of the gutter opening and presence of grating cover on the opening (i.e. "480 mm opening with grating cover" would refer to 480mm gutter opening with grating cover.)

As there is not an exact way of determining the success of the gutter openings, the videos are assessed and interpreted with particular focus on the following criteria and phenomena:

- Whether or not the water overshoots the gutter entirely
  - Observational estimation of the amount of overshoot
- "Backsplash" from the "bottom" of the gutter
- Observations at the "transition zone" between roof edge and gutter
- Effect of grating on runoff flow behavior

The observations are presented in an unbiased fashion but will be further discussed in chapter 5. Comparisons of the sizes of the gutter opening and the openings with or without grating coverings will also be explained in further detail in chapter 5.

It is important to note that the videos were filmed with a strong wide hemispherical distortion effect (fish-eye). This enables a wide field of view, which captures as much of the sample roof as possible. However, this can also cause a circular distortion at the edges of the image. An attempt was made to remove and correct for this effect, but this was unfortunately not possible. Therefore, the images in this thesis may appear distorted, and straight lines and objects may appear curved.

4.2.1 480 mm Gutter Opening

As these are the first images and video discussed, general observations regarding the behavior of the runoff flow seen in the majority of the trials is explained in detail.

As mentioned in Section 3.3.3, the experimental trials start with 18l/min runoff. This is shown in figure 4.1.

Multiple separated streams are seen"projecting" off the edge of the roof into the gutter in a curved trajectory reminiscent of a parabolic curve. The stream rarely lands further than one-third of the way into the gutter and breaks into droplets at the end of its "projection".

Then, the fire hoses are turned on and allowed to achieve "peak flow", illustrated in figure 4.2.

Figure 4.2shows that the flow splits into three streams, one on each end and one in the middle of the sample roof. The stream at the far right appears to be slightly smaller compared to the than the others streams, which can be confirmed from visual observations and footage from the hand-held video camera. The runoff appears to flow in a continuous film down the sample roof. This "sheet flow" appears to be moving with a wavelike frequency, indicating kinematic wave flow. The intensity of the trajectory of the water "projection" from the end of the roof into the gutter

Figure 4.1: Results from 480 mm opening with 18l/min runoff

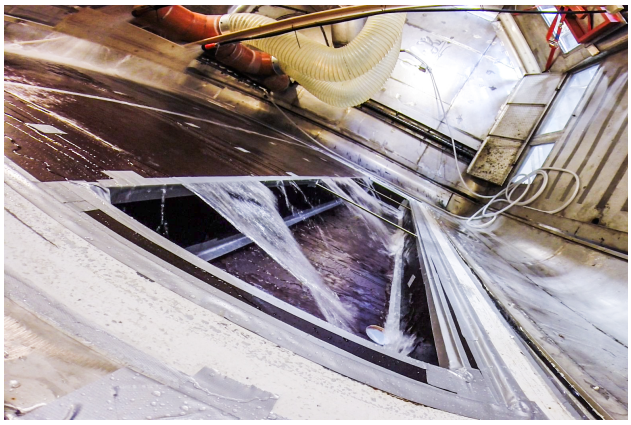

(a) Runoff at peak flow 480 mm opening

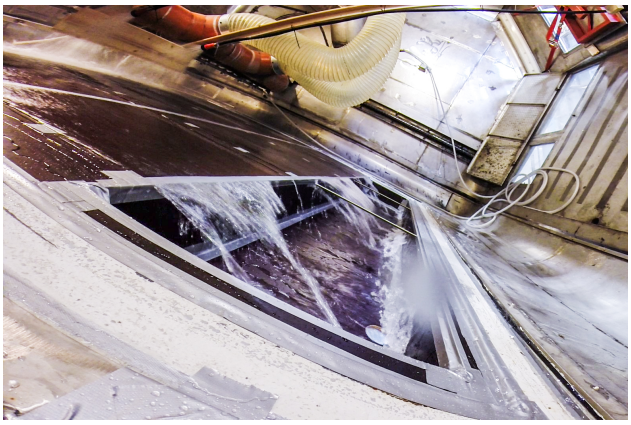

(b) Runoff at peak flow 480 mm opening

Figure 4.2: Peak runoff flow for 480 mm opening

appears to mimic this pattern of wavelike intensity as well. the "projection" of the water stream reaches the gutter sole approximately one-third to one-fourth the from bottom side of the gutter.

The water projection appears to flow off the roof edge in discrete turbulent sheet sections which taper and "break up" towards the end of the trajectory. The impact zone of this "free jet" creates a splash, which seems quite turbulent with some minimal back-splash. "Back-splash" is coined to describe when water splashes over the edge of the gutter in a reflected angle approximately perpendicular to the inflow's trajectory. A summary of the observations for this opening size and assessment of criteria outlined in section 4.2 is described in Table 4.2.

Table 4.2: Observations for 480 mm opening without grating cover

Criteria	**Observations**
Does Overshoot occur? Visual approximation	No overshoot occurs, the trajectory of inflow of water from the roof is inside gutter
Backsplash? Visual approximation	Backsplash does occur, though minimal amounts. Droplets of backsplash can be seen periodically

4.2.2 480 mm Gutter Opening with Grating Cover

Figure 4.3 shows the projection of runoff stream onto the grating with 18l/min. Due to grating covering the gutter, it is not possible to see exactly how far the streams project into the gutter.

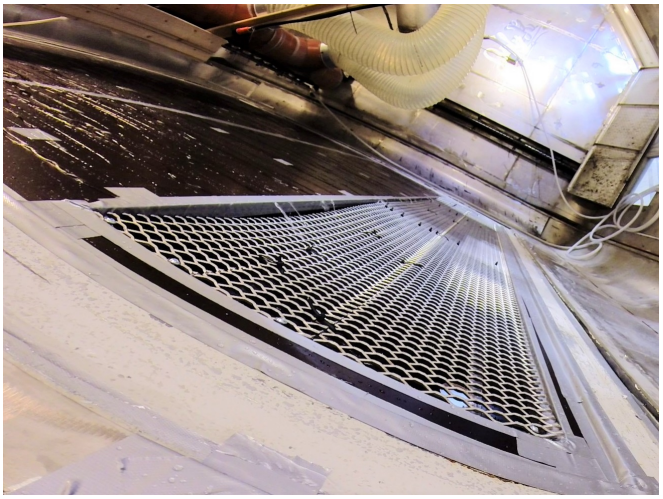

Figure 4.3: Results from 480 mm opening with grating cover with 18l/min runoff

The fire hoses are then turned on and allowed to achieve "peak flow", seen in figure 4.4.

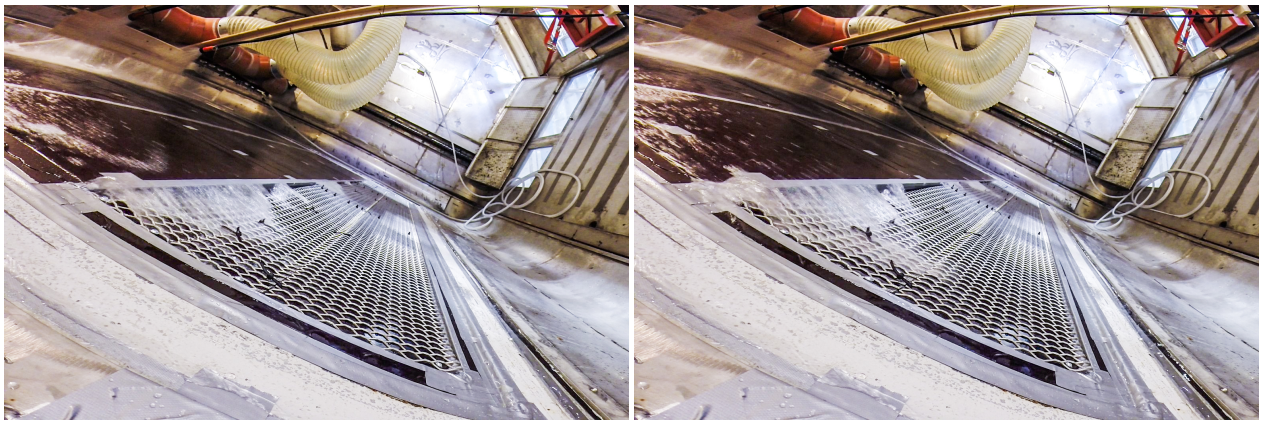

(a) Grating cover obscures projection (b) Runoff projection reaches 1/2 into gutter

Figure 4.4: Runoff at peak flow 480 mm opening with grating cover at different time instances

In the video for peak flow and its respective pictures, Figure 4.4, the runoff stream appears hindered and slowed by the grating. However, since the grating covers the interior of the gutter, a change in the parabolic trajectory of the runoff stream projection cannot be seen. Trickling of water from the exterior edge onto the RAWI box wall indicates back-splash. The video also shows indication that the back-splash occurs periodically rather than constantly. A summary of the observations for this opening size and assessment of criteria outlined in section 4.2 is described in Table 4.3.

4.2.3 240mm Gutter Opening

The runoff trajectory of 18 l/min for 240mm opening as seen in figure 4.5 is very similar to that in picture 4.1. The trickling stream "projections" reach approximately one-third into the gutter, but

Table 4.3: Observations for 480 mm opening with grating cover

Criteria	**Observations**
Does Overshoot occur? Visual approximation	No overshoot occurs, the trajectory of inflow of runoff water from the roof is inside gutter
Backsplash? Visual approximation	Backsplash does occur, though minimal amounts. Droplets of backsplash can be seen periodically
Effect of grating cover	Appears to slow down runoff flow or "catch" the runoff trajectory before the midpoint of the gutter opening

the streams appear to reach the gutter sole approximately at the midpoint. As Figure 4.5 appears to be very similar to Figures 4.3 and 4.1, this can be assumed is similar in all cases and no further figures of the water projection at 18 l/min will be presented in the Results section.

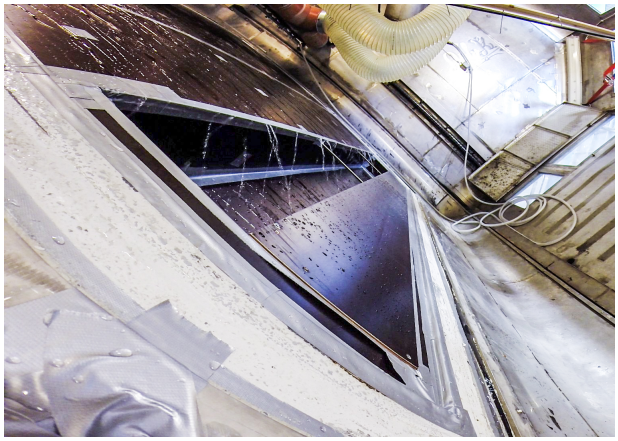

Figure 4.5: Results from 240 mm opening with grating cover with 18l/min runoff

(a) Example of back-splash (b) Water projection at approximate max

Figure 4.6: Runoff at peak flow 240 mm gutter opening at different time instances

When the fire-hoses were turned on, peak flow was achieved, as seen in figure 4.6. From figure 4.6, it appears that there is a lot of overshoot for this gutter opening size, especially considering the amount of water streaming down the corner closest to the camera. However, from examining the

videos, it appears that this water is flowing down the edge of the sample roof and funneled down the side of the gutter. The streaming water then experiences a hydraulic jump along the splice between the roof underneath the gutter, the edge and the RAWI-box frame. This is deduced by observing and comparing the streams on the far side of the RAWI-box, particularly the center stream. Even when neglecting for this distraction, one can see streaming water on the roof underneath the gutter. This water appears to come from the back-splash from when the stream "projection" hits the inside boards representing the bottom of the gutter design. A summary of the observations for this opening size and assessment of criteria outlined in section 4.2 is described in Table 4.4.

Table 4.4: Observations for 240 mm gutter opening

Criteria	**Observations**
Does Overshoot occur? Visual approximation	No overshoot occurs, the trajectory of inflow of water from the roof is inside gutter
Back-splash? Visual approximation	Back-splash occurs consistently throughout the run period. The back-splash creates steady, albeit small, streams of water flow down the roof underneath the gutter. These flows are concentrated around the 3 streams mentioned in section 4.2.

4.2.4 240 mm Gutter Opening with Grating Cover

This particular setup was tested three times in an attempt to measure the consistency and reliability of the water flow. Running the set-up three times would also give an indication of the consistency of the results. This particular point will be examined further in the chapter 5, but photos from the three trials will be presented here. It is important to note that the first run with this set-up experienced a rather large disturbance from a hydraulic jump due to loose taping on the transition zone above the gutter as seen in figure 4.7. The loose tape proved too distracting to garner

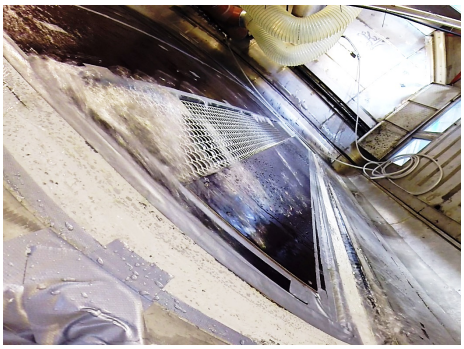

Figure 4.7: Results from 240 mm opening with grating cover, hydraulic jump from tape

significant results from the trial. The testing environment was remedied with additional tape, but the results from this set-up are taken from the other two videos. After identifying water flow down the edge of the roof and onto the roof section underneath the gutter as a disturbance, figure 4.8 indicate that there is no overshoot of runoff water. The grating appears to "slow" the flow of water and decrease the amount of back-splash streaming down the bottom section of the roof. However, in certain instances it appears that the water is lead down the metal mesh of the grating onto the bottom section of roof. This could be back-splash from the water stream striking the inside board cover, but it is difficult to determine due to the presence of the grating cover. A summary of the

(a) (b)

Figure 4.8: Runoff at peak flow 240 mm gutter opening with grating cover at different instances in time

observations for this opening size and assessment of criteria outlined in Section 4.2 is described in Table 4.5.

Table 4.5: Observations for 240 mm gutter opening with grating covers

Criteria	Observations
Does Overshoot occur? Visual approximation	No overshoot occurs, the trajectory of inflow of water from the roof is inside gutter
Backsplash? Visual approximation	Backsplash occurs consistently throughout the run period. The backsplash creates steady, albeit small, streams of water flow down onto the roof underneath the gutter. There is also some uncertainty if these streams are only backsplash or if the metal mesh of the grating cover channels water to the lower section of roof. These flows are concentrated around the three streams mentioned in section 4.2.
Effect of grating cover	Appears to slow down runoff flow or "catch" the runoff trajectory before 2/3rds into the opening of the gutter. Uncertainty if the grate channels water across gutter.

4.2.5 120mm Gutter Opening

The results from peak runoff flow for a 120mm gutter opening can be seen in figure 4.9.

From Figure 4.9 and the associated video, it is apparent that a large volume of water streams down onto the roof section below the gutter. This occurs underneath each of the three identified stream areas. There is quite a lot of splash from the impact when the stream projection hits the board representing the bottom/side board of the gutter. The impact is strong enough to spray droplets onto the camera and make spray visible from the third distinct flow furthest from the camera. This splash shoots quite a bit of water onto the bottom section of roof. The flow on this section of

(a) Runoff projection (b) Example of back-splash

Figure 4.9: Runoff at peak flow 120 mm gutter opening

the roof also appears to be in continuous film, which may look different than if it was just water spray. Though it is hard to discern the exact cause for this film, the runoff water which overshoots the gutter completely may cause this. A summary of the observations for this opening size and assessment of criteria outlined in Section 4.2 is described in Table 4.6.

Table 4.6: Observations for 120 mm gutter opening

Criteria	**Observations**
Does Overshoot occur? Visual approximation	Overshoot occurs. The trajectory of inflow of water is right on the edge of the gutter. Quite a bit of water flows down the bottom section of roof beneath the gutter.
Back-splash? Visual approximation	Back-splash occurs consistently throughout the run period. Spray is quite violent, with large droplets.

4.2.6 120 mm Gutter Opening with Grating Cover

For this particular set-up seen in Figure 4.10, the grate covering appears to bulge up past the plane of the roof due to the effect of the camera angle and undulation up from the bottom section of the roof. In actuality, the grating cover was exactly flush with the roof above it.

In figure 4.10 it is apparent that water flows down the bottom section of the roof below the gutter opening, in the three previously identified stream areas. The streams on the lowest section of roof appear to be narrow, when compared to figures 4.10. It appears as if the metal grate channels the water onto the roof below it. The stream closest to the camera appears to have minimal back-splash from water hitting the gutter opening edge. There appears to be more back-splash at the streams further away from the camera. This is also true for the spray created from the water stream hitting the joint on the bottom section of roof beneath the gutter. A summary of the observations for this opening size and assessment of criteria outlined in Section 4.2 is described in Table 4.7.

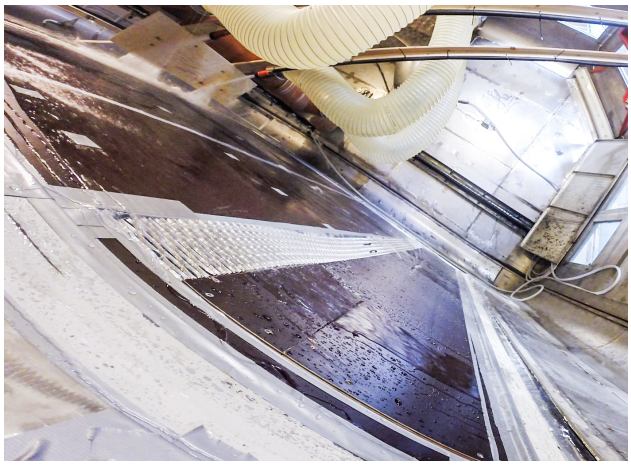

(a) Overshoot

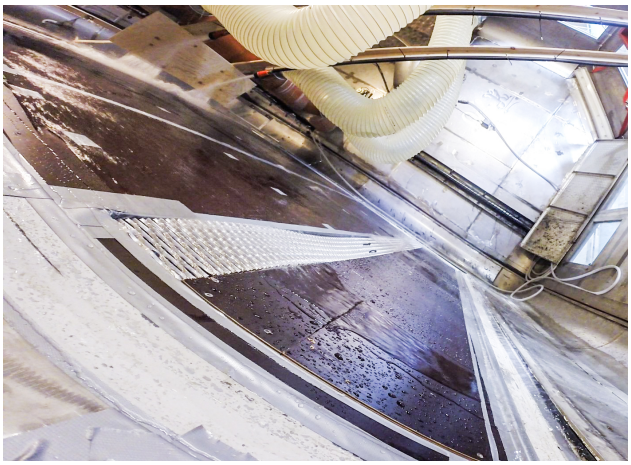

(b) Some back-splash

Figure 4.10: Runoff at peak flow 120 mm gutter opening

Table 4.7: Observations for 120 mm gutter opening with grating cover

Criteria	**Observations**
Does Overshoot occur? Visual approximation	Overshoot occurs. The metal mesh of the grating cover appears to channel water to the lower section of roof. These flows are concentrated around the three streams mentioned in section 4.2.
Back-splash? Visual approximation	Back-splash occurs consistently throughout the run period. Seems like there is less back-splash or less violent than 4.9 . Spray from joint on bottom section of roof.
Effect of grating cover	Might slow down runoff. Appears to channel water across the gutter opening. May also lessen the intensity of backs-plash created water hitting bottom edge/side of gutter.

4.2.7 Summary of Observations

Table 4.8 gives a holistic overview of all the observations done throughout the experiment with respect to the criteria mentioned in outlined in Section 4.2.

Table 4.8: Summary of Observations

	Criteria	**Observations**
480 gutter Gutter Opening	Does Overshoot occur? Visual approximation	No overshoot occurs, the trajectory of inflow of water from the roof is inside gutter
	Back-splash? Visual approximation	Back-splash does occur, though minimal amounts. Droplets of back-splash can be seen periodically
480mm Gutter Opening with grating cover	Does Overshoot occur? Visual approximation	No overshoot occurs, the trajectory of inflow of water from the roof is inside gutter
	Back-splash? Visual approximation	Back-splash does occur, though minimal amounts. Droplets of back-splash can be seen periodically
	Effect of grating cover	Appears to slow down runoff flow or "catch" the runoff trajectory before the midpoint of the gutter opening.
240 mm Gutter opening	Does Overshoot occur? Visual approximation	No overshoot occurs, the trajectory of inflow of water from the roof is inside gutter
	Back-splash? Visual approximation	Back-splash occurs consistently throughout the run period. The back-splash creates steady, albeit small, streams of water flow down the roof underneath the gutter. These flows are concentrated around the 3 streams mentioned in section 4.2.
240 mm Gutter Opening with Grating cover	Does Overshoot occur? Visual approximation	No overshoot occurs, the trajectory of inflow of water from the roof is inside gutter
	Back-splash? Visual approximation	Back-splash occurs consistently throughout the run period. The back-splash creates steady, albeit small, streams of water flow down the roof underneath the gutter. There is also some uncertainty if these streams are only back-splash or if the metal mesh of the grating channels water to the lower section of roof. These flows are concentrated around the 3 streams mentioned in section 4.2.
	Effect of grating cover	Appears to slow down runoff flow or "catch" the runoff trajectory before 2/3 of the gutter. Uncertainty if grate covering helps to "channel" water across gutter.
120 mm Gutter opening	Does Overshoot occur? Visual approximation	Overshoot occurs. The trajectory of inflow of water is right on the edge of the gutter. Quite a bit of water flows down the bottom section of roof.
	Back-splash? Visual approximation	Back-splash occurs consistently throughout the run period. Spray is quite violent, with large droplets.
120 mm Gutter opening with grating cover	Does Overshoot occur? Visual approximation	Overshoot occurs. The metal mesh of the grating cover appears to channel water to the lower section of roof. These flows are concentrated around the 3 streams mentioned in section 4.2.
	Back-splash? Visual approximation	Back-splash occurs consistently throughout the run period. Seems like there is less back-splash or less violent. Spray from joint on bottom section of roof.
	Effect of grating cover	Might slow down runoff. Appears to channel water across the gutter opening. May also lessen the intensity of back-splash created water hitting bottom edge/side of gutter.

Chapter 5

Analysis and Discussion

Although some analysis and interpretation occur in earlier parts of this thesis, a more detailed analysis will be presented in this chapter. As previously mentioned, the research questions are:

1. What are the current and future dimensioning rain loads for ZEB Laboratory in Trondheim?
2. How well does the architect's suggested design, with respect gutter opening, perform with regards to overshoot?
3. What rain gutter design will meet functional requirements while also maximizing solar energy potential?

Errors and uncertainties in data and experimental set-up are mentioned in this chapter, as they are imperative for understanding the limitations of the findings.

5.1 Rain loads

Rain loads are the basis for the experimental design. Though, not used directly as planned, the loads are used as a general design basis for the experiment and will be used in evaluating the risk involved with the subsequent design proposal. The rain load is perhaps the most significant factor when it comes to the hydraulic design of rain gutters. It is therefore important to gather reliable weather data. Data measurement in itself may be subject to uncertainties due to measurement methods, including wind effects[33].

5.1.1 Uncertainties in Rain Loads

Design rain loads are generally based on extreme rain loads, which naturally tend to be quite rare. Therefore, statistical extrapolation is necessary to estimate these rain loads [29]. The extrapolation process used by Met for the IDF curves used in the experiment is Gumbal extreme-value distribution [31]. The uncertainty of data sets increases with a lower number of measurement series and lower density of pluviometers. This is especially the case in places of complex topography, as the nature of convective showers are spatially variant. There is a relatively long time series of data for the meteorological station at Voll-Tyholt, but it is separated into two IDF curves based on location. This could affect the reliability and validity of the Voll IDF curve, as it has a shorter time series

to obtain extreme precipitation events. Coupled with the uncertainties in the data sets, the use of statistical extrapolation could also lead to overestimation or underestimation of extreme rain loads, particularly associated with long return periods [55].

5.1.2 Uncertainties in Future Rain Loads

Future rain loads are based on future climate models that attempt to predict how weather systems will behave in the future due to enhanced GHG in the atmosphere, and hence global warming. Due to the inherent complex nature of climate systems, climate projections are associated with large uncertainties. The uncertainties associated with rain load data will be further compounded by the uncertainties associated with the models and simulations. The uncertainties associated with climate projections can be subdivided into three categories:

Uncertainties associated with future anthropogenic GHG emissions

The uncertainties associated with anthropogenic GHG emissions, are mainly related to the development of global population and economy, technological factors such as energy efficiency and sources, and political climate policies. The release of potent GHG such as CO_2, N_2O, methane, and CFCs are associated with the combustion of fossil fuels, but agricultural practices and waste management practice also play a role. Emission amounts of other gases and particles that act as indirect forcings on climate systems are also uncertain. These uncertainties are somewhat accounted for in utilizing different RCP scenarios in simulations but there is no assurance that these emission scenarios are representative of actual future emission development. Even with a certain confidence in using different RCPs, there is also uncertainty of future climate development due to the knowledge gap between feedback sensitivity and forcings. [10, 33]

Uncertainties associated with natural variations

There is a knowledge gap in how the complex and non-linear climate systems react to random internal and external variations and forcings. The attempt to project future climate is complicated by the unpredictable natural of internal variations, which may greatly affect the climate system to larger degree than other forcings such as anthropogenic emissions [10]. These, sometimes random, internal variations can redistribute energy within the global climate system that can have greater impact on climatic variables on a regional scale. Examples include El-niña, El-niño and the Gulf Stream. Some external forcings include orbital changes and solar variability, but events that are more random such as volcanic eruptions could still have large impacts on the global climate system. [10, 33]

Uncertainties associated with models and simulations

As natural climate systems and interactions are not fully understood or known, the inability to describe these processes inherently limits the capabilities of models and simulations. Spatial and temporal resolution problems as well as analytic capabilities of modelling and simulation tools are also sources for uncertainties. (klima2100) The use of ensembles, or using predictions from many

different models, enhances model reliability of the results. The spread in ensemble simulations allow the results of climate predictions to be presented with uncertainties through a probability distribution. Post processing can also help minimize or calibrate systematic errors and uncertainties in projection. [10, 33]

As the data used in this thesis is from regional climate models, there are also uncertainties associated with down-scaling from global models. To improve reliability, utilizing different methods of down-scaling help determine accuracy of results[29, 33].

As climate factors are the expected relative change of expected future rainfall intensity compared to current values due to climate change, they are essentially based on climate projections. This entails that uncertainties associated with climate projections are also associated with climate factors [3]. To ensure reliability and chart uncertainty, several methods of calculating climate factors should be utilized [3].

5.2 Uncertainties in Runoff Calculations

As the volumetric runoff flow is the premise for designing the roof drainage system, appropriate calculation of these values is vital. The Rational Method is the recommended method for determining the peak flow for roof catchment systems by [39, 42]. The rational method was used as basis for design of the experimental set-up, but depended on a host of assumptions that did not incorporate the defining characteristics of ZEB Laboratory's roof. When considering the alternative approach, the hybrid method of the shallow water equations coupled with the manning equation, some critical assumptions were violated. This included the assumption for small angle approximation, as 30 °is a quite large angle, and the assumption that flow is laminar when in fact it is turbulent. In addition, there is an uncertainty of whether correlating the shallow water output with the manning equation is appropriate. For example, the viscous and relative roughness are not included in the manning equation and therefore not recommended for applications outside of normal-sized channels.

The results of the two methods proved to show quite similar results, as seen by Figures B.3-B.4 and B.17-B.18 and how well the time of concentration and the time to equilibrium compared B.9-B.10 and B.19-B.20 in appendix B.3. However, as the uncertainty associated with this new hybrid method was relatively high, the use of the rational method is recommended.

5.3 Sources of error and uncertainty in experiment

As the experiment can be considered a first of its type, as indicated by the lack of identified literature on the subject, there many of trials and tribulations. Therefore, the experiment was prone to uncertainty and error in the setup, which were hard to predict and account prior to the experimental process. This section will attempt to identify and illuminate issues and uncertainties in the experimental set-up and its measurements.

5.3.1 Measurement of runoff flow on roof

Initially, the experimental process was intended to test future and current rain runoff loads predicted by the runoff calculations done in section 3.2. However, it became apparent that these load values were vastly beyond the capacity of the RAWI-box – it could not supply the required amount of water. Therefore, the tactic was changed to instead experiment with the runoff loads that the modified set-up was able to achieve and then compare these loads to the runoff calculations for different durations and return-periods. The results could be used indicate the risk level which the developer would be able to accept in the final design. Fortunately, the maximum water quantities that the modified set-up could provide, around 180-200 l/min, were within range of the future runoff, so they were comparable to calculated rain loads. Ultimately, the extraordinary load placed on the RAWI-box by the modified set-up prevented testing of approximate present-day values. The present-day runoff flow quantity would have allowed for a basis of comparison and also given an indication of the reliability of the test results.

The use of a secondary water supply entailed that there was no automated method for measuring or controlling inflow to specific amounts, to compare the efficiency of gutter openings or to compare against calculated design runoff loads. The efficiency of interception could have been found by the drained amount as a percentage of the total inflow. Therefore, the only viable option for measuring water quantities was the method described in section 3.3.3, although this method was associated with significant uncertainties. The method only measured the water that entered the rain gutter and drained through the drainage holes in the span of 1 minute. Presumably, the runoff inflow was greater than this, as in some trials there was quite a lot of back-splash, and in some cases overshoot. The approach also did not take into account water that infiltrated into crevices or water that pooled in the gutter. This minimal quantity and uncertainty was ultimately accounted for by not initiating measurement of water quantity before peak flow presumably had occurred.

The measurement of the amount of water in the drainage bins was measured by pumping water out of the bins into 10 L buckets. The resolution of the measurement was therefore quite low, with an interval of ± 1 L. The stopwatch used to time the trials had a resolution of 0.01 seconds, but was prone to user observation errors of manual starting and stopping. This might have had a greater effect on flow measurement as more than 1 L could drain into the bins in the span of 1 second. All together, these factors affect the accuracy of the flow measurement, although there is ambiguity in the magnitude of the impact each factor has on the flow measurement. Therefore, using the trial runs for the 240 mm gutter opening for reliability purposes, one can distinguish the coarseness of the measurement. If considering all five of the flow measurements, the measurement uncertainty is $\pm 3l$ from $\Delta x = \frac{x_{max} - x_{min}}{2}$.

5.3.2 Video results

As there was no quantitative way of measuring the efficiency of the gutter, qualitative observations were used as the main source of evaluating gutter success. The GoPro Hero 3+ recorded video at 30 frames per second but in some cases, this was too coarse to determine the exact nature of the flow and identify occurring phenomena. The resolution of the image is also limiting, as the water in some cases cannot be clearly distinguished and zooming on distinct frames will blur or pixelate the image. Although using cameras with higher resolution and greater frame rate certainly

could improve the quality of the results, the use of multiple cameras may enhance the quality of observations and allow for valuable information extraction.

The use of only one camera restricted the experiment documentation to only one side and one angle of the sample roof. For example, in Figure 5.1, it is apparent that there is a splashing effect on the far side of the roof. When zoomed in on the specific area of the image, the quality of image does not allow for a clear interpretation of the frame. With multiple cameras in different locations, it might have been possible to discern what caused this disturbance on the far side of the roof. The limited view and angle of one camera also decreases the reliability and validity of the results. For example, it is difficult to identify whether the phenomena seen from one angle are significant and valid, or if it only occurs due to local effects.

Figure 5.1: Difficulty of identifying phenomena due to camera placement

5.3.3 Validity of experiment

In this case, the validity of the experiment is very much dependent on whether the runoff on the sample roof behaves similar as the runoff on the actual BIPV roof of the ZEB Laboratory. As water follows the path of least resistance, water flows tend to channel and rill when there are surface obstructions in the flow path. This could increase the depth of flow in certain areas and could cause discrete runoff jets at the downstream end of the roof. Perhaps the worst case of discrete jets, which cause overshoot, can be seen with steep corrugated metal roofs [45] with surface treatment. On a BIPV roof, the degree of this "channeling effect" would depend on local topography of the BIPVs and their framing and mounting structure. As most BIPVs have both horizontal and vertical joints, the horizontal joints may cancel out the effects of vertical channeling on the roof and slow the runoff flow.

Another point about joints and crevices is that it will cause disturbances in the flow that will cause turbulent flow to occur. This was seen in Figure 4.7. If the roof is riddled with protrusions, such as panels fasteners, down the length of the roof, this would increase the roughness of the roof and most likely slow the runoff flow.

The division into distinct streams that project off the downstream end of the roof into the gutter was detected in this experiment. In Figure 5.2, one can clearly identify these streams (marked by

red ovals). Though the division of the runoff into distinct streams and the consequent projection of runoff into the gutter is seen on the sample roof, this division of runoff appears to be primarily due to the way water was conveyed onto the sample roof. This division, due to the impact of the jets has been commented on earlier, and the effect was attempted assuaged by breaking up of the jet with boards. Ideally, water would have entered from above the sample roof in a continuous flow, in order to simulate runoff and avoid the turbulence created by the jet impact on the roof.

Figure 5.2: Runoff separation into streams

5.4 Analysis of Observations

General observations from the experiment indicate that the runoff flow tended to separate or converge into three streams of sheet flow when flowing down the sample roof. The high impact pressure and turbulence from the jets of water produced by the fire hoses appears to create "wakes" and the intersection of these "wakes" may cause the sheet flow to separate into streams. When these streams encounter the sample roof edge, they create three discrete jets as indicated in Figure 5.2. These jets have almost the same trajectory most of the trials, though it may be difficult to see it visually in some of the narrower gutter openings.

These trajectories are what cause overshoot when the gutter opening is insufficient. Therefore, it is of interest to try to model the trajectories of these projections to predict the size of gutter opening to avoid overshoot. Since these trajectories resemble the path of projectile motion, these equations were attempted with the velocity calculated in section in 3.2 for different runoff flows:

- 208 l/min: representative of worst case for future Trondheim and greatest measured amount
  - velocity: 0.89 m/s
- 185 l/min: runoff representative of test load
  - velocity: 0.85 m/s
- 140 l/min: runoff representative of current Trondheim runoff flow: m/s
  - velocity: 0.76 m/s

The trajectory equations for projectile motion:

$$y_{position} = v_0 sin(-\theta)t - \frac{1}{2}gt^2 \tag{5.1}$$

$$x_{position} = v_0 t cos\theta \tag{5.2}$$

Where θ refers to the angle of the slope, 30 °, and the velocity as per the three cases outlined above. For the y position, as the velocity is down along the roof the angle is negative from the horizon. There multitude of assumptions for the use of these equations in this case but the main ones are:

- v_0: initial velocity, considered to be the same velocity of the water flow entering the roof
- The projectile is assumed to be in a two-dimensional space as the projectile motion occurs in while in one plane but in reality the trajectory occurs in three dimensions.
- Object is a particle
- Air resistance or drag is neglected; therefore stream break-up is also neglected
- Fluid-fluid interactions and turbulence are neglected

Though it is clearly optimistic to use these trajectory equations for examining the motion of the runoff projection, it is an attempt to describe this motion. The x and y positions in time, from equations 5.1 and 5.2, were graphed with the slope of the roof in a 1:1 aspect ratio, to give the trajectory comparisons in Figures 5.3a and 5.3b.

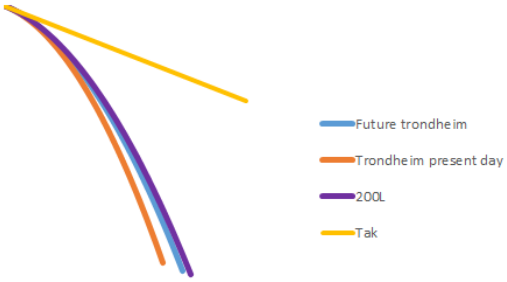

(a) 240mm gutter opening

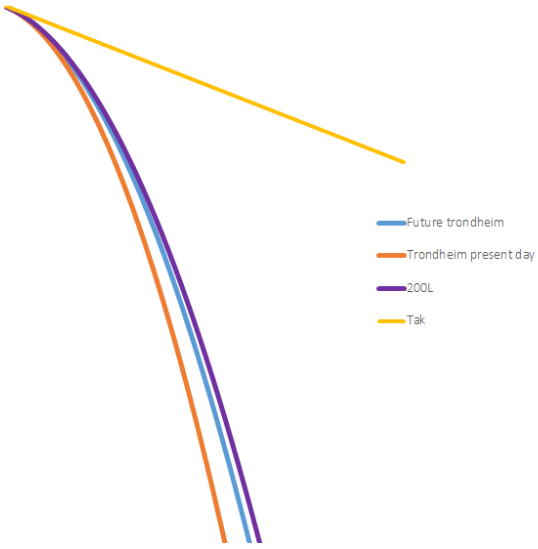

(b) 480mm gutter opening

Figure 5.3: Theoretical runoff projection trajectory in comparison to gutter opening

The graphed trajectory overlaid on images from the experiment by scaling the projection according to the length and angle of the gutter opening in the photos. The graphs were also angled in a 3D program to allow for depth perspective. Examples can be seen in the following Figures 5.4a and 5.4b.

From both Figures 5.4a and 5.4b, it is apparent that the runoff projection follows the same trajectory as the projectile motion trajectories to a certain extent. At the start of the projection trajectory where the water seems to be a more cohesive stream, further along the trajectory it seems like drag forces break apart the jet and cause turbulence. This suggests that with precise

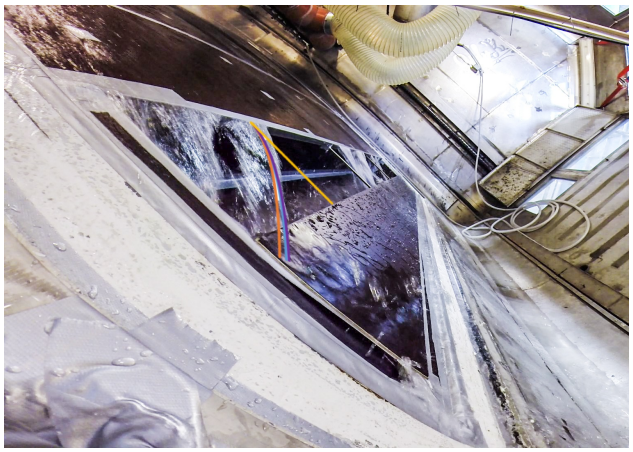

(a) 240mm gutter opening in comparison to experiment

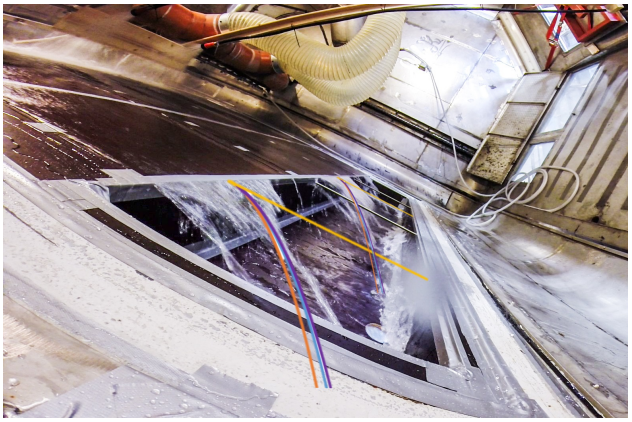

(b) 480mm gutter opening in comparison to experiment

Figure 5.4: Theoretical runoff projection trajectory in comparison experiment

measurement of velocity and with correction for drag effects, one could use trajectory equations to predict theoretical runoff projection [56].

5.4.1 Gutter size evaluation

One of the main objectives of the experiment was to evaluate the success of the different sizes of the gutter openings. This evaluation is done by comparing the opening sizes against each other. The color coding of the editing of the photos is as follows:

- Red: relating to overshoot
- Blue: relating to back-splash
- Green: flow on bottom roof section

Note! The photos only seem like they are at different angles, as the camera angle may have changed slightly from one trial to another because the camera had to be removed to charge the battery.

480 mm vs 240 mm gutter opening

From Figures in 5.5 it is obvious that both preform relatively similar when it comes to overshoot, indicated by the red circles. There appears to be no overshoot as the runoff projection is completely within the gutter. The difference between these two gutter opening sizes is mainly the back-splash from the runoff projection hitting the board that represents the bottom side of the gutter. This is seen with the blue circles in both Figure 5.5a and 5.5b but is especially noticeable in Figure 5.5b. The 240mm has definitely more back-splash than the 480 mm gutter.

240 mm vs 120 mm gutter opening

From Figures in 5.6, one can see that there is definitely more back-splash in the 120 mm case both in quantity and intensity, as indicated by the blue circles. Overshoot, indicated by the red circle

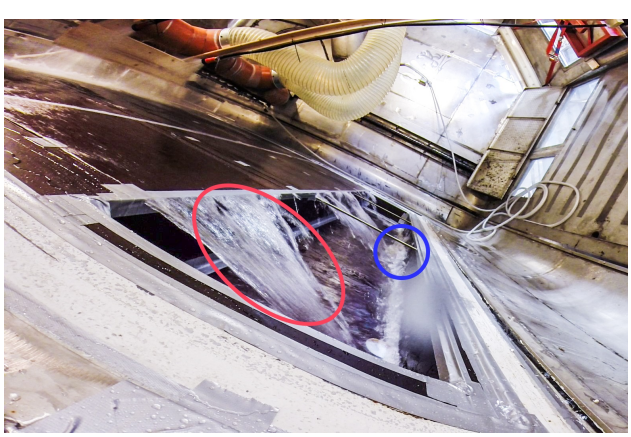

(a) 480 mm gutter evaluation

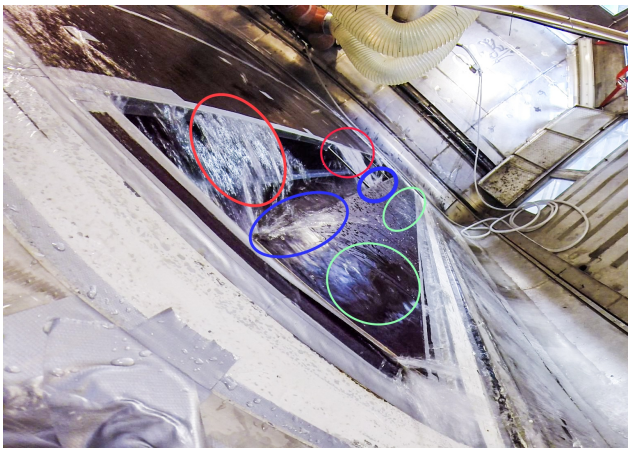

(b) 240mm gutter evaluation

Figure 5.5: Comparison and evaluation of 480mm and 240mm gutter opening

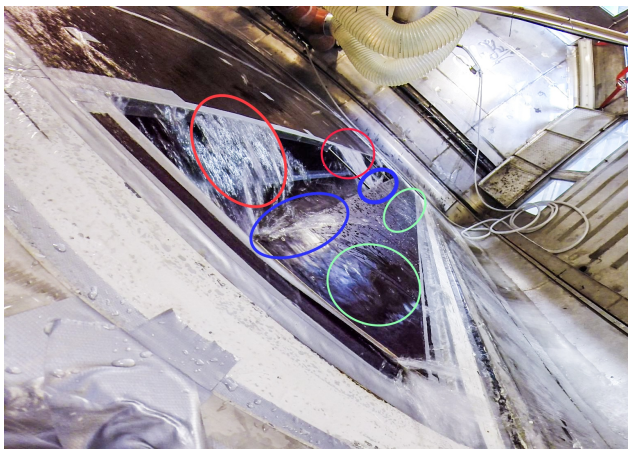

(a) 240 mm gutter evaluation

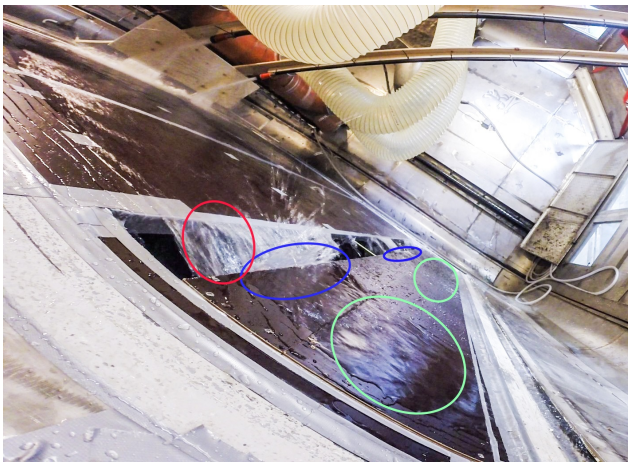

(b) 120mm gutter evaluation

Figure 5.6: Comparison and evaluation of 240mm and 120mm gutter opening

in Figure 5.6b, seems to be occurring in the 120 mm case especially considering the quantity and consistency of water flow on the roof underneath the gutter. When comparing the two green circles in Figures 5.6a and 5.6b, the 120mm case seems to have too much water flow for it to be solely related to the increase in back-splash.

The main observations drawn from section 5.4.1 is that the smaller the opening size, the greater the chance of overshoot and the greater amount and intensity and turbulence of the back-splash. The cohesion is the runoff projection seems to be greater in the smaller of gutter openings, as break-up of the projection occurs further along in the runoff's trajectory than the gutter allows. From the evaluation of gutter opening size alone, one can conclude that although a 240 mm gutter opening is sufficient for overshoot, smaller openings closer to 120mm risk overshoot and considerable amounts of back-splash.

5.4.2 Back-splash

The cause of the increase in back-splash quantity and intensity as the opening size decreases may be related to the water projection impact zone, where the water projection hits the bottom side of the gutter, is closer to the opening of the gutter. The break-up of the stream due to drag effects in larger openings, may cause the runoff projection to have a lesser intensity in this cases as well. An illustration in Figure 5.7 attempts to explain what could be causing back-splash.

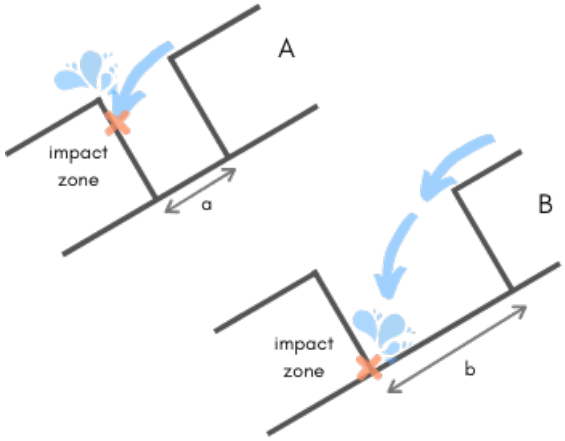

Figure 5.7: The impact zone of the runoff trajectory at to different gutter openings, $a < b$

As the opening increases in Figure 5.7 from a and b, the trajectory of the runoff projection moves the impact along the bottom side of the gutter. Although there seems to be some degree of back-splash in most of the gutter opening sizes, the back-splash appears to be significantly greater in quantity and intensity for smaller opening sizes. The distance between the impact zone and the opening of the gutter seems to impact the back-splash landing. The closer the distance, the greater the quantity of back-splash landing outside the gutter. The cohesion of the water projection is greater at the start of the trajectory before the drag breaks up and the decreases energy of the projection. Thus, the runoff projections for smaller gutter openings have greater energy on impact, causing bigger splashes.

5.4.3 Effect of Grating Cover

The effect of the grating covers were predicted to slow the velocity of the runoff flow in such a manner that the runoff would more readily be intercepted by the gutter. The covering of the gutter and the resolution of the camera made it hard to visually interpret the results to understand the exact mechanisms occurring with runoff flow over the grating cover. Table 4.8, summarized the apparent effects of the grating cover on the different sizes of gutter openings. For all gutter openings, the grating cover seemed to minimize the back-splash effect, which suggests that a partial covering is enough to prevent back-splash. However, for the smaller gutter openings, the grating cover seemed like it could also be channeling water across the gutter opening. Example shown in Figure 5.8.

As the holes in the grating covering were parallel, as Figure 5.9a, instead of horizontal to flow, this could have led to channeling of water as in Figure 5.8. Therefore, the plan was to test the grating holes that were horizontal to flow, as in Figure 5.9b, as this will not provide “pathways” for the

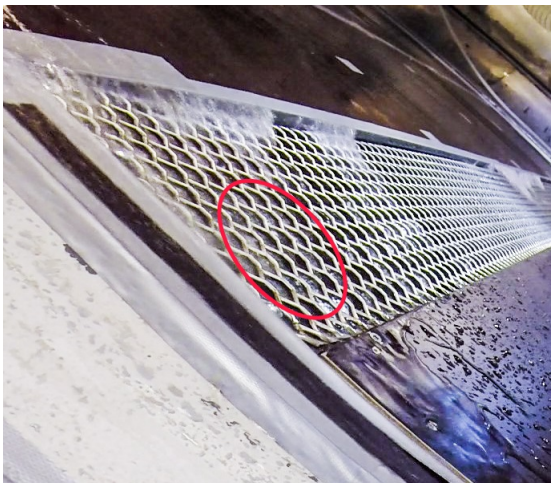

Figure 5.8: Grating cover conveying runoff, indicated by "film" inside holes

water flow to cross the gutter opening. The misalignment in the RAWI-box prevented this from being tested.

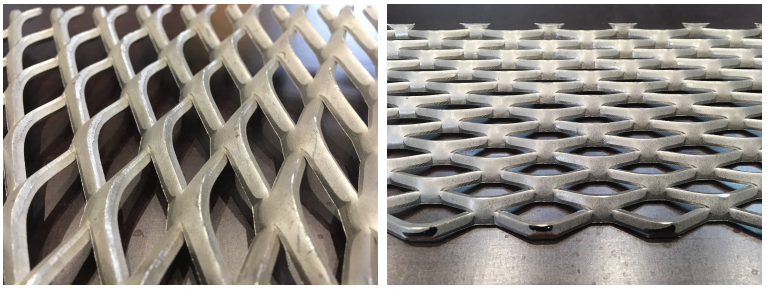

(a) Grating holes are vertical (b) Grating holes are horizontal

Figure 5.9: Direction of holes in grating cover

When comparing the same gutter opening with and without grating covers, it definitely seems like the grating cover could improve interception. An indication of this could be the amount of water flow on the bottom section of roof beneath the gutter. Figure 5.10 compares the effect of grating cover for 120 mm gutter opening. From Figure 5.10, it is obvious that the gutter covering has an effect on the flow on the bottom section of roof. Table 4.1 indicates that there is not too much difference in the amount of inflow, and therefore the gutter covering could have had noticeable effect on the amount of water intercepted. This is possibly due to the fact that impact and friction provided by the grating dissipates energy of the runoff projection. If the grating cover does in fact channel water across the gutter opening, this is considerably less than the amount of water prevents from leaving the gutter.

5.5 Hydraulic Capacity of the Gutters

The experimental set-up has been used primarily to determine the gutter size opening based on the gutter's capability of capturing runoff flow. In cases, like the ZEB Laboratory, were the roofs allow for large volumes of water to gain significant velocity, this interception is largely based on preventing overshoot. However, if the gutter is insufficiently design for hydraulic capacity, the

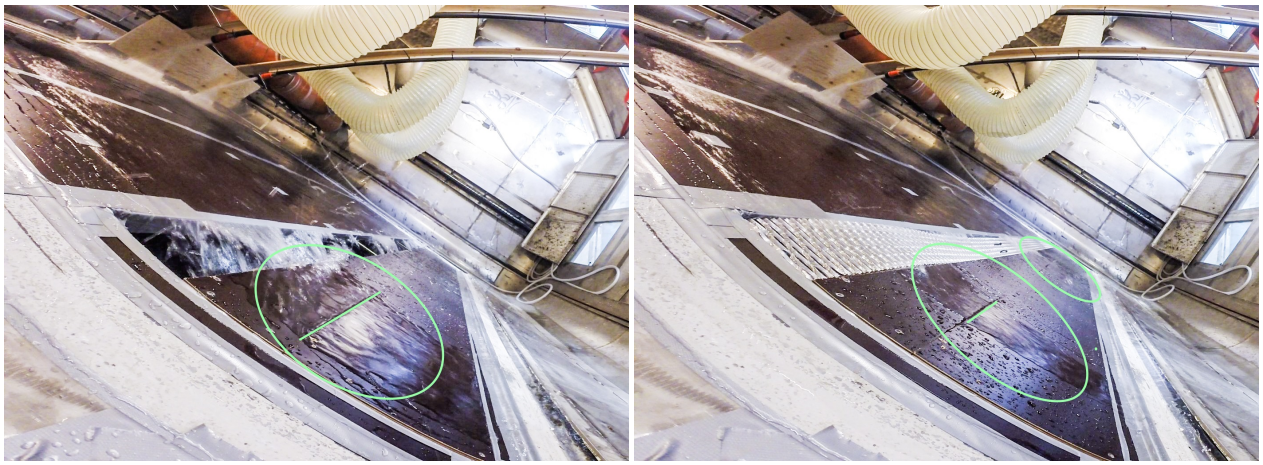

(a) 120 mm gutter opening without grating cover (b) 120 mm gutter opening with grating cover

Figure 5.10: Comparison of the effect of grating cover on 120 mm gutter opening

gutter could overflow, which would lower the interception efficiency and represents gutter failure. Therefore, it is essential to ensure that the hydraulic capacity of the gutter exceeds the design runoff flow from the roof catchment area. The equations 2.12 and 2.13 for capacity of hydraulically short internal gutters were therefore used. The values for the dimension variables, presented in Figure 5.11, used in the calculation of the different opening widths are presented in Table 5.1.

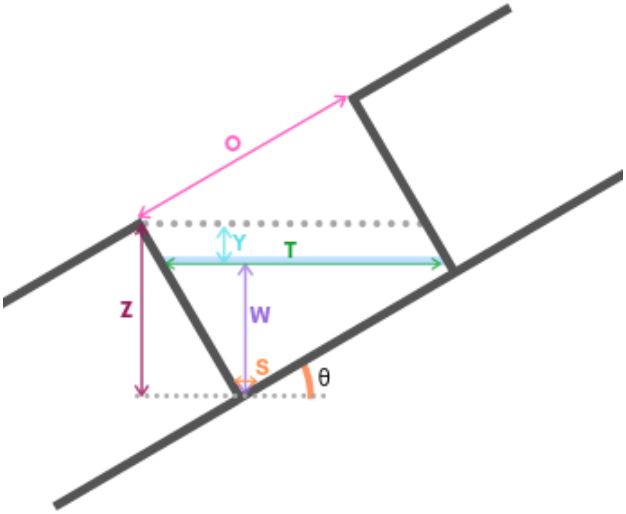

Figure 5.11: Illustration of gutter dimension variables for ZEB Laboratory

Opening sizes below 200 mm gutter opening are excluded from this calculation, as those widths were deemed insufficient from the experiments. It should also be noted that the thickness of roof layer (measured from bottom of the gutter) is dependent on the thickness of the BIPVs, and therefore a minimum of 220mm was used. This 220mm is height of the ventilation gap and an additional 20 mm for the BIPVs. In reality, this value will likely be higher and therefore all opening sizes will be sufficient in capacity if they have acceptable capacity with a 220mm roof layer thickness.

The results of the hydraulic design capacity are presented in Figure 5.12. The graph presents the hydraulic design capacity and capacity of the internal gutter without shape and depth factor. This was done because the design capacity appeared to increase slightly compared to the opening's

Table 5.1: Variables for Hydraulic Design of Opening sizes

	Gutter Opening in mm				
O, Opening [mm]	200.0	240.0	245.0	300.0	480.0
Roof angle	30.0	30.0	30.0	30.0	30.0
Thickenss of roof layer, X [mm]	220.0	220.0	220.0	220.0	220.0
Z, total depth [mm]	190.5	190.5	190.5	190.5	190.5
width at Z [mm]	230.9	277.1	282.9	346.4	440.0
Y, Freeboard [mm]	57.2	57.2	57.2	57.2	57.2
W, design height [mm]	133.4	133.4	133.4	133.4	133.4
T, width at W [mm]	98.9	145.1	150.9	214.4	308.0
S, sole [mm]	0.0	0.0	0.0	0.0	0.0
Aw [mm^2]	25853.0	28252.3	28487.3	30119.2	36960.0
W/T	1.3	0.9	0.9	0.6	0.4
Fd	1.1	1.0	1.0	0.9	0.8
S/T	-	-	-	-	-
Fs (triangle)	0.893	0.893	0.893	0.893	0.893
Qsv	12.5	13.9	14.1	15.1	19.5
Qn	12.0	12.2	12.2	12.0	14.1
Ql (l/s)	10.8	11.0	11.0	10.8	12.7

dimension. It is apparent from the graph that the shape and depth factor counter the prospective increase in capacity.

The greatest total runoff flow from the conservative rational method, gathered from Table B.4, was 37.35 l/s for a duration of 2 minutes and with a return period of 200 years for the entire roof. The ZEB Laboratory roof will most likely have three drainage outlets with a maximum of 4 meters between each outlet. The capacity of the individual gutter lengths should therefore be 6.21 l/s. This value was plotted against the design capacities in Figure 5.12 to indicate that the gutter sizes mentioned were all satisfactory in terms of hydraulic capacity.

Extra Section of Roof

The extra section of roof that has been excluded from calculations has been mentioned in several sections of this thesis. In reality, this section will provide another 80 m^2 to collect rainwater that needs to be drained. The planned solution is that edge section of the roof has a gutter that follows the angle of the roof. It is therefore assumed that the rainwater from the contributing area will not gain enough velocity to overshoot this angled gutter. This section of gutter then combines with the horizontal gutter for the rest of the roof and drains into the drainage outlets located along main gutter section. However, this results in increased drainage load on the nearest drain to this "extra" section of roof. Thus, the gutter lengths of other drainage sections may need to be adjusted to account for the need for increased capacity at this drainage outlet. Further analysis regarding the speed of the runoff conveyed in this gutter might be necessary as the gutter would be quite steep.

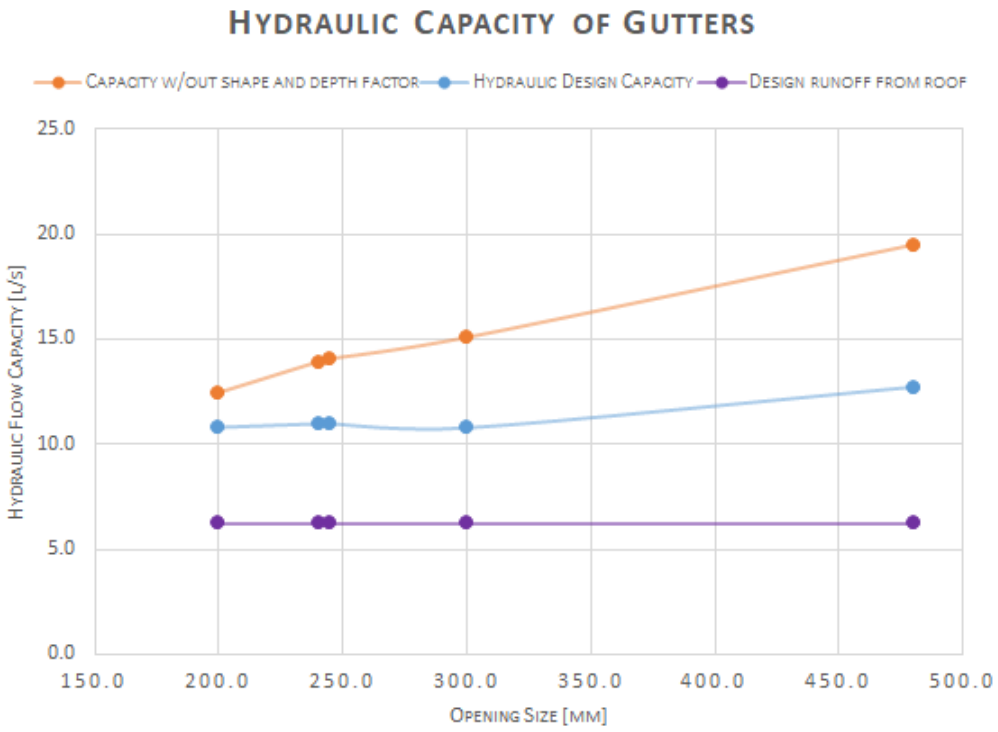

Figure 5.12: Graph of Hydraulic Capacity of Different Openings

This could cause high velocity at the drainage outlet where the two sections of gutter meet.

5.6 Implications of Design

The ultimate goal of this thesis is to provide a recommendation for gutter design that can be utilized on the roof of the ZEB Laboratory, which will ensure appropriate interception of runoff rainwater from the roof without being over-dimensioned. The original architect solution with a 480 mm gutter opening performs indisputably well with respect to both overshoot, back-splash, and overtopping, but could perhaps be considered over-dimensioned.

5.6.1 Recommendations

A gutter opening size of at least 300 mm [42] for internal gutter is recommended by the European standards, though this investigation has lead to the conclusion that 240mm could be sufficient based on performance. Overall, a gutter opening size close to 240mm is the best compromise as no overtopping or overshoot occurs and there is a moderate amount of back-splash. Considering the presence of a grating cover appears to slow flow of moderate gutter openings, a range of 200-300mm for gutter opening can be recommended.

As discussed in section 5.4.2, back-splash can be attributed to water splashing on the bottom side of the gutter near the opening. Thus ensuring that the impact zone of the water projection is closer to the sole of the gutter without decreasing gutter opening could prevent back-splash from being a problem. A suggested solution is shown in Figure 5.13.

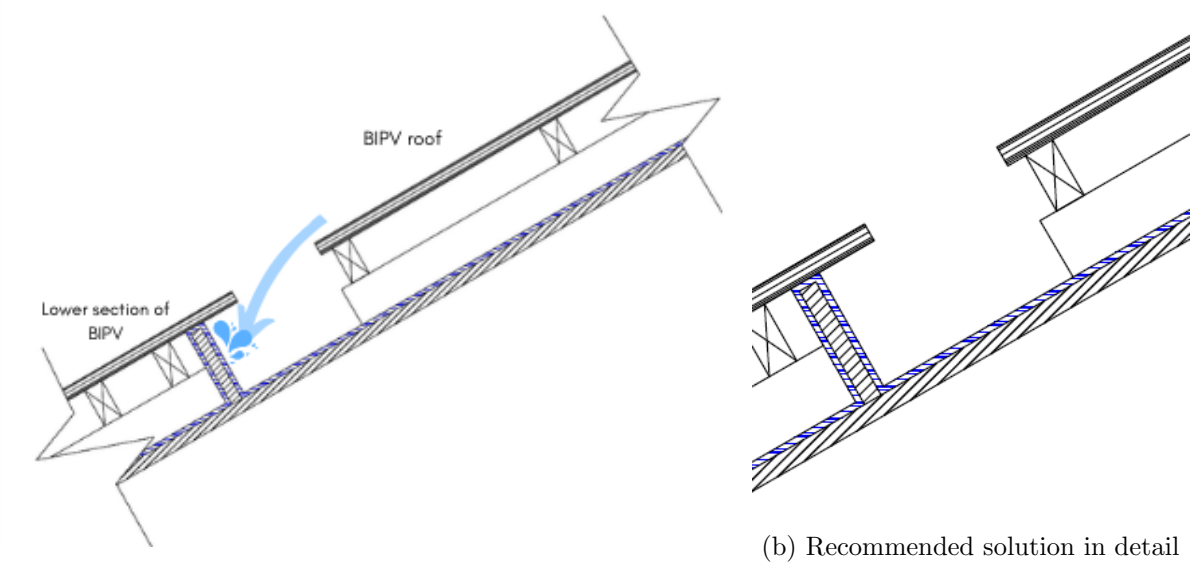

(a) Recommended solution with regards to back-splash

(b) Recommended solution in detail

Figure 5.13: Recommended design solution to avoid back-splash, without specified dimensions

Here the lower section of BIPV roof is placed so it overhangs the gutter slightly, thus enabling a larger gutter and the overhang would prevent back-splash from leaving the gutter completely. This gutter recommendation would of course require a more thorough feasibility investigation, especially considering the electronics associated with BIPVs. Ventilation openings and flashing are not considered in this recommendation design and the construction issues associated with the complex structure could lead to construction issues.

The final decision of absolute gutter width would depend on the level of risk that building owner is willing to accept. The risk level depends on both the gutter design and subsequent hydraulic performance, but also the probability of storm occurrence that will cause exceedance of the system. The probability of exceedance of a storm event can be expressed: $P_r = 1 - (1 - \frac{1}{T})^{L_y}$ where L_y: is the lifetime of the building, in this case 60 years, and T is the return period of the storm, both expressed in years.

Table 5.2 summarizes the probability of exceedance for different runoff quantities for the ZEB Laboratory, based on future rain loads in Trondheim. The runoff flow quantities that are less than or equal to the corresponding runoff flows tested in the experiment are highlighted. The recommendations that have been made so far are therefore applicable for these values and exceedance probabilities. Considering that the tested values have a relatively low probability of exceedance throughout the entire lifetime, one can conclude that the design recommendations are applicable.

If the recommendation of an opening of 240 mm is followed,5.8 m^2 of roof is freed from roof gutter to be available for BIPVs. Though this might not seem like much, with the efficiency of the selected BIPVs [57] and irradiation for Trondheim, could produce 1303 kWh/yr.

5.6.2 Other considerations

Even though the hydraulic interception characteristics of the roof gutters are probably one of the most important aspects of roof gutter design, many other characteristics not considered in this thesis are pertinent to the final design. Although snow loads are not considered to be the dimensioning

Table 5.2: Exceedance probabilities for tested runoff quantities for specified duration events

	Q: Runoff rate (l/min) pr roof length for specified duration				
Probability of exceedance during lifetime	1 min	2 min	3 min	5 min	10 min
100 %	28.69	25.03	22.28	18.94	13.98
100 %	41.43	39.27	35.23	27.94	18.36
99.8 %	49.86	48.70	43.81	33.88	21.25
95.4 %	57.97	57.74	52.03	39.59	24.04
91.4 %	60.54	60.62	54.64	41.40	24.92
70.2 %	73.32	74.41	67.16	50.33	29.62
45.3 %	81.73	83.81	75.71	56.26	32.51
26.0 %	90.14	93.18	84.24	62.18	35.38

aspect for the ZEB Laboratory, it is important to consider the how the snow load will affect the gutter's capacity and structure. Thus, the design might need to be modified slightly to accommodate these loads. The recommendations that have been made in this thesis have not considered the feasibility of construction of design details concerning water tightness and ventilation. These are important aspects to consider in preventing moisture damage to the interior of the building from the roof.

Maintenance is necessary for the roof drainage system to function properly, it is recommended that the roof gutter be cleaned for debris at least once annually and joints and connections checked regularly [58]. The drainage systems components therefore need to be accessible for maintenance and repairs. Material choice may have an effect on the longevity of the system and the need for maintenance, therefore using materials that are well suited for these purposes are vital for the ZEB Laboratory.

The conveying capabilities of the gutters themselves and drainage outlets are also be pertinent to the overall performance of the roof drainage system and should be evaluated.

Chapter 6

Conclusion

The purpose of this thesis was to calculate the dimensions of the internal roof gutter for the ZEB Laboratory to ensure proper hydraulic functionality for expected future rain loads while maintaining optimal use of the south-facing area for solar energy production.

Future rain loads are inherently associated with uncertainties due to the complexity of climate systems and also the exacerbation of greenhouse gases in the atmosphere. Therefore, conservative climate factors of 1.4 and 1.5 [34] were utilized when estimating rainfall intensity and consequent runoff.

The experiment was designed and completed to evaluate the performance of various sizes of gutter opening qualitatively, and their ability to prevent roof runoff from overshooting the gutter. As the substantial mechanical and water loads placed on the RAWI-box were well beyond its capabilities, the experiment was only partially completed and therefore the reliability of the results could be question. Despite uncertainties in the experiments, the results were valuable in shaping gutter design. Although only discrete widths of opening sizes 480 mm, 240 mm, and 120 mm were tested, some general deductions regarding opening sizes can be made from the observations. A decrease in opening size is associated with a higher risk of overshoot and an increase in frequency and intensity of back-splash. The runoff projection is more cohesive and dense at the start of the trajectory and then breaks up, presumably due to drag forces. As the bottom side of the gutter meets the runoff projection's trajectory in a place with higher energy, the back-splash increases.

The grating covers, tested in the experiment, seem to decrease the energy of the projection stream for all sizes of the gutter openings. This decreases the overshoot quantity in those cases and decreases the intensity and frequency of back-splash. These findings suggest that a grating size around the range of 200-300 mm will be most viable with regards to overshoot and back-splash, where smaller openings are appropriate, depending on the use of grating cover. To fulfill the functional requirements, it is recommended to use a 240 mm gutter opening. The suggested gutter opening sizes also perform satisfactorily with regards to theoretical hydraulic capacity and the potential for overtopping.

A suggested solution to avoid back-splash was also tested, where a portion of roof below the gutter overhangs into the gutter seen in Figure 5.13. This would effectively maintain the gutter opening size but increase the hydraulic capacity of the gutter and block back-splash. If the recommended 240 mm gutter opening size is used instead of the 480 mm gutter suggested by the architect, the area for BIPVs on the roof could increase by 5.7 m^2, with the potential to produce 1303 kWh annually.

Further investigations to generalize the observations from this experiment, could be useful in future gutter design for buildings with large mono-pitched BIPV roofs.

Chapter 7

Suggestions for Further Work

There are many different adaptations, tests and alterations that could have been attempted within the framework of the experiment that were not completed due to time and monetary constraints. Based on the knowledge and experience gained from the completed tests and trials, , the following are suggestions for further research and work:

- Improvements to the experimental set-up and procedure to increase reliability of data: Finding a method that could accurately measure inflow and outflow within the experiment's boundaries would give a quantitative measure of efficiency of the gutter interception. This would ultimately make optimization of design more unambiguous. A method that eliminates wakes and the turbulence of jet impacts, and instead distributes inflow like a sheet, would lead to a truer experiment. As mentioned in section 5.3.2, using multiple cameras with higher image resolution and a greater number of frames per second in different locations would allow for the recording and analysis of phenomena such as back-splash and the runoff projection.
- Include various experimental variables for testing to increase the robustness and validity of data and give a more conclusive and holistic understanding of gutters: This would improve applicability, as generalized observations for BIPV roof gutters could be formulated into standards and building recommendations. This could include testing different roof slopes, roof surface materials, and gutter shapes. Different roof surface topographies, such as a corrugated roof, would give an indication of "worst case" scenario when the flow separates into jets at the roof edge. A greater variety of runoff flow rates would also allow for a more holistic comparison and discussion regarding risk level acceptance.
- A more thorough investigation into the effect of grating covers on the roof runoff: Other investigation variables could be direction of the hole pattern, shape and size of holes and slope of system.
- Development of a runoff model that is suitable to use on roof catchments: Ideally the model would be able to incorporate parameters that vary for roofs and give outputs such as runoff flow rate, depth of flow at downstream end and velocity of flow. This would help characterize behavior at the edge of the roof and gutter, and predict behavior of runoff into the gutter.

References

[1] Karl Berger et al. "Internatonal Definitions of BIPV". In: vol. T15-04. IEA-PVPS. IEA, Aug. 2018. ISBN: ISBN: 978-3-906042-73-2.

[2] V. Masson-Delmotte et al. "Global Warming of 1.5°C. An IPCC Special Report on the impacts of global warming of 1.5°C above pre-industrial levels and related global greenhouse gas emission pathways, in the context of strengthening the global response to the threat of climate change, sustainable development, and efforts to eradicate poverty". In: Annex I: Glossary. 2018.

[3] Kim H Paus et al. *METODER FOR BEREGNING AV KLIMAFAKTORER FOR FREMTIDIG NEDBØRINTENSITET*. 2015.

[4] Sintef Byggforsk. *Energieffektive bygninger. Begreper og definisjoner*. Tech. rep. 473.003. SINTEF Byggforskserien, Dec. 2015. URL: https://www.byggforsk.no/dokument/4153/energieffektive_bygninger_begreper_og_definisjoner.

[5] World Meteorological Organization and United Nations Educational Scientific and Cultural Organization. "International Glossary of Hydrology". In: 3rd ed. WMO- No. 385. WMO, UNESCO, Sept. 2012.

[6] Clayton T. Crowe, Donald F. Elger, and John A. Roberson. 8th ed. John Wiley and Sons, 2005. ISBN: 0-471-48737-6.

[7] Wilfried Brutsaert. Cambridge University Press, 2005. ISBN: 978-0-521-82479-8. URL: https://app.knovel.com/hotlink/toc/id:kpHAI00009/hydrology-an-introduction/hydrology-an-introduction.

[8] Sintef Byggforsk. *Nullutslippsbygninger (ZEB) Retningslinjer og beregningsmetoder*. Tech. rep. 473.020. SINTEF Byggforskserien, Aug. 2017. URL: https://www.byggforsk.no/dokument/5177/nullutslippsbygninger_zeb_retningslinjer_og_beregningsmetoder.

[9] Tor Helge Dokka et al. *A Norwegian ZEB Definition Guideline*. Tech. rep. 2016.

[10] V. Masson-Delmott et al. *Global Warming of 1.5 °C: Summary for Policymakers above pre-industrial levels and related global greenhouse gas emission pathways, in the context of strengthening the global response to the threat of climate change, sustainable development, and efforts to eradicate poverty*. Tech. rep. IPCC- Intergovernmental Panel on Climate Change, 2018, p. 26.

[11] International Energy Agency and The United Nations Environment Programme. *2018 Global Status Report Towards a zero-emission, efficient and resilient buildings and construction sector*. Tech. rep. The Global Alliance for Buildings and Construction, 2018, p. 73. URL: https://www.globalabc.org/uploads/media/default/0001/01/f64f6de67d55037cd9984cc29308f3609829797a.pdf.

[12] Council of the European Union European Parliament. *DIRECTIVE 2010/31/EU OF THE EUROPEAN PARLIAMENT AND OF THE COUNCIL of 19 May 2010 on the energy performance of buildings*. Official Journal of the European Union. June 2010.

[13] Link Arkitektur and Veidekke. *ZEB Laboratory*. 2019.

[14] SINTEF. *ZEB Flexible Lab - Konseptbeskrivelse forprosjekt*.

[15] Norsk Klimaservicesenter. *Klimaprofil Sør-Trøndelag:Et kunnskapsgrunnlag for klimatilpasning*. Norsk Klimaservicesenter. July 2017. URL: https://cms.met.no/site/2/klimaservicesenteret/klimaprofiler/klimaprofil-s%C3%B8r-tr%C3%B8ndelag/_attachment/12039?_ts=15dcb459a0a.

[16] Veidekke Multiconsult- Karianne Skrindo. *Bygningsfysiske premisser*. ZEB-Flexible Lab,418722-RIBfy-RAP-001. 2017.

[17] Link Arkitektur. *ZEB Laboratory*. 2019.

[18] Link Arkitektur. *ZEB Laboratory Detaljer Klimaskall*. 2019.

[19] IEA. *Technology Roadmap: Solar Photovoltaic Energy*. 2014.

[20] Jarand Hole. *Solenergi*. NVE. June 2014. URL: https://www.nve.no/energiforsyning/solenergi/?ref=mainmenu.

[21] FME SUSOLTECH, Solenergiklyngen, Norsk Solenergiforening, and BIPV Norway. *Muligheter og utfordringer knyttet til Bygnings Integrerte solceller (BIPV) i Norge 2018*. 2018.

[22] A. G. Imenes and J. Kanters. "3D solar maps for the evaluation of building integrated photovoltaics in future city districts: A norwegian case study". In: *2016 IEEE 43rd Photovoltaic Specialists Conference (PVSC)*. June 2016, pp. 3141–3146. DOI: 10.1109/PVSC.2016.7750245.

[23] Weller D et al. *Detail Practice - Photovoltaics : Technology, Design, Construction*. Walter de Gruyter GmbH, 2010. ISBN: 9783034615709. URL: https://ebookcentral.proquest.com/lib/ntnu/detail.action?docID=1075522.

[24] Dr.Hein van der Zeeuw. *Manual for BIPV Projects*. Odersun AG. Sept. 2011.

[25] Isa Zanetti et al. *Building Integrated Photovoltaics; Product Overview for solar building skins*. SUPSI-SEAC BIPV. Status-Report. 2017.

[26] Gullbrekken L, Kvande T, and Time B. "Roof-integrated PV in Nordic climate - Building physical challenges". In: *Energy Procedia* 78 (2015), pp. 1962–1967. ISSN: 18766102. DOI: 10.1016/j.egypro.2015.11.382.

[27] Kristjansdottir T et al. "Embodied greenhouse gas emissions from PV systems in Norwegian residential Zero Emission Pilot Buildings". In: *Solar Energy* 133 (2016), pp. 155–171. ISSN: 0038-092X. DOI: 10.1016/J.SOLENER.2016.03.063.

[28] Sintef Byggforsk and MET. *Klimadata for dimensjonering mot regnpåkjenning*. Tech. rep. 451.031. SINTEF Byggforskserien, Aug. 2013. URL: https://www.byggforsk.no/dokument/3331/klimadata_for_dimensjonering_mot_regnpaakjenning.

[29] Eirik Førland et al. *Dimensjonerende korttidsnedbør*. Tech. rep. 2016.

[30] Roger A. Pielke and Fritz P. Loewe, eds. *Climate*. Encyclopedia Britannica, inc., 2019. URL: https://www.britannica.com/science/climate-meteorology.

[31] MET Klimaservicesenter. *Nedbørintensitet- IVF kurver*. URL: https://klimaservicesenter.no/faces/desktop/idf.xhtml.

[32] Trondheim Kommune. *Beregning av overvannsmengde: Dimensionering avledning og fordrøyningsvolum*. Tech. rep. 2015.

[33] L.M. Andreassen et al. *Klima i Norge 2100*. Tech. rep. 2016.

[34] Anita Verpe Dyrrdal and Eirik J. Førland. *Klimapåslag for korttidsnedbør Anbefalte verdier for Norge*. Tech. rep. 2019.

[35] Kim Robert Lisø andTore Kvande. Byggforsk, 2007. ISBN: 9788253609607.

[36] Luke Verstraten et al. "Sensitivity of Australian roof drainage structures to design rainfall variability and climatic change". In: *Building and Environment* 161 (2019), p. 106230. ISSN: 0360-1323. DOI: https://doi.org/10.1016/j.buildenv.2019.106230. URL: http://www.sciencedirect.com/science/article/pii/S0360132319304408.

[37] Luke Verstraten, Terry Lucke, and Geoffrey O'Loughlin. "Comparing empirical water depth observations of a box gutter roof drainage system to three different international design guidelines". In: *Journal of Building Engineering* 12 (2017), pp. 178–187. ISSN: 2352-7102. DOI: https://doi.org/10.1016/j.jobe.2017.06.004. URL: http://www.sciencedirect.com/science/article/pii/S2352710217300396.

[38] R W P May. *Manual for the Design of Roof Drainage Systems: A Guide to the use of European Standard BS EN 12056-3:2000*. Mar. 2003.

[39] Standard Norge. *Gravity drainage systems inside buildings Part3: Roof drainage, layout and calculation*. Tech. rep. NS 12056-3:2000. Standard Norge, Oct. 2000.

[40] Henrik Svaland Aas. *Hydraulisk utforming av nedløp fra gateavrenning*. Master Thesis, Norwegian Institute of Technology. June 2015.

[41] Louis Blendermann. *Controlled Stormwater Drainage*. Industrial Press, 1979. ISBN: 0-8311-1123-2.

[42] British Standards Institution. *Gravity drainage systems inside buildings Part 3: Roof drainage, layout and calculation*. Tech. rep. BS EN 12056-3:2000. British Standards Institution, Oct. 2000.

[43] Urban Drainage Standards Committee of the Standards Development Council of the Environmental and Water Resources Institute of the American Society of Civil Engineers and American Society of Civil Engineers (ASCE) Staff. American Society of Civil Engineers, 2005. ISBN: 9780784471241.

[44] Gwilym T. Still and Terry Thomas. *THE OPTIMUM SIZING OF GUTTERS FOR DOMESTIC ROOFWATER HARVESTING*. University of Warwick. Dec. 2002.

[45] J. Zankowski et al. "Gutter design and selection for roof rainwater catchment systems". In: *2013 IEEE Global Humanitarian Technology Conference (GHTC)*. Aug. 2013, pp. 226–231. DOI: 10.1109/GHTC.2013.6713685.

[46] J.A. Swaffield, M. Escarameia, and D.P. Campbell. "Unsteady roof gutter flow: Development and application of simulation". In: *Building Services Engineering Research and Technology* 20.1 (1999), pp. 29–39. DOI: 10.1177/014362449902000106. URL: https://doi.org/10.1177/014362449902000106.

[47] "Large-scale experimental wind-driven rain exposure investigations of building integrated photovoltaics". In: *Solar Energy* 90 (2013), pp. 179–187. ISSN: 0038-092X. DOI: https://doi.org/10.1016/j.solener.2013.01.003.

[48] Erlend Andenæs. *Wind-driven rain exposure and assessment of building integrated photovoltaic systems*. Master Thesis, Norwegian Institute of Technology. June 2016.

[49] Anna Fedorova et al. *Large-Scale Laboratory Investigation of Building Integrated Photovoltaics - A Review of Methods and Opportunities*. Mar. 2017.

[50] NordTest. *Roofs: Water-tightness under pulsating air pressure*. Nordtest method NT Build 421. May 1993.

[51] Aoife M. O'Brien and Conor Mc Guckin. "The Systematic Literature Review Method: Trials and Tribulations of Electronic Database Searching at Doctoral Level". In: *SAGE Research Methods Cases* 61 (2016). DOI: https://dx.doi.org/10.4135/9781446273050155953 81.

[52] Anthony J. Onwuegbuzie and Rebecca K. Frels. Sage Publications Ltd, 2016. ISBN: 9781446248928.

[53] Claes Wohlin. "Guidelines for Snowballing in Systematic Literature Studies and a Replication in Software Engineering". In: *Proceedings of the 18th International Conference on Evaluation and Assessment in Software Engineering*. EASE '14. London, England, United Kingdom: ACM, 2014, 38:1–38:10. ISBN: 978-1-4503-2476-2. DOI: 10.1145/2601248.2601268. URL: http://doi.acm.org/10.1145/2601248.2601268.

[54] Link Arkitektur. *Manning's Equation and Table of N Values*. Engineering and Technical Data R-15, E.J. Prescott.

[55] Anita Verpe Dyrrdal et al. "Estimating extreme areal precipitation in Norway from a gridded dataset". In: *Hydrological Sciences Journal* 61.3 (2016), pp. 483–494. DOI: 10.1080/02626667.2014.947289. URL: https://doi.org/10.1080/02626667.2014.947289.

[56] Ben Trettel and Ofodike A. Ezekoye. *Theoretical Range and Trajectory of a Water Jet*. 2015.

[57] Sunpower. *SunPower X-Series: X21-350-BLK DC*.

[58] Sintef Byggforsk. *Takrenner og nedløp*. Tech. rep. 525.921. SINTEF Byggforskserien, Sept. 2017. URL: https://www.byggforsk.no/dokument/411/takrenner_og_nedloep.

Appendices

Appendix A

IDF Curves

Current and Future IDF Curves for Weather stations in Trondhiem

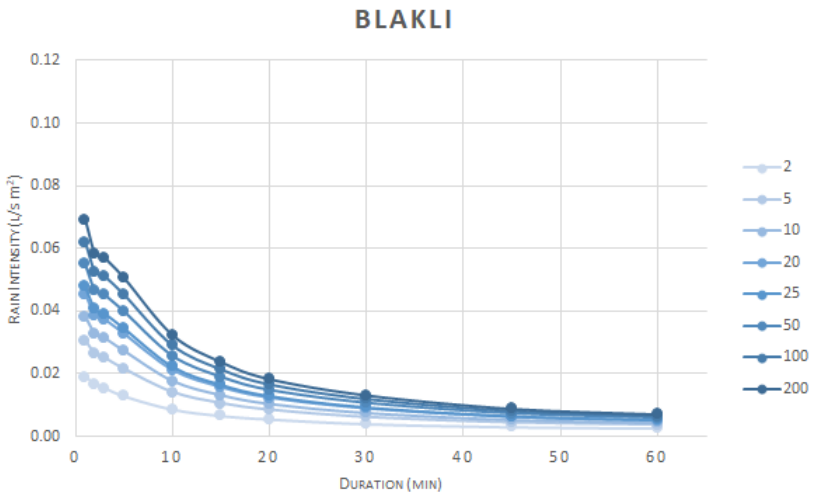

Figure A.1: IDF Curve for Blakli weather station [31]

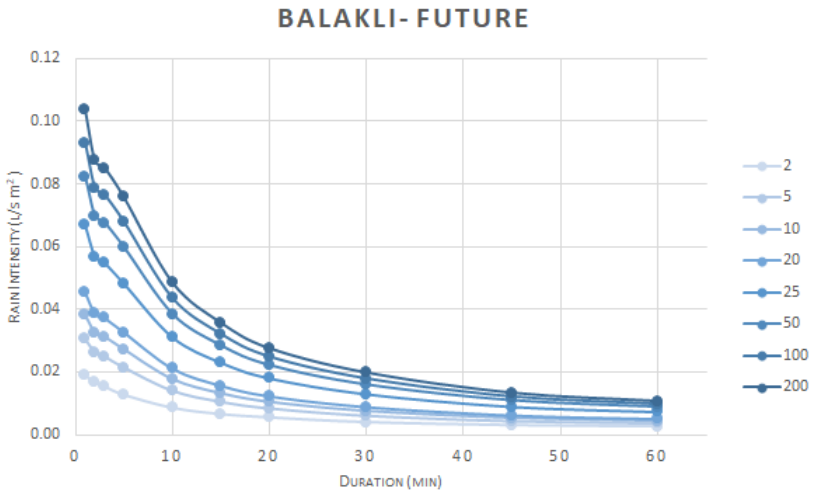

Figure A.2: Future IDF Curve for Blakli weather station [31]

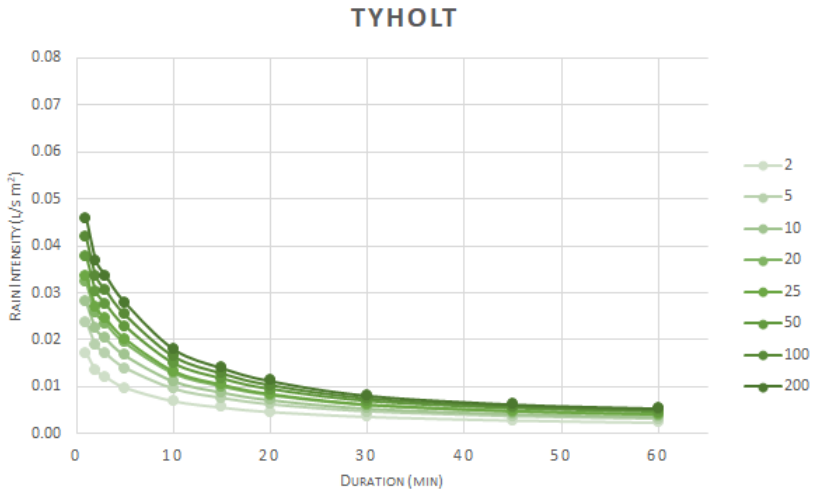

Figure A.3: IDF Curve for Tyholt weather station [31]

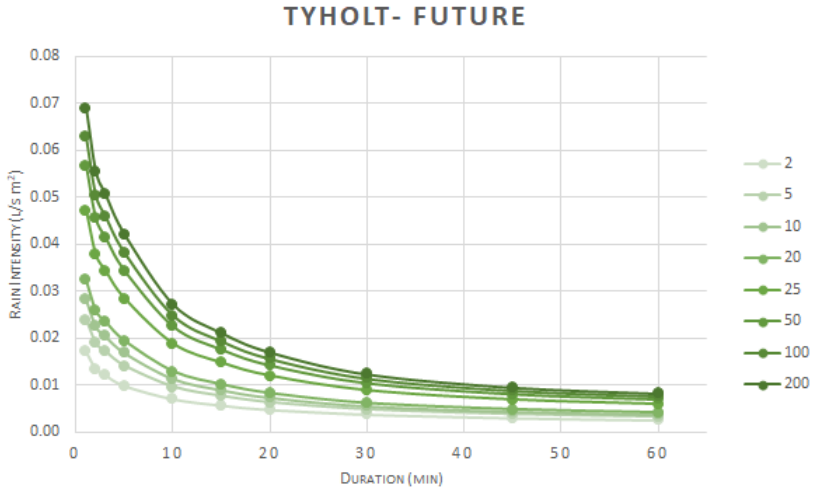

Figure A.4: Future IDF Curve for Tyholt weather station [31]

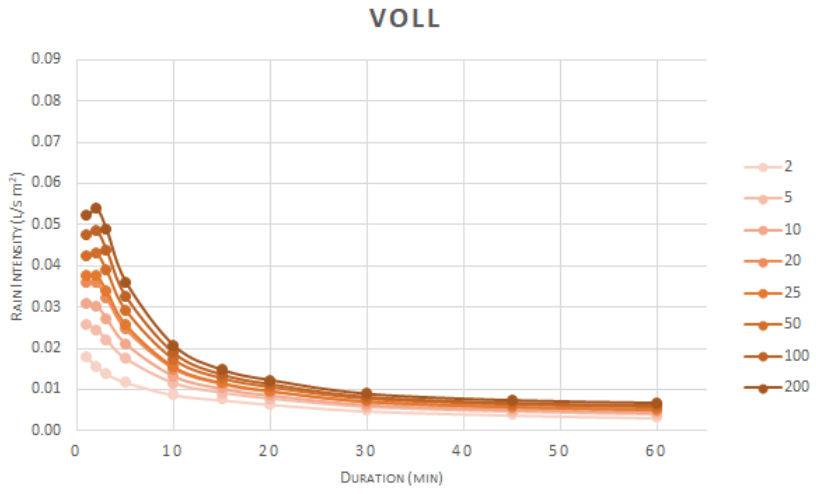

Figure A.5: IDF Curve for Voll weather station [31]

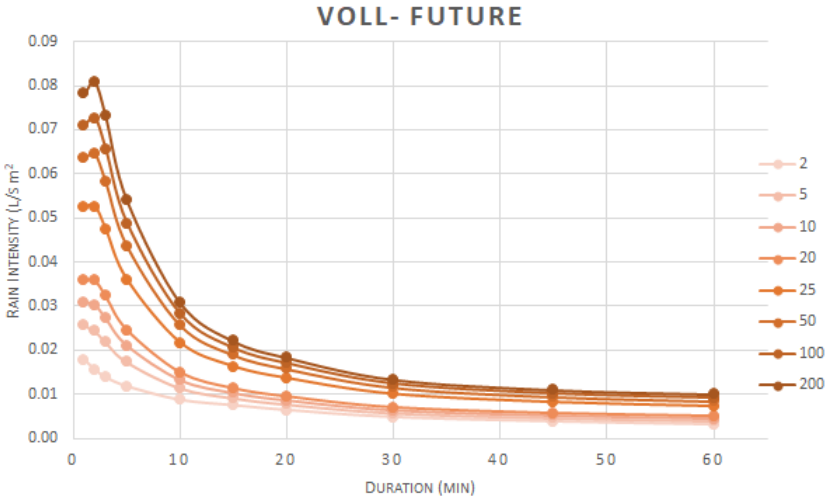

Figure A.6: Future IDF Curve for Voll weather station [31]

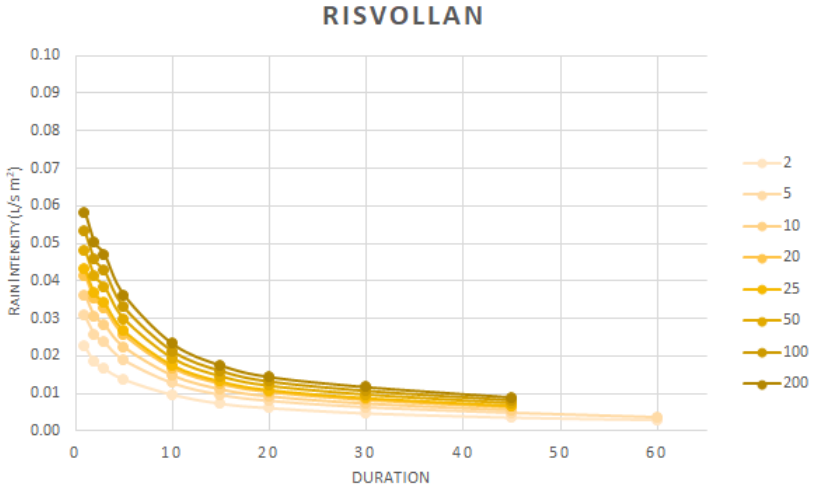

Figure A.7: IDF Curve for Risvollan weather station [31]

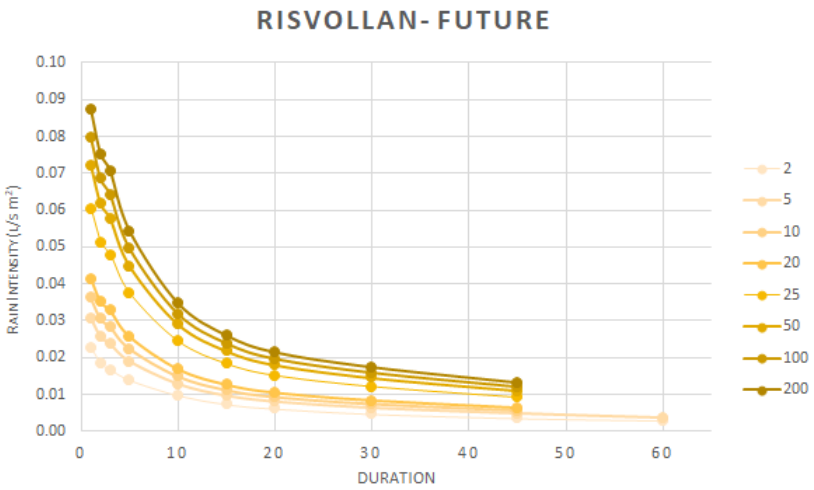

Figure A.8: Future IDF Curve for Risvollan weather station [31]

Appendix B

Runoff Quantities

B.1 IDF Data

IDF Data used in calculations in Section 3.2.1. The IDF data used is presented in Figure B.1 and B.2.

	Return Value for precipitation (l/s*Ha)									
Return Period (yr)	1 min	2 min	3 min	5 min	10 min	15 min	20 min	30 min	45 min	60 min
2	177.7	155	138	117.3	86.6	74.6	63.7	47.8	37.8	31
5	256.6	243.2	218.2	173	113.7	91.2	77	57.1	45.8	39.1
10	308.8	301.6	271.3	209.8	131.6	102.2	85.8	63.3	51.1	44.5
20	359	357.6	322.2	245.2	148.9	112.7	94.2	69.3	56.2	49.6
25	374.9	375.4	338.4	256.4	154.3	116	96.9	71.2	57.9	51.3
50	423.8	430.1	388.2	290.9	171.2	126.3	105.2	77	62.8	56.3
100	472.4	484.4	437.6	325.2	187.9	136.5	113.4	82.7	67.8	61.3
200	521	538.6	486.9	359.4	204.5	146.7	121.6	88.5	72.7	66.3

Figure B.1: IDF Data for Voll [31]

	Returverdi for precipitation (l/s*Ha)									
Return Period (yr)	1 min	2 min	3 min	5 min	10 min	15 min	20 min	30 min	45 min	60 min
2	248.78	217.00	193.20	164.22	121.24	104.44	89.18	66.92	52.92	43.40
5	359.24	340.48	305.48	242.20	159.18	127.68	107.80	79.94	64.12	54.74
10	432.32	422.24	379.82	293.72	184.24	143.08	120.12	88.62	71.54	62.30
20	502.60	500.64	451.08	343.28	208.46	157.78	131.88	97.02	78.68	69.44
25	524.86	525.56	473.76	358.96	216.02	162.40	135.66	99.68	81.06	71.82
50	635.70	645.15	582.30	436.35	256.80	189.45	157.80	115.50	94.20	84.45
100	708.60	726.60	656.40	487.80	281.85	204.75	170.10	124.05	101.70	91.95
200	781.50	807.90	730.35	539.10	306.75	220.05	182.40	132.75	109.05	99.45

Figure B.2: Future IDF Data for Voll

B.2 Rational Method

Runoff quantities from calculations in Section 3.2.1 in figures B.3 - B.10.

	Rational Method- Entire Roof Q: Runoff rate (l/s)									
Return Period (yr)	1 min	2 min	3 min	5 min	10 min	15 min	20 min	30 min	45 min	60 min
2	8.22	7.17	6.38	5.42	4.00	3.45	2.94	2.21	1.75	1.43
5	11.86	11.24	10.09	8.00	5.26	4.22	3.56	2.64	2.12	1.81
10	14.28	13.94	12.54	9.70	6.08	4.72	3.97	2.93	2.36	2.06
20	16.60	16.53	14.90	11.34	6.88	5.21	4.36	3.20	2.60	2.29
25	17.33	17.36	15.64	11.85	7.13	5.36	4.48	3.29	2.68	2.37
50	19.59	19.88	17.95	13.45	7.91	5.84	4.86	3.56	2.90	2.60
100	21.84	22.39	20.23	15.03	8.69	6.31	5.24	3.82	3.13	2.83
200	24.09	24.90	22.51	16.62	9.45	6.78	5.62	4.09	3.36	3.07

Figure B.3: Volumetric runoff flow rate for entire roof [l/s]

	Entire Roof Q: Runoff rate (l/s)									
Return Period (yr)	1 min	2 min	3 min	5 min	10 min	15 min	20 min	30 min	45 min	60 min
2	11.50	10.03	8.93	7.59	5.61	4.83	4.12	3.09	2.45	2.01
5	16.61	15.74	14.12	11.20	7.36	5.90	4.98	3.70	2.96	2.53
10	19.99	19.52	17.56	13.58	8.52	6.61	5.55	4.10	3.31	2.88
20	23.24	23.15	20.85	15.87	9.64	7.29	6.10	4.49	3.64	3.21
25	24.27	24.30	21.90	16.60	9.99	7.51	6.27	4.61	3.75	3.32
50	29.39	29.83	26.92	20.17	11.87	8.76	7.30	5.34	4.36	3.90
100	32.76	33.59	30.35	22.55	13.03	9.47	7.86	5.74	4.70	4.25
200	36.13	37.35	33.77	24.92	14.18	10.17	8.43	6.14	5.04	4.60

Figure B.4: Future volumetric runoff flow rate for entire roof [l/s]

	q:runoff l/s per meter width (drainage length)									
Return Period (yr)	1 min	2 min	3 min	5 min	10 min	15 min	20 min	30 min	45 min	60 min
2	0.34	0.30	0.27	0.23	0.17	0.14	0.12	0.09	0.07	0.06
5	0.49	0.47	0.42	0.33	0.22	0.18	0.15	0.11	0.09	0.08
10	0.59	0.58	0.52	0.40	0.25	0.20	0.16	0.12	0.10	0.09
20	0.69	0.69	0.62	0.47	0.29	0.22	0.18	0.13	0.11	0.10
25	0.72	0.72	0.65	0.49	0.30	0.22	0.19	0.14	0.11	0.10
50	0.81	0.83	0.75	0.56	0.33	0.24	0.20	0.15	0.12	0.11
100	0.91	0.93	0.84	0.63	0.36	0.26	0.22	0.16	0.13	0.12
200	1.00	1.04	0.94	0.69	0.39	0.28	0.23	0.17	0.14	0.13

Figure B.5: Volumetric runoff flow rate pr meter drainage length [l/s]

B.3 Hybrid Method- Shallow water and Manning

Results from the calculation method presented in section 3.2.2 in Figures B.11- B.20.

	q:runoff l/s per meter width (drainage length)									
Return Period (yr)	1 min	2 min	3 min	5 min	10 min	15 min	20 min	30 min	45 min	60 min
2	0.48	0.42	0.37	0.32	0.23	0.20	0.17	0.13	0.10	0.08
5	0.69	0.65	0.59	0.47	0.31	0.25	0.21	0.15	0.12	0.11
10	0.83	0.81	0.73	0.56	0.35	0.28	0.23	0.17	0.14	0.12
20	0.97	0.96	0.87	0.66	0.40	0.30	0.25	0.19	0.15	0.13
25	1.01	1.01	0.91	0.69	0.42	0.31	0.26	0.19	0.16	0.14
50	1.22	1.24	1.12	0.84	0.49	0.36	0.30	0.22	0.18	0.16
100	1.36	1.40	1.26	0.94	0.54	0.39	0.33	0.24	0.20	0.18
200	1.50	1.55	1.40	1.04	0.59	0.42	0.35	0.26	0.21	0.19

Figure B.6: Future volumetric runoff flow pr meter drainage length [l/s]

	entire sample roof runoff (l/min)									
Return Period (yr)	1 min	2 min	3 min	5 min	10 min	15 min	20 min	30 min	45 min	60 min
2	54.72	47.73	42.50	36.12	26.67	22.97	19.62	14.72	11.64	9.55
5	79.02	74.89	67.20	53.28	35.01	28.09	23.71	17.58	14.10	12.04
10	95.10	92.88	83.55	64.61	40.53	31.47	26.42	19.49	15.74	13.70
20	110.56	110.12	99.22	75.51	45.85	34.71	29.01	21.34	17.31	15.27
25	115.45	115.61	104.21	78.96	47.52	35.72	29.84	21.93	17.83	15.80
50	130.51	132.45	119.55	89.58	52.72	38.89	32.40	23.71	19.34	17.34
100	145.48	149.17	134.76	100.15	57.86	42.04	34.92	25.47	20.88	18.88
200	160.44	165.86	149.94	110.68	62.98	45.18	37.45	27.25	22.39	20.42

Figure B.7: Volumetric runoff flow rate for entire sample roof [l/min]

	entire sample roof runoff (l/min)									
Return Period (yr)	1 min	2 min	3 min	5 min	10 min	15 min	20 min	30 min	45 min	60 min
2	76.61	66.83	59.50	50.57	37.34	32.16	27.46	20.61	16.30	13.37
5	110.63	104.85	94.07	74.59	49.02	39.32	33.20	24.62	19.75	16.86
10	133.13	130.03	116.97	90.45	56.74	44.06	36.99	27.29	22.03	19.19
20	154.78	154.17	138.91	105.71	64.20	48.59	40.61	29.88	24.23	21.38
25	161.63	161.85	145.90	110.54	66.52	50.01	41.78	30.70	24.96	22.12
50	195.77	198.68	179.32	134.38	79.08	58.34	48.60	35.57	29.01	26.01
100	218.22	223.76	202.14	150.22	86.80	63.05	52.38	38.20	31.32	28.32
200	240.67	248.80	224.91	166.02	94.47	67.77	56.17	40.88	33.58	30.63

Figure B.8: Future volumetric runoff flow rate for entire sample roof [l/min]

	Time of concentration [s]									
Return Period (yr)	1 min	2 min	3 min	5 min	10 min	15 min	20 min	30 min	45 min	60 min
2	36.88	38.95	40.81	43.55	49.17	52.19	55.59	62.36	68.50	74.16
5	31.84	32.53	33.97	37.28	44.09	48.16	51.53	58.08	63.44	67.58
10	29.57	29.85	31.14	34.51	41.59	46.02	49.35	55.74	60.72	64.17
20	27.84	27.88	29.07	32.43	39.59	44.25	47.54	53.75	58.45	61.45
25	27.36	27.35	28.50	31.85	39.03	43.74	47.01	53.17	57.76	60.62
50	26.05	25.90	26.98	30.28	37.44	42.28	45.49	51.53	55.91	58.41
100	24.94	24.70	25.72	28.96	36.07	40.99	44.14	50.08	54.22	56.46
200	23.99	23.67	24.64	27.83	34.87	39.82	42.93	48.74	52.73	54.71

Figure B.9: Time of concentration for entire roof length [s]

Time of concentration [s]										
Return Period (yr)	1 min	2 min	3 min	5 min	10 min	15 min	20 min	30 min	45 min	60 min
2	36.88	38.95	40.81	43.55	49.17	52.19	55.59	62.36	68.50	74.16
5	31.84	32.53	33.97	37.28	44.09	48.16	51.53	58.08	63.44	67.58
10	29.57	29.85	31.14	34.51	41.59	46.02	49.35	55.74	60.72	64.17
20	27.84	27.88	29.07	32.43	39.59	44.25	47.54	53.75	58.45	61.45
25	27.36	27.35	28.50	31.85	39.03	43.74	47.01	53.17	57.76	60.62
50	26.05	25.90	26.98	30.28	37.44	42.28	45.49	51.53	55.91	58.41
100	24.94	24.70	25.72	28.96	36.07	40.99	44.14	50.08	54.22	56.46
200	23.99	23.67	24.64	27.83	34.87	39.82	42.93	48.74	52.73	54.71

Figure B.10: Future time of concentration for entire roof length [s]

Return Period (yr)	1 min	2 min	3 min	5 min	10 min	15 min	20 min	30 min	45 min	60 min
2	261.35	227.97	202.96	172.52	127.37	109.72	93.69	70.30	55.59	45.59
5	377.39	357.68	320.92	254.44	167.22	134.13	113.25	83.98	67.36	57.51
10	454.17	443.58	399.01	308.56	193.55	150.31	126.19	93.10	75.15	65.45
20	528.00	525.94	473.87	360.63	218.99	165.75	138.54	101.92	82.66	72.95
25	551.38	552.12	497.70	377.10	226.94	170.61	142.52	104.72	85.16	75.45
50	623.30	632.57	570.94	427.84	251.79	185.75	154.72	113.25	92.36	82.80
100	694.78	712.43	643.60	478.29	276.35	200.76	166.78	121.63	99.72	90.16
200	766.26	792.14	716.11	528.59	300.77	215.76	178.84	130.16	106.92	97.51

Figure B.11: Reynolds number for current runoff

Reynolds Number										
Return Period (yr)	1 min	2 min	3 min	5 min	10 min	15 min	20 min	30 min	45 min	60 min
2	365.89	319.15	284.15	241.53	178.31	153.60	131.16	98.42	77.83	63.83
5	528.35	500.76	449.28	356.21	234.11	187.78	158.55	117.57	94.30	80.51
10	635.83	621.01	558.62	431.99	270.97	210.43	176.67	130.34	105.22	91.63
20	739.20	736.31	663.42	504.88	306.59	232.05	193.96	142.69	115.72	102.13
25	771.93	772.96	696.78	527.94	317.71	238.85	199.52	146.60	119.22	105.63
50	934.95	948.85	856.41	641.76	377.69	278.63	232.08	169.87	138.54	124.20
100	1042.17	1068.64	965.40	717.43	414.53	301.13	250.17	182.45	149.57	135.23
200	1149.39	1188.21	1074.16	792.88	451.15	323.64	268.26	195.24	160.38	146.27

Figure B.12: Future reynolds number for current runoff

depth of flow (mm)										
Return Period (yr)	1 min	2 min	3 min	5 min	10 min	15 min	20 min	30 min	45 min	60 min
2	0.85	0.81	0.77	0.72	0.63	0.60	0.56	0.50	0.46	0.42
5	0.99	0.97	0.93	0.84	0.71	0.65	0.61	0.54	0.49	0.46
10	1.08	1.06	1.02	0.91	0.75	0.68	0.63	0.56	0.51	0.49
20	1.15	1.14	1.09	0.98	0.79	0.71	0.66	0.58	0.53	0.51
25	1.17	1.17	1.12	0.99	0.80	0.72	0.66	0.59	0.54	0.51
50	1.23	1.24	1.18	1.05	0.84	0.74	0.69	0.61	0.56	0.53
100	1.29	1.30	1.25	1.10	0.87	0.76	0.71	0.62	0.57	0.55
200	1.34	1.36	1.31	1.15	0.90	0.79	0.73	0.64	0.59	0.57

Figure B.13: Depth of flow at downstream end at peak flow [mm]

depth of flow (mm)										
Return Period (yr)	1 min	2 min	3 min	5 min	10 min	15 min	20 min	30 min	45 min	60 min
2	0.98	0.93	0.88	0.83	0.73	0.69	0.64	0.57	0.52	0.48
5	1.15	1.12	1.07	0.97	0.81	0.74	0.69	0.61	0.56	0.53
10	1.24	1.23	1.17	1.05	0.87	0.78	0.73	0.64	0.59	0.56
20	1.32	1.32	1.26	1.12	0.91	0.81	0.75	0.66	0.61	0.58
25	1.35	1.35	1.29	1.15	0.93	0.82	0.76	0.67	0.62	0.59
50	1.46	1.47	1.41	1.25	0.99	0.88	0.81	0.71	0.66	0.63
100	1.53	1.55	1.48	1.31	1.03	0.90	0.84	0.74	0.68	0.65
200	1.60	1.62	1.55	1.36	1.07	0.93	0.86	0.76	0.70	0.67

Figure B.14: Future depth of flow at downstream end at peak flow [mm]

Manning formula, speed of flow m/s										
Return Period (yr)	1 min	2 min	3 min	5 min	10 min	15 min	20 min	30 min	45 min	60 min
2	0.62	0.60	0.58	0.55	0.51	0.49	0.47	0.43	0.41	0.39
5	0.69	0.68	0.66	0.62	0.55	0.52	0.49	0.46	0.43	0.41
10	0.73	0.72	0.70	0.65	0.57	0.53	0.51	0.47	0.44	0.43
20	0.76	0.76	0.73	0.68	0.59	0.55	0.52	0.48	0.45	0.44
25	0.77	0.77	0.74	0.69	0.60	0.55	0.53	0.48	0.46	0.44
50	0.79	0.80	0.77	0.71	0.61	0.57	0.54	0.49	0.47	0.45
100	0.82	0.82	0.80	0.74	0.63	0.58	0.55	0.50	0.48	0.46
200	0.84	0.85	0.82	0.76	0.65	0.59	0.56	0.51	0.49	0.47

Figure B.15: Speed downstream end at peak flow [m/s]

Manning formula, speed of flow speed m/s										
Return Period (yr)	1 min	2 min	3 min	5 min	10 min	15 min	20 min	30 min	45 min	60 min
2	0.68	0.66	0.64	0.61	0.56	0.54	0.51	0.48	0.45	0.42
5	0.76	0.75	0.72	0.68	0.60	0.57	0.54	0.50	0.47	0.45
10	0.80	0.79	0.77	0.71	0.63	0.59	0.56	0.51	0.48	0.47
20	0.83	0.83	0.81	0.75	0.65	0.60	0.57	0.53	0.50	0.48
25	0.84	0.84	0.82	0.76	0.66	0.61	0.58	0.53	0.50	0.49
50	0.89	0.89	0.87	0.80	0.69	0.63	0.60	0.55	0.52	0.51
100	0.92	0.93	0.90	0.83	0.71	0.65	0.61	0.56	0.53	0.52
200	0.94	0.95	0.93	0.85	0.72	0.66	0.63	0.57	0.54	0.53

Figure B.16: Future speed downstream end at peak flow [m/s]

Q = flow entire sample roof (l/min)										
Return Period (yr)	1 min	2 min	3 min	5 min	10 min	15 min	20 min	30 min	45 min	60 min
2	84.90	77.24	71.30	63.78	51.87	46.90	42.17	34.81	29.80	26.16
5	109.68	105.64	97.93	83.34	62.43	53.73	47.91	39.19	33.84	30.48
10	124.92	122.86	114.05	95.28	69.01	58.05	51.55	41.99	36.39	33.20
20	138.93	138.54	128.71	106.24	75.13	62.06	54.92	44.63	38.78	35.68
25	143.25	143.39	133.25	109.62	77.00	63.29	55.99	45.45	39.56	36.49
50	156.27	157.92	146.84	119.77	82.74	67.09	59.21	47.91	41.77	38.83
100	168.82	171.86	159.87	129.56	88.25	70.77	62.32	50.28	43.98	41.10
200	181.03	185.38	172.50	139.04	93.60	74.37	65.37	52.64	46.09	43.32

Figure B.17: Volumetric runoff flow rate for entire sample roof [l/min]

Q = flow entire sample roof (l/min)										
Return Period (yr)	1 min	2 min	3 min	5 min	10 min	15 min	20 min	30 min	45 min	60 min
2	84.90	77.24	71.30	63.78	51.87	46.90	42.17	34.81	29.80	26.16
5	109.68	105.64	97.93	83.34	62.43	53.73	47.91	39.19	33.84	30.48
10	124.92	122.86	114.05	95.28	69.01	58.05	51.55	41.99	36.39	33.20
20	138.93	138.54	128.71	106.24	75.13	62.06	54.92	44.63	38.78	35.68
25	143.25	143.39	133.25	109.62	77.00	63.29	55.99	45.45	39.56	36.49
50	156.27	157.92	146.84	119.77	82.74	67.09	59.21	47.91	41.77	38.83
100	168.82	171.86	159.87	129.56	88.25	70.77	62.32	50.28	43.98	41.10
200	181.03	185.38	172.50	139.04	93.60	74.37	65.37	52.64	46.09	43.32

Figure B.18: Future volumetric runoff flow rate for entire sample roof [l/min]

Time to equilibrium (s)										
Return Period (yr)	1 min	2 min	3 min	5 min	10 min	15 min	20 min	30 min	45 min	60 min
2	48.00	52.00	55.67	61.25	73.29	80.09	88.00	104.53	120.42	135.79
5	38.76	39.99	42.59	48.76	62.39	71.08	78.59	93.95	107.25	117.98
10	34.83	35.30	37.53	43.57	57.24	66.44	73.70	88.33	100.42	109.13
20	31.93	32.00	33.98	39.80	53.24	62.71	69.73	83.68	94.85	102.23
25	31.14	31.12	33.03	38.78	52.14	61.65	68.57	82.34	93.17	100.18
50	29.02	28.78	30.52	36.05	49.06	58.64	65.32	78.59	88.75	94.75
100	27.27	26.89	28.50	33.80	46.46	56.02	62.48	75.32	84.78	90.04
200	25.79	25.30	26.81	31.91	44.23	53.70	59.97	72.35	81.33	85.92

Figure B.19: Time to equilibrium [s]

Time to equilibrium (s)										
Return Period (yr)	1 min	2 min	3 min	5 min	10 min	15 min	20 min	30 min	45 min	60 min
2	39.47	42.73	45.72	50.27	60.07	65.60	72.03	85.45	98.33	110.78
5	31.92	32.92	35.04	40.08	51.19	58.27	64.38	76.86	87.65	96.36
10	28.70	29.09	30.91	35.85	47.00	54.50	60.40	72.30	82.11	89.18
20	26.32	26.38	28.00	32.76	43.74	51.46	57.17	68.52	77.59	83.58
25	25.68	25.66	27.23	31.93	42.84	50.60	56.23	67.43	76.23	81.92
50	23.02	22.83	24.20	28.54	38.75	46.24	51.46	61.81	69.73	74.39
100	21.64	21.34	22.61	26.78	36.71	44.20	49.24	59.27	66.64	70.73
200	20.47	20.09	21.27	25.29	34.96	42.38	47.28	56.95	63.94	67.52

Figure B.20: Future time to equilibrium [s]

Appendix C

Byggindustri Article

FRA EKSPERTENE: NTNU

Takrenne for BIPV-tak

ZEB-laboratoriet er NTNU og SINTEF sitt nye nullutslippslaboratorium i Trondheim. Det 19 meter lange taket vil bestå av bygningsintegrerte solcellepaneler. Størrelsen på taket og glattheten til taktekningen er utfordrende med tanke på håndtering av takvann fra kraftige regnskyll. Vi har derfor testet takrennen for forventede regnmengder om 100 år for å sikre en optimal utforming.

Katalin Sandor Johansen og Anna Eknes Stagrum
Institutt for bygg- og miljøteknikk

ZEB-laboratoriet har hele takflaten vendt mot sør for optimal strømproduksjon med solceller.
Illustrasjon: LINK Arkitektur/Veidekke

ZEB-laboratoriet skal bli et kontor- og undervisningsbygg for forskning og utvikling av teknologi. Målsettingen er å demonstrere gjennomføringen av et klimatilpasset ZEB-COM bygg. For å oppnå ZEB-COM kravet skal byggets fornybare energiproduksjon kompensere for klimagassutslipp fra bygging, drift og materialfremstilling over en livssyklus på 60 år. Dette innebærer at bygget må være meget energieffektivt, men løsningene må også ha lavest mulig klimagassutslipp i et livssyklusperspektiv. Et viktig tiltak er å redusere materialbruken så mye som mulig.

Bygningsintegrerte PV-panel (BIPV)

Produksjon av elektrisitet er basert på solceller. ZEB-laboratoriet er orientert direkte mot sør med et 19 meter langt skråtak på 30°. Dette gjør taket og den sørvendte fasaden til effektive arealer for høsting av solenergi. 525 m² med svært effektive solceller skal brukes på taket. Samtidig skal solcellene være bygningsintegrerte (BIPV) for å erstatte den tradisjonelle taktekningen. BIPV-systemet må derfor være så regntett som mulig for å unngå fuktproblemer.

For ZEB-laboratoriet blir taket en stor, tett og meget glatt overflate som under kraftige regnskyll vil føre store mengder vann i høy fart ned langs taket mot ytterkanten (raften). En utvendig takrenne, tilstrekkelig stor nok til å fange alt vannet, vil skygge for solceller i øvre del av fasaden og dermed redusere energiproduksjon. Løsningen blir en innvendig takrenne som er integrert i takflaten. For å optimalisere solcellearealet og for å påse at det arkitektoniske uttrykket blir bevart, har vi utforsket hvor smal takrenneåpning kan være før den ikke klarer å fange takvannet.

Laboratorieforsøk

Intens korttidsnedbør gir størst utfordring med tanke på å fange takvannet. Høyere nedbørintensitet gir mer vann og høyere fart på vannet som strømmer nedover taket, og dermed økt fare for at vannet renner over takrennen. Et prøvetak på 2,8 x 2,8m ble bygget for å undersøke takrennens evne til å fange regnvannet. SINTEF sin RAWI (Rain and Wind) boks ble brukt til å teste regnmengder som det 19 meter lange taket kan få. Taket ble testet på 30° vinkel.

Ettersom ZEB-bygget har en levetid på 60 år, er det viktig at takrennen også klarer å håndtere nedbørsmengder som kommer i fremtiden. Dagens dimensjonerende regnmengde i Trondheim for prøvetaket er på 100 l/min. Med klimapåslag for framtidssituasjonen har vi testet prøvetaket for 180 l/min. I tillegg til størrelsen på takrenneåpningen har vi sett på effekten av å benytte en rist over rennen for å «lede» vannet ned i rennen.

Anbefaling

Opprinnelig foreslått løsning i prosjektet var en takrenne med åpning på 480 mm. Forsøkene viser at en halvering av denne størrelsen vil være tilstrekkelig for å fange opp regn fra de største regnskyllene. Med rist, kan åpningen reduseres ytterligere. Med bakgrunn i prøvingen kan vi altså halvere takrenneåpningen, noe som gir oss 6 m² ekstra takflate til å montere solceller på. I tillegg gir smalere takrenne med rist et bedre arkitektonisk uttrykk.

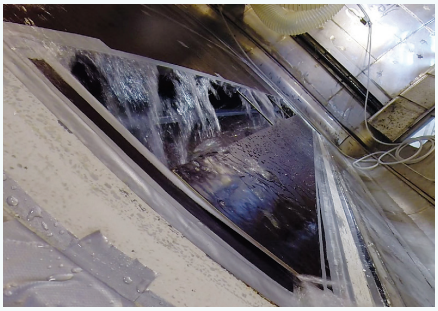

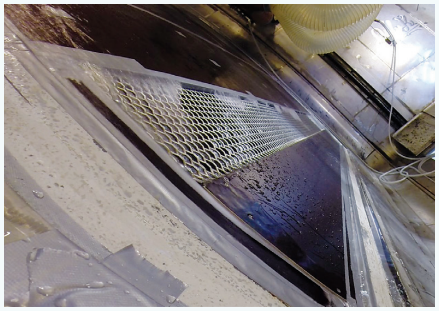

Kraftige regnskyll på glatt taktekning gir mye vann som renner i stor fart nedover taket. Med for smal takrenneåpning vil ikke vannet bli fanget av takrennen. Bruk av rist kan lede vannet ned i rennen og samtidig hindre at løv blokkerer taknedløpene.